

Growth of nanostructures by cluster deposition : experiments and simple models

Pablo Jensen*

Département de Physique des Matériaux, Université Claude Bernard Lyon-1, 69622 Villeurbanne Cédex, France

This paper presents a comprehensive analysis of simple models useful to analyze the growth of nanostructures obtained by cluster deposition. After detailing the potential interest of nanostructures, I extensively study the first stages of growth (the submonolayer regime) by kinetic Monte-Carlo simulations. These simulations are performed in a wide variety of experimental situations : complete condensation, growth with reevaporation, nucleation on defects, total or null cluster-cluster coalescence The main scope of the paper is to help experimentalists analyzing their data to deduce which of those processes are important and to quantify them. A software including all these simulation programs is available at no cost on request to the author. I carefully discuss experiments of growth from cluster beams and show how the mobility of the clusters on the surface can be measured : surprisingly high values are found. An important issue for future technological applications of cluster deposition is the relation between the size of the incident clusters and the size of the islands obtained on the substrate. An approximate formula which gives the ratio of the two sizes as a function of the melting temperature of the material deposited is given. Finally, I study the atomic mechanisms which can explain the diffusion of the clusters on a substrate and the result of their mutual interaction (simple juxtaposition, partial or total coalescence ...).

I. INTRODUCTION

Growth of new materials with tailored properties is one of the most active research directions for physicists. As pointed out by Silvan Schweber in his brilliant analysis of the evolution of physics after World War II : "An important transformation has taken place in physics : As had previously happened in chemistry, an ever larger fraction of the efforts in the field [are] being devoted to the study of novelty [creation of new structures, new objects and new phenomena] rather than to the elucidation of fundamental laws and interactions [...] Condensed matter physics has indeed become the study of systems that have never before existed." [1]

Among these new materials, those presenting a structure controlled down to the nanometer scale are being extensively studied [2–8]. There are different ways to build up nanostructured systems [8] : atomic deposition [9], mechanical milling [10], chemical methods [7,11], gas-aggregation techniques [5,12,13] ... Each of these techniques has its own advantages, but, as happens with atomic deposition techniques, the requisites of *control* (in terms of characterization and flexibility) and *efficiency* (in terms of quantity of matter obtained per second) are generally incompatible. As a physicist wishing to understand the details of the processes involved in the building of these nanostructures, I will focus in this review on a carefully *controlled* method : low energy cluster deposition [13]. Clusters are large "molecules" containing typically from 10 to 2000 atoms, and have been studied for their specific physical properties (mostly due to their large surface to volume ratio) which are *size dependent* and different from both the atoms and the bulk material [4,14–17]. By depositing *preformed* clusters on a substrate, one can build nanostructures of two types : in the submonolayer range, separated (and hopefully ordered) nanoislands, and for higher thicknesses, thin films or cluster assembled materials (CAM). The main advantage of the cluster deposition technique is that one can carefully control the building block (i.e. the cluster) and characterize the growth mechanisms. By changing the *size* of the incident clusters one can change the growth mechanisms [18,19] and the characteristics of the materials. For example, it has been shown that by changing the mean size of the incident carbon clusters, one can modify the properties of the carbon film, from graphitic to diamond-like [20].

This review is organized as follows. First, I present briefly the interest of nanostructures, both in the domain of nanoislands arranged on a substrate and as nanostructured, continuous films. I also review the different strategies employed to deposit *clusters* on a substrate : by accelerating them or by achieving their soft-landing. The scope of this section is to convince the reader that cluster deposition is a promising technique for nanostructure growth in a variety of domains, and therefore deserves a careful study. In Section III, models for cluster deposition are introduced. These models can also be useful for *atomic* deposition in some simple cases, namely when aggregation is irreversible. The models are adapted here to the physics of *cluster* deposition. In this case, reevaporation from the substrate can be important (as opposed to the usual conditions of Molecular Beam Epitaxy), cluster-cluster aggregation is always irreversible (as opposed to the possibility of bond breaking for atoms [21]) and particle-particle *coalescence* is possible. After a brief presentation of Kinetic Monte-Carlo (KMC) simulations, I show how the submonolayer regime

can be studied in a wide variety of experimental situations : complete condensation, growth with reevaporation, nucleation on defects, formation of two and three dimensional islands ... Since I want these models to be useful for experimentalists, Section V is entirely devoted to the presentation of a strategy on how to analyze experimental data and extract microscopic parameters such as diffusion and evaporation rates. I remind the reader that a simple software simulating all these situations is available at no cost on simple request to the author. Section VI analyzes in detail several experiments of cluster deposition. These studies serve as examples of the recipes given in Section V to analyze the data and also to demonstrate that clusters can have surprisingly large mobilities (comparable to atomic mobilities) on some substrates. A first interpretation of these intriguing results at the atomic level is given in Section VII, where the kinetics of cluster-cluster coalescence is also studied. The main results of this Section are that high cluster mobilities can be achieved provided the cluster does not find an epitaxial arrangement on the substrate and that cluster-cluster coalescence can be much slower than predicted by macroscopic theories.

A note on terminology : The structures formed on the surface by aggregation of the clusters are called islands. This is to avoid the possible confusion with the terms usually employed for atomic deposition where the clusters are the islands formed by aggregation of atoms on the surface. Here, the clusters are *performed* in the gas phase *before* deposition. I use *coverage* for the actual portion of the surface covered by the islands and *thickness* for the total amount of matter deposited on the surface (see also Table I).

II. INTEREST AND BUILDING OF NANOSTRUCTURES

Before turning to the heart of this paper - the growth of nanostructures by cluster deposition - I think it is appropriate to show why one wants to obtain nanostructures at all and how these can be prepared experimentally. Due to the technological impetus, a tremendous amount of both experimental and theoretical work has been carried out in this field, and it is impossible to summarize every aspect of it here. For a recent and rather thorough review, see Ref. [8] where the possible technological impact of nanostructures is also addressed. Actually, several journals are entirely devoted to this field [22]. The reader is also referred to the enormous number of World Wide Web pages (about 6000 on nanostructures), especially those quoted in Ref. [23]. A short summary of the industrial interest of nanostructures [24] and introductory reviews on the interest of "Nanoscale and ultrafast devices" [25] or "Optics of nanostructures" [26] have appeared recently.

There are two distinct (though related) domains where nanostructures can be interesting for applications. The first stems from the desire of miniaturization of electronic devices. Specifically, one would like to grow organized nanometer size islands with specific electronic properties. As a consequence, an impressive quantity of deposition techniques have been developed to grow carefully controlled thin films and nanostructures from atomic deposition [9]. While most of these techniques are complex and keyed to specific applications, Molecular Beam Epitaxy (MBE) [27] has received much attention from the physicists [28], mainly because of its (relative) simplicity. The second subfield is that of nanostructured materials [8], as thin or thick films, which show (mechanical, catalytic, optical) properties different from their microcrystalline counterparts [5,6,11,29,30].

I will now briefly review the two subfields since cluster deposition can be used to build both types of nanostructures. Moreover, some of the physical processes studied below (such as cluster-cluster coalescence) are of interest for both types of structure.

A. Organized nanoislands

There has been a growing interest for the fabrication of organized islands of nanometer dimensions. One of the reasons is the obvious advantage of miniaturizing the electronic devices both for device speed and density on a chip (for a simple and enjoyable introduction to the progressive miniaturization of electronics devices, see Ref. [31]). But it should be noted that at these scales, shrinking the size of the devices does also change their properties, owing to quantum confinement effects. Specifically, semiconductor islands smaller than the Bohr diameter of the bulk material (from several nm to several tens of nm) show interesting properties : as their size decreases, their effective bandgap increases. The possibility to tailor the electronic properties of a given material by playing on its size has generated a high level of interest in the field of these *quantum dots* [32]. But quantum dots are not the only driving force for obtaining organized nanoislands. Isolated nanoparticles are also interesting as model catalysts (see Refs. [33,34] and Chapter 12 of Ref. [8]). Clearly, using small particles increases the specific catalytic area for a given volume. More interesting, particles smaller than 4-5 nm in diameter might show specific catalytic properties, different from the bulk [34,35], although the precise mechanisms are not always well identified (Chapter 12 of Ref. [8]). One possibility is the increase, for small particle sizes, of the proportion of low coordination atoms (corners, kinks) whose electronic

(and therefore catalytic) properties are expected to be different from bulk atoms. For even smaller particles (1-2 nm), the interaction with the substrate can significantly alter their electronic properties [36]. Recently, there have been attempts at *organizing* the isolated islands to test the consequences on the catalytic properties [37]. Obtaining isolated clusters on a surface can also be interesting to study their properties. For example, Schaefer et al. [38] have obtained isolated gold clusters onto a variety of substrates to investigate the elastic properties of *single* nanoparticles by Atomic Force Microscopy (AFM).

Let me now briefly turn on to the possible ways of obtaining such organized nanoislands. Deposition of atoms on carefully controlled substrates is the main technique used presently by physicists to try to obtain a periodic array of nanometer islands of well-defined sizes. A striking example [39] of organized nanoislands is given in Fig. 1. These triangular islands have been grown on the dislocation network formed by the second Ag atomic layer on Pt(111). Beautiful as these triangles are, they have to be formed by nucleation and growth on the substrate, and therefore the process is highly dependent on the interaction of the adatoms with the substrate (energy barriers for diffusion, possibility of exchange of adatoms and substrate atoms, ...). This drastically limits the range of possible materials that can be grown by this method. However, the growth of strained islands by heteroepitaxy is under active study, since stress is a force which can lead to order, and even a tunable order, as observed for example in the system $PbSe/Pb_{1-x}Eu_xTe$ [40] (see Refs. [41,42] for further details on stress).

In this review, I will focus on an alternative approach to form nanoislands on substrates : instead of growing them by atom-atom aggregation *on* the substrate, a process which dramatically depends on the idiosyncrasies of the substrate and its interaction with the deposited atoms, one can prepare the islands (as free clusters) *before* deposition and then deposit them. It should be noted that the cluster structure can be extensively characterized *prior to* deposition by several in-flight techniques such as time-of-flight spectrometry, photo-ionization or fragmentation [43]. Moreover, the properties of these building blocks can be adjusted by changing their *size*, which also affects the growth mechanisms, and therefore the film morphology [18,19]. A clear example of the possibility to change the film morphology by varying only the mean cluster size has been given a few years ago by Fuchs et al. [18] (Fig. 2) and this study has been completed recently by Brechignac's group for larger cluster sizes [19]. There are several additional interests for depositing clusters. First, these are grown in extreme nonequilibrium conditions, which allows to obtain metastable structures or alloys. It is true that neither islands grown on a substrate are generally in equilibrium, but the quenching rate is very high in a beam, and the method is more flexible since one avoids the effects of nucleation and growth on a specific substrate. For example, PdPt alloy clusters - which are known to have interesting catalytic properties - can be prepared with a precise composition (corresponding to the composition of the target rod, see below) and variable size and then deposited on a surface [44]. The same is true for SiC clusters where one can modify the electronic properties of the famous C_{60} clusters by introducing in a controlled way Si atoms before deposition [45]. This allows to tune within a certain range the properties of the films by choosing the preparation conditions of the preformed clusters. It might also be anticipated that cluster nucleation is less sensitive to impurities than atomic nucleation. Atomic island growth can be dramatically affected by them, as exemplified by the celebrated case of the different morphologies of Pt islands grown on Pt(111) [46] which were actually the result of CO contamination at an incredibly low level : 10^{-10} mbar [47]. Instead, clusters, being larger entities, might interact less specifically with the substrate and its impurities. There is still no systematic way of organizing the clusters on a surface. One could try to pin them on selected sites such as defects or to encapsulate the clusters with organic molecules before deposition in order to obtain ordered arrays on a substrate [48].

B. Nanostructured materials

Although my main focus in this review is the understanding of the first stages of growth, it is worth pointing out the interest of thicker nanostructured films (for a recent review of this field, see Ref. [8]). It is known [5,6,29] that the (magnetic, optical and mechanical) properties of these films can be intrinsically different from their macrocrystalline counterparts. The precise reasons for this are currently being investigated, but one can cite the presence of a significant fraction (more than 10 %) of atoms in configurations different from the bulk configuration, for example in grain boundaries [2]. It is reasonable to suppose that both dislocation generation and mobility may become significantly difficult in nanostructured films [5]. For example, recent studies of the mechanical deformation properties of nanocrystalline copper [49] have shown that high strain can be reached before the appearance of plastic deformation. A review of the effects of nanostructuration on the mechanical response of solids is given by Weertman and Averback in chapter 13 of Ref. [8]. Another interesting property of these materials is that their crystalline order is intermediate between that of the amorphous materials (first neighbor order) and of crystalline materials (long range order). It is given by

the size of the crystalline cluster, which can be tuned. For example, for random magnetic materials, by varying the size of the clusters, and consequently of the ferromagnetic domain, one can study the models of amorphous magnetic solids [50].

C. How can one deposit clusters on surfaces?

After detailing the potential interests of nanostructures, I now address the practical preparation methods by *cluster* deposition. Two main variants have been explored. Historically, the first idea has been to produce beams of *accelerated* (ionized) clusters and take advantage of the incident kinetic energy to enhance atomic mobility even at low substrate temperatures. This method does not lead in general to nanostructured materials, but to films similar to those obtained by atomic deposition, with sometimes better properties. A more recent approach is to deposit neutral clusters, with *low energy* to preserve their peculiar properties when they reach the surface. The limit between the two methods is roughly at a kinetic energy of 0.1 to 1 eV/atom.

1. Accelerated clusters

The Japanese group of Kyoto University was the first to explore the idea of depositing clusters with high kinetic energies (typically a few keV) to form thin films [51]. The basic idea of the Ionized Cluster Beam (ICB) technique is that the cluster breaks upon arrival and its kinetic energy is transferred to the adatoms which then have high lateral (i.e. parallel to the substrate) mobilities on the surface. This allows in principle to achieve epitaxy at low substrate temperatures, which is interesting to avoid diffusion at interfaces or other activated processes. Several examples of good epitaxy by ICB have been obtained by Kyoto's group : Al/Si [52] which has a large mismatch and many other couples of metals and ceramics on various crystalline substrates such as Si(100), Si(111) . . . Molecular Dynamics (MD) simulations have supported this idea of epitaxy by cluster spreading [53]. The reader is referred to Yamada's reviews [51] for an exhaustive list of ICB applications, which also includes high energy density bombardment of surfaces to achieve sputter yields significantly higher than obtained from atomic bombardment [54].

However, the physics behind these technological successes is not clear. In fact, the very presence of a significant fraction of large clusters in the beam seems dubious [55,56]. There is some experimental evidence [51] offered by Kyoto's group to support the effective presence of a significant fraction of large clusters in the beam, but the evidence is not conclusive. In short, it is difficult to make a definite judgement about the ICB technique. There is no clear proof of the presence of clusters in the beam and the high energy of the incident particles renders difficult any attempt of modelling. Kyoto's group has clearly shown that ICB does lead to good quality films in many cases but it is not clear how systematic the improvement is when compared to atomic deposition techniques.

Haberland's group in Freiburg has developed recently a different technique called Energetic Cluster Impact (ECI) where a better controlled beam of energetic clusters is deposited on surfaces [57]. Freiburg's group has shown that accelerating the clusters leads to improvements in some properties of the films : depositing slow clusters (energy per atom 0.1 eV) produces metal films which can be wiped off easily, but accelerating them before deposition (up to 10 eV per atom) results in strongly adhering films [58]. MD simulations of cluster deposition [58] have explained qualitatively this behavior : while low energetic clusters tend to pile up on the substrate leaving large cavities, energetic clusters lead to a compact film (Fig. 3). It is interesting to note that, even for the highest energies explored in the MD simulations (10 eV per atom), no atoms were ejected from the cluster upon impact. The effect of film smoothening is only due to the flattening of the cluster when it touches the substrate. Some caution on the interpretation of these simulations is needed because of the very short time scales which can be simulated (some ps). Similar MD simulations of the impact of a cluster with a surface at higher energies have also been performed [59]. Recently, Palmer's group [60] has studied the interaction of Ag clusters on graphite for various incident kinetic energies (between 15 and 1500 eV). They have shown that, for *small* (Ag_3) clusters, the probability of a cluster penetrating the substrate or not critically depends on its orientation relative to the substrate.

2. Low energy clusters

Another strategy to grow nanostructures with cluster beams consists in depositing *low energy* particles [13,19,48,61–65]. Ideally, by depositing the clusters with low kinetic energies, one would like to conserve the memory of the free cluster phase [13] to form thin films with original properties. Since the kinetic energy is of the order of 10 eV per cluster [66], i.e. a few meV per atom which is negligible compared to the binding energy of an atom in the

cluster, no fragmentation of the clusters is expected upon impact on the substrate. Fig. 3 suggests that the films are porous [58,67], which is interesting to keep one of the peculiarities of the clusters : their high surface/volume ratio which affects all the physical (structural, electronic) properties as well as the chemical reactivity (catalysis). Concerning deposition of carbon clusters, experiments [13,20] as well as simulations [68] have shown that the carbon clusters preserve their identity in the thick film. Another interesting type of nanostructured film grown by cluster deposition is the growth of cermets by combining a cluster beam with an atomic beam of the encapsulating material [69]. The point is that the size of the metallic particles is determined by the incident cluster size and the concentration by the ratio of the two fluxes. Then, these two crucial parameters can be varied independently, in contrast to the cermets grown from atomic beams and precipitation upon annealing.

Cluster beams are generated by different techniques : Multiple Expansion Cluster Source (MECS, [38]), gas-aggregation [12,13,61,70,71] ... All these techniques produce a beam of clusters with a distribution of sizes, with a dispersion of about half the mean size. For simplicity, I will always refer to this mean size. In gas-aggregation techniques, an atomic vapor obtained from a heated crucible is mixed with an inert gas (usually Ar or He) and the two are cooled by adiabatic expansion, resulting in supersaturation and cluster formation. The mean cluster size can be monitored by the different source parameters (such as the inert gas pressure) and can be measured by a time of flight mass spectrometer. For further experimental details on this technique, see Refs. [13,72]. To produce clusters of refractory materials, a different evaporation technique is needed : laser vaporization [13,72,73]. A plasma created by the impact of a laser beam focused on a rod of is thermalized by injection of a high pressure He-pulse (typically, 3-5 bars during 150 to 300 μ s), which permits the cluster growth. The mean cluster size is governed by several parameters such as the helium flow, the laser power and the delay time between the laser shot and the helium pulse. As a consequence of the pulsed laser shot, the cluster flux reaching the surface is not continuous but *chopped*. Typical values for the chopping parameters are : active portion of the period $\simeq 100\mu$ s and chopping frequency $f = 10$ Hz.

3. Other approaches

Alternatively, one can deposit accelerated clusters onto a buffer layer which acts as a "mattress" to dissipate the kinetic energy. This layer is then evaporated, which leads to cluster soft-landing onto the substrate [74,75]. The advantage of this method is that it is possible to select the mass of the ionized clusters before deposition. However, it is difficult with this technique to reach high enough deposition rates to grow films in reasonable times. Vitomirov et al [76] deposited *atoms* onto a rare-gas buffer layer : the atoms first clustered on top and within the layer which was afterwards evaporated, allowing the clusters to reach the substrate. Finally, deposition of clusters from a Scanning Tunneling Microscope (STM) tip has been shown to be possible, both theoretically [77] and experimentally [78].

III. MODELS OF PARTICLE DEPOSITION

I describe in this section simple models which allow to understand the first stages of film growth by low energy cluster deposition. These models can also be useful for understanding the growth of islands from *atomic* beams in the submonolayer regime in *simple* cases, namely (almost) perfect substrates, irreversible aggregation, etc. and they have allowed to understand and quantify many aspects of the growth : for a review of analysis of atomic deposition with this kind of models, see Refs. [28,39,79,80]. The models described below are similar to previous models of diffusing particles that aggregate, but such "cluster-cluster aggregation" (CCA) models [81] do not incorporate the possibility of continual injection of new particles via deposition, an essential ingredient for thin film growth.

Given an experimental system (substrate and cluster chemical nature), how can one predict the growth characteristics for a given set of parameters (substrate temperature, incoming flux of clusters ...)?

A first idea - the "brute-force" approach - would be to run a Molecular Dynamics (MD) simulation with ab-initio potentials for the particular system one wants to study. It should be clear that such an approach is bound to fail since the calculation time is far too large for present-day computers. Even using empirical potentials (such as Lennard-Jones, Embedded Atom or Tight-Binding) will not do because there is an intrinsically large time scale in the growth problem : the mean time needed to fill a significant fraction of the substrate with the incident particles. An estimate of this time is fixed by t_{ML} , the time needed to fill a monolayer : $t_{ML} \simeq 1/F$ where F is the particle flux expressed in monolayers per second (ML/s). Typically, the experimental values of the flux are lower than 1ML/s, leading to $t_{ML} \geq 1$ s. Therefore, there is a time span of about 13 decades between the typical vibration time (10^{-13} s, the lower time scale for the simulations) and t_{ML} , rendering hopeless any "brute-force" approach.

There is a rigorous way [82] of circumventing this time span problem : the idea is to "coarsen" the description by defining *elementary processes*, an approach somewhat reminiscent of the usual (length, energy) renormalization of particle physics [1]. One "sums up" all the short time processes (typically, atomic thermal vibrations) in effective parameters (transition rates) valid for a higher level (longer time) description. I will now briefly describe this rigorous approach and then proceed to show how it can be adapted to cluster deposition.

A. Choosing the elementary processes

Voter [82] showed that the interatomic potential for any system can be translated into a finite set of parameters, which then provides the exact dynamic evolution of the system. Recently, the same idea has been applied to Lennard-Jones potentials [83] by using only *two* parameters. The point is that these coarse-grained, lattice-gas approach needs orders of magnitude less computer power than the MD dynamics described above. One can understand the basic idea by the following simple example : for the MD description of the diffusion of an atom by hopping, one has to follow in detail its motion at the picosecond scale, where the atom mainly oscillates in the bottom of its potential well. Only rarely at this time scale will the atom jump from site to site, which is what one is interested on. Voter showed that, provided some conditions are met concerning the separation of these two time scales, and restricting the motion to a regular (discrete) lattice (see [82] for more details), one could replace this "useless" information by an effective parameter taking into account all the detailed motion of the atom within the well (including the correlations between the motions of the atom and its neighbors) and allowing a rapid evaluation of its diffusion rate.

Unfortunately, this rigorous approach is not useful for *cluster* deposition, because the number of atomic degrees of freedom (configurations) is too high. Instead, one chooses - from physical intuition - a "reasonable" set of elementary processes, whose magnitudes are used as *free parameters*. This allows to understand the role of each of these elementary processes during the growth and then to fit their value from experiments (Fig. 4). These are the models which I will study in this paper, with precise examples of parameter fit (see section VI). Examples of such fits from experimental data for *atomic* deposition include homoepitaxial growth of GaAs(001) [84], of Pt(100) [85] or several metal(100) surfaces [86]. Of course, fitting is not very reliable when there are too many (almost free) parameters. An interesting alternative are intermediate cases, where parameters are determined from known potentials but with a simplified fitting procedure taking into account what is known experimentally of the system under study : see Ref. [87] for a clear example of such a possibility.

B. Predicting the growth from the selected elementary processes

To be able to adjust the values of the elementary processes from experiments, one must first predict the growth from these processes. The oldest way is to write "rate-equations" which describe in a mean-field way the effect of these processes on the number of isolated particles moving on the substrate (called monomers) and islands of a given size. The first author to attempt such an approach for growth was Zinsmeister [88] in 1966, but the general approach is similar to the rate-equations first used by Smoluchovsky for particle aggregation [89]. In the seventies, many papers dealing with better mean-field approximations and applications of these equations to interpret experimental systems were published. The reader is referred to the classical reviews by Venables and co-workers [90,91] and Stoyanov and Kaschiev [92] for more details on this approach. More recently, there have been two interesting improvements. The first is by Villain and co-workers which have simplified enormously the mathematical treatment of the rate-equations, allowing one to understand easily the results obtained in a variety of cases [93,94]. Pimpinelli et al. have recently published a summary of the application of this simplified treatment to many practical situations using a unified approach [95]. The second improvement is due to Bales and Chrzan [96] who have developed a more sophisticated self-consistent rate-equations approach which gives better results and allows to justify many of the approximations made in the past. However, these analytical approaches are mean-field in nature and cannot reproduce all the characteristics of the growth. Two known examples are the island morphology and the island size distribution [96].

The alternative approach to predict the growth are Kinetic Monte-Carlo (KMC) simulations. KMC simulations are an extension of the usual Monte Carlo [97–99] algorithm and provide a rigorous way of calculating the dynamical evolution of a complicated system where a large but *finite* number of random processes occur at given rates. KMC simulations are useful when one chooses to deal with only the slowest degrees of freedom of a system, these variables being only weakly coupled to the fast ones, which act as a heat bath [99]. The "coarsened" description of film growth (basically, diffusion) given above is a good example [82,96,100–103], but other applications [99] of KMC simulations include interdiffusion in alloys, slow phase separations . . . The principle of KMC simulations is straightforward : one uses a list of all the possible processes together with their respective rates ν_{pro} and generates the time evolution of

the system from these processes taking into account the random character of the evolution. For the simple models of film growth described below, systems containing up to 4000 x 4000 lattice sites can be simulated in a reasonable time (a few hours), which limits the finite size effects usually observed in this kind of simulation. Let me now discuss in some detail the way KMC simulations are implemented to reproduce the growth, once a set of processes has been defined, with their respective ν_{pro} taking arbitrary values or being derived from known potentials.

There are two main points to discuss here : the physical correctness of the dynamics and the calculation speed. Concerning the first point, it should be noted that, originally [97], Monte Carlo simulations aimed at the description of the *equations of state* of a system. Then, "the MC method performs a "time" averaging of a model with (often artificial) stochastic kinetics [...] : time plays the role of a label characterizing the sequential order of states, and need not be related to the physical times" [104]. One should be cautious therefore on the precise Monte Carlo scheme used for the simulation when attempting at describing the kinetics of a system, as in KMC simulations. For example, there are doubts [105,106] about some simulation work [107,108] carried out using Kawasaki dynamics. This point is discussed in great detail in Ref. [106].

Let me address now the important problem of the calculation speed. One could naively think of choosing a time interval Δt smaller than all the relevant times in the problem, and then repeat the following procedure :

- (1) choose one particle randomly
- (2) choose randomly one of the possible processes for this particle
- (3) calculate the probability p_{pro} of this process happening during the time interval Δt ($p_{pro} = \nu_{pro}\Delta t$)
- (4) throw a random number p_r and compare it with p_{pro} : if $p_{pro} < p_r$ perform the process, if not go to the next step
- (5) increase the time by Δt and goto (1)

This procedure leads to the correct kinetic evolution of the system but might be extremely slow if there is a large range of probabilities p_{pro} for the different processes (and therefore some $p_{pro} \ll 1$). The reason is that a significant fraction of the loops leads to rejected moves, i.e. to no evolution at all of the system.

Instead, Bortz et al. [109] have proposed a clever approach to eliminate *all* the rejected moves and thus reduce dramatically the computational times. The point is to choose not the particles but the *processes*, according to their respective rate and the number of possible ways of performing this process (called Ω_{pro}). This procedure can be represented schematically as follows :

- (1) update the list of the possible ways of performing the processes Ω_{pro}
- (2) randomly select one of the process, *weighting* the probability of selection by the process rate ν_{pro} and Ω_{pro} :

$$p_{pro} = (\nu_{pro}\Omega_{pro}) / \left(\sum_{processes} \Omega_{pro}\nu_{pro} \right)$$
- (3) randomly select a particle for performing this process
- (4) move the particle
- (5) increase the time by $dt = \left(\sum_{processes} \Omega_{pro}\nu_{pro} \right)^{-1}$
- (6) goto (1)

A specific example of such a scheme for cluster deposition is given below (Section III C). Note that the new procedure implies a less intuitive increment of time, and that one has to create (and update) a list of all the Ω_{pro} constantly, but the acceleration of the calculations is worth the effort.

A serious limitation of KMC approaches is that one has to assume a finite number of local environments (to obtain a finite number of parameters) : this confines KMC approaches to regular lattices, thus preventing a rigorous consideration of elastic relaxation, stress effects . . . everything that affects not only the *number* of first or second nearest neighbors but also their precise position. Indeed, considering the precise position as in MD simulations introduces a *continuous* variable and leads to an infinite number of possible configurations or processes. Stress effects can be introduced approximately in KMC simulations, for example [110] by allowing a variation of the bonding energy of an atom to an island as a function of the island size (the stress depending on the size), but it is unclear how meaningful these approaches are (see also Refs. [111]). I should quote here a recent proposition [112] inspired on the old Frenkel-Kontorova model [113] which allows to incorporate some misfit effects in rapid simulations. It remains to explore whether such an approach could be adapted to the KMC scheme.

C. Basic elementary processes for cluster growth

What is likely to occur when clusters are deposited on a surface ? I will present here the elementary processes which will be used in cluster deposition models : deposition, diffusion and evaporation of the clusters and their interaction on the surface (Figs. 5 and 6). The influence of surface defects which could act as traps for the particles is also addressed.

A simple physical rationale for choosing only a limited set of parameters is the following (see Fig. 7). For any given system, there will be a "hierarchy" of time scales, and the relevant ones for a growth experiment are those much lower than $t_{ML} \simeq 1/F$. The others are too slow to act and can be neglected. The hierarchy of time scales (and therefore the relevant processes) depend of course on the precise system under study. It should be noted that for *cluster* deposition the situation is somewhat simpler than for atom deposition [114] since many elementary processes are very slow. For example, diffusion of clusters on top of an already formed island is very low [115], cluster detachment from the islands is insignificant and edge diffusion is not an elementary process at all since the cluster cannot move as an entity over the island edge (as I will discuss in section VII B, the equivalent process is cluster-cluster coalescence by atomic motion). Let me now discuss in detail each of the elementary processes useful for cluster deposition.

The first ingredient of the growth, *deposition*, is quantified by the flux F , i.e. the number of clusters that are deposited on the surface per unit area and unit time. The flux is usually uniform in time, but in some experimental situations it can be pulsed, i.e. change from a constant value to 0 over a given period. Chopping the flux can affect the growth of the film significantly [116], and I will take this into account when needed (Section VI B 3).

The second ingredient is the *diffusion* of the clusters which have reached the substrate. I assume that the diffusion is brownian, i.e. the particle undergoes a random walk on the substrate. To quantify the diffusion, one can use both the usual diffusion coefficient D or the diffusion time τ , i.e. the time needed by a cluster to move by one diameter. These two quantities are connected by $D = d^2/(4\tau)$ where d is the diameter of the cluster. Experiments show that the diffusion coefficient of a cluster can be surprisingly large, comparable to the atomic diffusion coefficients. The diffusion is here supposed to occur on a perfect substrate. Real surfaces always present some defects such as steps, vacancies or adsorbed chemical impurities. The presence of these defects on the surface could significantly alter the diffusion of the particles and therefore the growth of the film. I will include here one simple kind of defect, a perfect trap for the clusters which definitively prevents them from moving.

A third process which could be present in growth is *re-evaporation* of the clusters from the substrate after a time τ_e . It is useful to define $X_S = \sqrt{D\tau_e}$ the mean diffusion length on the substrate before desorption.

The last simple process I will consider is the *interaction* between the clusters. The simplest case is when aggregation is irreversible and particles simply remain juxtaposed upon contact. This occurs at low temperatures. At higher temperatures, cluster-cluster coalescence will be active (Fig. 6). Thermodynamics teaches us that coalescence should always happen but without specifying the kinetics. Since many clusters are deposited on the surface per unit time, kinetics is here crucial to determine the shape of the islands formed on the substrate. A total comprehension of the kinetics is still lacking, for reasons that I will discuss later (Section VII B). I note that the shape of the clusters and the islands on the surface need not be perfectly spherical, even in the case of total coalescence. Their interaction with the substrate can lead to half spheres or even flatter shapes depending on the contact angle. Contrary to what happens for atomic deposition, a cluster touching an island forms a huge number of atom-atom bonds and will not detach from it. Thus, models including *reversible* particle-particle aggregation [21] are not useful for cluster deposition.

The specific procedure to perform a rapid KMC simulation of a system (linear size L) when deposition, diffusion and evaporation of the monomers are included is the following. The processes are : deposition of a particle ($\nu_{depo} = F$, $\Omega_{depo} = L^2$ (it is possible to deposit a particle on each site of the lattice)), diffusion of a monomer ($\nu_{diff} = 1/\tau$, $\Omega_{diff} = \rho L^2$ where ρ is the monomer density on the surface) and evaporation of a monomer ($\nu_{evap} = 1/\tau_e$, $\Omega_{evap} = \rho L^2$). For each loop, one calculates two quantities $p_{drop} = F/(F + \rho(\frac{1}{\tau_e} + \frac{1}{\tau}))$ and $p_{dif} = (\rho/\tau)/(F + \rho(\frac{1}{\tau_e} + \frac{1}{\tau}))$. Then, one throws a random number p ($0 < p < 1$) and compare it to p_{drop} and p_{dif} . If $p < p_{drop}$, a particle is deposited in a random position; if $p > p_{drop} + p_{dif}$, a monomer (randomly selected) is removed, otherwise we just move a randomly chosen monomer. After each of these possibilities, one checks whether an aggregation has taken place (which modifies the number of monomers on the surface, and therefore the number of possible diffusion or evaporation moves), increase the time by $dt = 1/(FL^2 + \rho L^2(\frac{1}{\tau_e} + \frac{1}{\tau}))$ and go to the next loop.

The usual game for theoreticians is to combine these elementary processes and predict the growth of the film. However, experimentalists are interested in the reverse strategy : from (a set of) experimental results, they wish to understand which elementary processes are actually present in their growth experiments and what are the magnitudes of each of them, what physicists call understanding a phenomenon. The problem, of course, is that with so many processes, many combinations will reproduce the same experiments (see specific examples below). Then, some clever guesses are needed to first identify which processes are present. For example, if the saturation island density does not change when flux (or substrate temperature) is changed, one can guess that nucleation is mostly occurring on defects of the surface.

In view of these difficulties, next section is devoted to predict the growth when the microscopic processes (and their values) are known. After, in Section V, I propose a detailed procedure to identify and quantify the microscopic process from the experiments. Finally, Section VI reviews the experimental results obtained for cluster deposition.

IV. PREDICTING GROWTH WITH COMPUTER SIMULATIONS

The scope of this section is to find formulas or graphs to deduce the values of the microscopic processes (diffusion, evaporation ...) from the observed experimental quantities (island density, island size histograms ...). The "classical" studies [90–92] have focused on the evolution of the concentration of islands on the surface as a function of time, and especially on the saturation island density, i.e. the maximum of the island density observed before reaching a continuous film. The reason is of course the double possibility to calculate it from rate-equations and to measure it experimentally by conventional microscopy. I will show other interesting quantities such as island size distributions which are measurable experimentally and have been recently calculated by computer simulations [117–122].

I will study the two limiting cases of pure juxtaposition and total coalescence (which are similar to two and three dimensional growth in atomic deposition terminology) separately. Experimentally, the distinction between the two cases can be made by looking at the shape of the supported islands : if they are circular (and larger than the incident clusters) they have been formed by total coalescence; if ramified by pure juxtaposition (see several examples below, section VI).

In both cases, I analyze how the growth proceeds when different processes are at work : diffusion, evaporation, defects acting as traps, island mobility ... In the simulations, I often take the diffusion time τ to be the unit time : in this case, the flux is equivalent to the normalized flux ϕ (see the Table) and the evaporation time corresponds to τ_e/τ . The growth is characterized by the kinetics of island formation, the value of the island concentration at saturation N_{sat} (i.e. the maximum value reached before island-island coalescence becomes important) and the corresponding values of the thickness e_{sat} and condensation coefficient C_{sat} , useful when evaporation is important (the condensation coefficient is the ratio of matter actually present on the substrate over the the total number of particles sent on the surface (also called the thickness $e = Ft$), see Table I).

I also give the island size distributions corresponding to each growth hypothesis. These have proven useful as a tool for experimentalists to distinguish between different growth mechanisms [115,121,122]. By *size* of an island, I mean the surface it occupies on the substrate. For "two dimensional" islands (i.e. formed by pure juxtaposition), this is the same as the island mass, i.e. its number of monomers. For "three dimensional" islands (formed by total coalescence), their projected surface is the easiest quantity to measure by microscopy. It should be noted that for three dimensional islands, their projected surface for a given mass depends on their shape, which is assumed here to be pyramidal (close to a half-sphere). It has been shown [86,101] that by normalizing the size histograms, one obtains a "universal" size distribution independent of the coverage, the flux or the substrate temperature for a large range of their values.

A. Pure juxtaposition : growth of one cluster thick islands

I first study the formation of the islands in the limiting case of pure juxtaposition. This is done for several growth hypothesis. The rate-equations treatment is given in Appendix A.

1. Complete condensation

Let me start with the simplest case where only diffusion takes place on a perfect substrate (no evaporation). Fig 8a shows the evolution of the monomer (i.e. isolated clusters) and island densities as a function of deposition time.

We see that the monomer density rapidly grows, leading to a rapid increase of island density by monomer-monomer encounter on the surface. This goes on until the islands occupy a small fraction of the surface, roughly 0.1% (Fig. 9a). Then, islands capture efficiently the monomers, whose density decreases. As a consequence, it becomes less probable to create more islands, and their number increases more slowly. When the coverage reaches a value close to 15% (Fig. 9b), coalescence will start to decrease the number of islands. The maximum number of islands at saturation N_{sat} is thus reached for coverages around 15%. Concerning the dependence of N_{sat} as a function of the model parameters, it has been shown that the maximum number of islands per unit area formed on the surface scales as $N_{sat} \simeq (F/D)^{1/3}$ [90,92]. Recent simulations [96,115] and theoretical analysis [93] have shown that the precise relation is $N_{sat} = 0.53(F\tau)^{0.36}$ for the *ramified* islands produced by pure juxtaposition (Fig. 10).

It should be noted that if cluster diffusion is vanishingly small, the above relation does not hold : instead, film growth proceeds as in the percolation model [123], by random paving of the substrate. An experimental example of such a situation has been given in Ref. [124].

2. Evaporation

What happens when evaporation is also included ? Fig 8b shows that now the monomer density becomes roughly a *constant*, since it is now mainly determined by the balancing of deposition and evaporation. As expected, the constant concentration equals $F\tau_e$ (solid line). Then the number of islands increases linearly with time (the island creation rate is roughly proportional to the square monomer concentration, see Appendix A). One can also notice that only a small fraction (1/100) of the monomers do effectively remain on the substrate, as shown by the low condensation coefficient value at early times. This can be understood by noting that the islands grow by capturing only the monomers that are deposited within their "capture zone" (comprised between two circles of radius R and $R + X_S$). The other monomers evaporate before reaching the islands. When the islands occupy a significant fraction of the surface, they capture rapidly the monomers. This has two effects : the monomer density starts to decrease, and the condensation coefficient starts to increase. Shortly after, the island density saturates and starts to decrease because of island-island coalescence. Fig. 10 shows the evolution of the maximum island density in the presence of evaporation. A detailed analysis of the effect of monomer evaporation on the growth is given in Ref. [117], where is also discussed the regime of "direct impingement" which arises when $X_S \leq 1$: islands are formed by *direct impingement* of incident clusters as first neighbors of previously adsorbed clusters, and grow by direct impingement of clusters on the island boundary. A summary of the results obtained in the various regimes spanned as the evaporation time τ_e decreases is given in Appendix A.

3. Defects

I briefly treat now the influence of a very simple kind of defect : a perfect trap for the diffusing particles. If a particle enters such a defect site, it becomes trapped at this site forever. If such defects are present on the surface [125] they will affect the growth of the film only if their number is higher than the number of islands that would have been created without defects (for the same values of the parameters). If this is indeed the case, monomers will be trapped by the defects at the very beginning of the growth and the number of islands equates the number of defects, whatever the diffusivity of the particles. The kinetics of island formation is dramatically affected by the presence of defects, the saturation density being reached almost immediately (Fig. 11).

4. Island mobility

The consequences of the mobility of small islands have not received much attention. One reason is that it is difficult to include island mobility in rate equations treatments. A different (though related!) reason is that (atomic) islands are expected to be almost immobile in most homoepitaxial systems. However, several studies have shown the following consequences of island mobility for the pure juxtaposition case and in the absence of evaporation. First, the saturation island density is changed [93,102,126–128] : one obtains $N_{sat} = 0.3(F/D)^{.42}$ (Fig. 10) if all islands are mobile, with a mobility inversely proportional to their size [102]. Second, the saturation island density is reached for very low coverages (Fig. 11 and Ref. [102]). This can be explained by a dynamical equilibrium between island formation and coalescence taking place at low coverages thanks to island diffusion. If only monomers are able to move, islands can coalesce (static coalescence) only when the coverage is high enough (roughly 10-15%, [93,117]). Then, the saturation island density is reached in this case for those coverages. Instead, when islands can move, the so called dynamical coalescence starts from the beginning of the growth and the balance is established at very low coverages [102]. Third, the island size distribution is sharpened by the mobility of the islands [118,120,127,128]. To my knowledge, there is no prediction concerning the growth of films with evaporation when islands are mobile.

5. Island size distributions

Fig 12 shows the evolution of the *rescaled* [101,121] island size distributions as a function of the evaporation time for islands formed by juxtaposition [117]. Size distributions are normalized by the mean island size in the following way : one defines $p(s/s_m) = n_s/N_t$ as the probability that a randomly chosen island has a surface s when the average surface per island is $s_m = \theta/N_t$, where n_s stands for the number of islands of surface s , N_t is the total number of islands and θ for the coverage of the surface. It is clear that the distributions are significantly affected by the evaporation, smaller islands becoming more numerous when evaporation increases. This trend can be qualitatively understood by noting that new islands are created continuously when evaporation is present, while nucleation rapidly becomes negligible

in the complete condensation regime. The reason is that islands are created (spatially) homogeneously in the last case, because the positions of the islands are correlated (through monomer diffusion), leaving virtually no room for further nucleation once a small portion of the surface is covered ($\theta \sim 0.05$). In the limit of strong evaporation, islands are nucleated randomly on the surface, the fluctuations leaving large regions of the surface uncovered. These large regions can host new islands even for relatively large coverages, which explains that there is a large proportion of small ($s < s_m$) islands in this regime.

B. Total coalescence : growth of three dimensional islands

If clusters coalesce when touching, the results are slightly different from those given in the preceding section, mainly because the islands occupy a smaller portion of the substrate at a given thickness. Therefore, in the case of complete condensation for example, saturation arises at a higher thickness (Fig. 11) even if the *coverage* is approximately the same (matter is "wasted" in the dimension perpendicular to the substrate). However, the main qualitative characteristics of the growth correspond to those detailed in the preceding section. Fig. 13 shows the evolution of the maximum island density in that case, where the three-dimensional islands are assumed to be roughly half spheres (actually, pyramids were used in these simulations which were originally intended for atomic deposition [129]). The analytical results obtained from a rate-equations treatment are given in Appendix B. If the islands are more spherical (i.e. the contact angle is higher), a simple way to adapt these results on the kinetic evolution of island concentration (Fig. 11) is to multiply the thickness by the appropriate form factor, 2 for a sphere for example. Indeed, if islands are spherical, the same coverage is obtained for a thickness double than that obtained for the case of half-spheres (there are two identical half spheres). This is a slight approximation since one has to assume that the capture cross section (which governs the growth) is identical for the two shapes : this is not exactly true [117] but is a very good approximation.

Fig. 14 shows the evolution of the *rescaled* island size distributions for three dimensional islands (pyramids) in presence of evaporation. I recall that size means here the projected surface of the island, a quantity which can be measured easily by electron microscopy. We note the same trends as for the pure juxtaposition case.

Fig. 15 shows the evolution of the *rescaled* island size distributions for pyramidal islands nucleating *on defects*. Two main differences can be noted. First, the histograms are significantly narrower than in the preceding case, as had already been noted in experimental studies [130]. This can be understood by noting that all islands are nucleated at almost the same time (at the very beginning of growth). The second point is that the size distributions are sensitive to the actual coverage of the substrate, in contrast with previous cases. In other words, there is no perfect rescaling of the data obtained at different coverages, even if rescaling for different fluxes or diffusion times has been checked.

C. Other growth situations

I briefly address in this paragraph other processes which have not been analyzed here. A possible (but difficult to study) process is a long range interaction between particles (electrostatical or through the substrate). There is some experimental evidence of this kind of interaction for the system Au/KCl(100) [131] but to my knowledge, it has never been incorporated in growth models. Chemical impurities adsorbed on the substrate can change the growth in conventional vacuum, and these effects are extremely difficult to understand and control [132]. Of course, many other possible processes have not been addressed in this review, such as the influence of strain, of extended defects as steps or vacancy islands ...

V. HOW TO ANALYZE EXPERIMENTAL DATA

Figures 10, 13 constitute in some sense "abacuses" from which one can determine the value of the microscopic parameters (diffusion, evaporation) if the saturation island density is known. The problem is : does the measured island density correspond to the defect concentration of the surface or to homogeneous nucleation? If the latter is true : which curve should be used to interpret the data? In other words, is evaporation present in the experiments

and what is the magnitude of τ_e ? I will now give some tricks to first find out which processes are relevant and then how they can be quantified.

Let's concentrate first on the presence of defects. One possibility is to look at the evolution of N_{sat} with the flux. As already explained, if this leaves unaffected the saturation density, nucleation is occurring on defects. A similar test can be performed by changing the substrate temperature, but there is the nagging possibility that this changes the defect concentration on the surface. It is also possible to study the kinetics of island nucleation, i.e. look at the island concentration as a function of thickness or coverage. The presence of defects can be detected by the fact that the maximum island density is reached at very low coverages (typically less than 1%, see Fig. 11) and/or by the fact that the nucleation rate (i.e. the derivative of the island density) scales as the flux and not as the square flux : see Section 3 of Ref. [92] for more details. One should be careful however to check that all the islands, even those containing a few particles, are visible in the microscope images. This is a delicate point for atomic deposition [133] but should be less restrictive for clusters since each cluster has already a diameter typically larger than a nanometer. Of course all this discussion assumes that the defects are of the "ideal" kind studied here, i.e. perfect traps. If atoms can escape from the defects after some time, the situation is changed but I am unaware of studies on this question.

The question of evaporation is more delicate. First, one should check whether particle reevaporation is important. In principle, this can be done by measuring the condensation coefficient, i.e. the amount of matter present on the surface as a function of the amount of matter brought by the beam. If possible, this measure leaves no ambiguity. Otherwise, the kinetics of island creation is helpful. If the saturation is reached at low thicknesses ($e_{sat} \leq .5 ML$), this means that evaporation is not important. Another way of detecting particle evaporation is by studying the evolution of the saturation island density with the flux : in the case of 2D growth (Fig. 10), the exponent is 0.36 when evaporation is negligible but roughly 0.66 when evaporation significantly affects the growth [117]. There are similar differences for 3d islands : the exponent changes from 0.29 to 0.66 [134] (Fig. 13). Suppose now that one finds that evaporation is indeed important : before being able to use Fig. 10 or Fig. 13, one has to know the precise value of τ_e . One way to find out is to make a precise fit of the kinetic evolution of the island density or the condensation coefficient (see Section VIB2 for an example). In next paragraph, I show how to find τ_e if one knows only the *saturation* values of the island density and the thickness.

As a summary, here is a possible experimental strategy to analyze the growth. First, get a series of micrographs of submonolayer films as a function of the thickness. The distinction between the pure juxtaposition and total coalescence cases can be easily made by comparing the size of the supported islands to the (supposedly known) size of the incident clusters. Also, if the islands are spherical, this means that coalescence has taken place, if they are ramified that clusters only juxtapose upon contact. Of course, all the intermediate cases are possible (see the case of gold clusters below). One can calculate the ratio of deposited thickness over the coverage : if this ratio is close to 1, islands are flat (i.e. one cluster thick), otherwise three dimensional (unless there is evaporation).

From these micrographs, it is possible to measure the island density as a function of the thickness. Fig. 11 should be now helpful to distinguish between the different growth mechanisms. For example, if the saturation island density is obtained for large thicknesses (typically more than 1ML), then evaporation is certainly relevant and trying to measure the condensation coefficient is important to confirm this point. It is clear from Figs. 10, 13 that the knowledge of N_{sat} alone cannot determine τ_e since many values of τ and τ_e can lead to the same N_{sat} . In the 2D case, the values of the microscopic parameters can be obtained by noting that the higher the evaporation rate, the higher the amount of matter "wasted" for film growth (i.e. re-evaporated). One therefore expects that the smaller τ_e , the higher e_{sat} , which is confirmed by Fig. 16a. Therefore, from the (known) value of e_{sat} , one can determine the value of the evaporation parameter $\eta = F\tau X_S^6$ (Fig. 16a). Once η is known, X_S is determined from Fig. 16b since N_{sat} is known. $F\tau$ can afterwards be determined (from X_S and η). This is only valid for $X_S \gg 1$ [117], a condition always fulfilled in experiments.

The 3d case is more difficult since the same strategy (measuring N_{sat} and e_{sat}) fails. The reason is that in the limit of high evaporation, e_{sat} goes as $e_{sat} \sim N_{sat}^{-1/2}$, thus bringing no independent information on the parameters [134]. The same is true for the condensation coefficient at saturation C_{sat} , which is a *constant*, i.e. independent of the value of τ_e or the normalized flux (see Fig. 17b). This counterintuitive result (one would think that the higher the evaporation rate, the smaller the condensation coefficient at saturation) can be understood by noting that *in this limit*, islands only grow by direct impingement of particles within them [134] and therefore X_S (or τ_e) has no effect on the growth. Fortunately, in many experimental situations, the limit of high evaporation is not reached and one "benefits" from (mathematical) crossover regimes where these quantities do depend on the precise values of τ_e . Figs. 17 give the evolutions of C_{sat} and e_{sat} as a function of N_{sat} for different values of τ_e and F . Then, knowing e_{sat} and N_{sat} leads to an estimation of τ_e from Fig. 17a which can be confirmed with Fig. 17b provided C_{sat} is known.

To conclude, let me note that a saturation thickness much smaller than 1ML can also be attributed to island

mobility. This is a subtle process and it is difficult to obtain any information on its importance. We note that interpreting data as not affected by island diffusion when it is actually present leads to errors on diffusion coefficients of one order of magnitude or more depending on the value of $F\tau$ (see Fig. 10). Finally, one should be careful in interpreting the N_t vs. thickness curves since most observations are not made in real time (as in the computer simulations) and there can be post-deposition evolutions (see for example Ref. [135] for such complications in the case of atomic deposition).

VI. EXPERIMENTAL RESULTS

I review in this section the experimental results obtained these last years for low-energy cluster deposition, mainly in the submonolayer regime. The scope is double : first, I want to give some examples on how to analyze experiments (as indicated in Section V) and second, I will show that from a comparison of experiments and models one can deduce important physical quantities characterizing the interaction of a cluster with a surface (cluster diffusivity) and with another cluster (coalescence). The following can be read with profit by those interested only in atomic deposition as examples of interpretation since these elementary processes are relevant for some cases of atomic deposition. One should be careful that some mechanisms which are specific to atomic deposition (transient mobility, funnelling, ...) are not discussed here (see [136]). Also, growth without cluster diffusion has to be interpreted in the framework of the percolation model as indicated above [124].

Before analyzing experimental data, it is important to know how to make the connection between the units used in the programs and the experimental ones (see also Table I). In the program, the unit length is the diameter of a cluster. In the experiments, it is therefore convenient to use as a surface unit the *site*, which is the projected surface of a cluster $\pi d^2/4$ where d is the mean *incident* cluster diameter. The flux is then expressed as the number of clusters reaching the surface per second per site (which is the same as ML/s) and the island density is given per site. The thickness is usually computed in cluster monolayers (ML), obtained by multiplying the flux by the deposition time. The coverage - the ratio of the area covered by the supported islands over the total area - has to be measured on the micrographs.

A. A simple case : Sb_{2300} clusters on graphite HOPG

I start with the case of antimony clusters containing 2300 (± 600) atoms deposited on graphite HOPG since here the growth has been thoroughly investigated [115]. I first briefly present the experimental procedure and then the results and their interpretation in terms of elementary processes.

1. Experimental procedure

As suggested in the preceding Section, various samples are prepared for several film thicknesses, incident fluxes and the substrate temperatures. For films grown on Highly Oriented Pyrolytic Graphite (HOPG), before deposition at room temperature, freshly cleaved graphite samples are annealed at 500°C during 5 hours in the deposition chamber (where the pressure is $\simeq 10^{-7}$ Torr) in order to clean the surface. The main advantage of HOPG graphite conveniently annealed is that its surfaces consist mainly of defect-free large terraces ($\simeq 1\mu m$) between steps. It is also relatively easy to observe these surfaces by electron or tunneling microscopy [115]. Therefore, deposition on graphite HOPG is a good choice to illustrate the interplay between the different elementary processes which combine to lead to the growth. After transfer in air, the films are observed by Transmission Electron Microscopy (TEM) (with JEOL 200CX or TOP CON electron microscopes operating at 100 kV in order to improve the contrast of the micrographs).

2. Results

Fig. 18a shows a general view of the morphology of the antimony submonolayer film for $e = 0.14$ ML and $T_s = 353K$. A detailed analysis [115] of this kind of micrographs shows that the ramified islands are formed by the juxtaposition of particles which have the same size distribution as the free clusters of the beam. From this, we can infer two important results. First, clusters do not fragment upon landing on the substrate as indicated in the introduction. Second, antimony clusters remain juxtaposed upon contact and do not coalesce to form larger particles (option (a) of Fig. 6).

From a qualitative point of view, Fig. 18a also shows that the clusters are able to *move* on the surface. Indeed, since the free clusters are deposited at random positions on the substrate, it is clear that, in order to explain the aggregation of the clusters in those ramified islands, one has to admit that the clusters move on the surface. How can this motion be quantified? Can we admit that diffusion and pure juxtaposition are the only important physical phenomena at work here?

Fig. 19a shows the evolution of the island density as a function of the deposited thickness. We see that the saturation island density N_{sat} is reached for $e \simeq 0.15ML$. This indicates that evaporation or island diffusion are not important in this case. Therefore, we guess that the growth should be described by a simple combination of deposition, diffusion of the incident clusters and juxtaposition. This has been confirmed in several ways. I only give three different confirmations, directing the reader to Ref. [115] for further details. First, a comparison of the experimental morphology and that predicted by models including only deposition, diffusion and pure juxtaposition shows a very good agreement (Fig. 18b). Second, Fig. 19b shows that the saturation island density accurately follows the prediction of the model when the flux is varied. I recall that if the islands were nucleated on defects of the surface, the density would not be significantly affected by the flux.

Having carefully checked that the experiments are well described by the simple DDA model, I can confidently use Fig. 10 to quantify the diffusion of the clusters. As detailed in Ref. [115], one first measures the saturation island density for different substrate temperatures. The normalized fluxes ($F\tau$) are obtained from Fig. 10. Knowing the experimental fluxes, one can derive the diffusion times and coefficients. The result is a surprisingly high mobility of Sb_{2300} on graphite, with diffusion coefficients of the same order of magnitude as the atomic ones, i.e. $10^{-8}cm^2s^{-1}$ (Fig. 19c).

The magnitude of the diffusion coefficient is so high that we wondered whether there was any problem in the interpretation of the data, in despite of the very good agreement between experiments and growth models described above. For example, one could think of a linear diffusion of the incoming clusters, induced by the incident kinetic energy of the cluster in the beam (the cluster could "slide" on the graphite surface). This seems unrealistic for two reasons : first, in order to explain the low island density obtained in the experiments (see above), it should be assumed that the cluster, which has a low kinetic energy (less than 10 eV), can travel at least several thousand nanometers before being stopped by friction with the substrate. This would imply that the diffusion is just barely influenced by the substrate, which only slows down the cluster. In this case, it is difficult to explain the large changes observed in the island density when the substrate temperature varies. Second, we have deposited antimony clusters on a graphite substrate tilted to 30° from its usual position (i.e. perpendicular to the beam axis). Then, a linear diffusion of the antimony clusters arising from their incident kinetic energy would lead to anisotropic islands (they would grow differently in the direction of tilt and its perpendicular). Experiments [115] show that there is no difference between usual and tilted deposits. Therefore we can confidently believe that Sb_{2300} clusters perform a very rapid Brownian motion on graphite surfaces. A similar study has been carried out for Sb_{250} on graphite, showing the same order of magnitude for the mobility of the clusters [115]. The microscopic mechanisms that could explain such a motion will be presented in section VII.

B. Other experiments

In this subsection, I try to analyze data obtained in previous studies [62,137]. I provide *possible* (i.e. not in contradiction with any of the data) explanations, with the respective values of the microscopic processes. I stress that the scope here is not to make precise fits of the data, but rather to identify the microscopic processes at work and obtain good guesses about their respective values.

1. Slightly accelerated Ag_{160} clusters on HOPG

Palmer's group [62] has investigated the growth of films by Ag_{160} cluster deposition. Fig. 20 shows the ramified morphology of a submonolayer deposit. Although no precise fit is possible given the limited experimental data, the island density and size shows that Ag_{160} clusters are mobile on HOPG.

2. Sb_{36} on a-C

Small antimony clusters are able to move on amorphous carbon, as demonstrated by Figs. 21, and by the fact that the films are dramatically affected by changing the incident flux [137].

Fig. 21a shows that these small clusters gather in large islands and coalesce upon contact. The island density is shown in Fig. 21b. The maximum is reached for a very high thickness ($e \simeq 1.8\text{ML}$), which can only be explained by supposing that there is significant reevaporation of Sb_{36} clusters from the surface. Evaporation of small antimony clusters (Sb_n with $n \leq 100$) from a-C substrates has also been suggested by other authors [19]. A fit, using $\tau_e = 20$ deduced from Fig. 17a gives, with $F\tau = 10^{-5}$ for $F = 6 \cdot 10^{-3}$ clusters $\text{site}^{-1}\text{s}^{-1}$, leading to $\tau \sim 2 \cdot 10^{-3}\text{s}$, $D = 2 \cdot 10^{-12}\text{cm}^2/\text{s}$, $\tau_e = .04\text{s}$ and $X_S \sim 6 \text{ nm}$ before evaporation, and a condensation coefficient of .2 when the maximum island density is reached. However, some authors have argued [18] that the condensation coefficient is not so low. It is interesting to try a different fit of the data – in better agreement with this indication – to give an idea of the uncertainties of the fits. For this, I assume that the deposited islands are spherical (solid line of Fig. 21b) by the procedure described in Section IV. Here I have taken $F\tau = 3 \cdot 10^{-6}$ for $F = 6 \cdot 10^{-3}$ clusters $\text{site}^{-1}\text{s}^{-1}$, leading to $\tau \sim 5 \cdot 10^{-4}\text{s}$, $\tau_e = .04\text{s}$ corresponding to $D = 8 \cdot 10^{-12}\text{cm}^2/\text{s}$, and $X_S \sim 11 \text{ nm}$ before evaporation, and a condensation coefficient of .5 when the maximum island density is reached. Note that the condensation coefficient is, as expected, higher than in the previous fit and that the agreement with the experimental island densities for the lowest thicknesses is better. Comparing the two fits, it can be seen that the difference in the diffusion coefficient is a factor of 4, and a factor 2 in the X_S . This means that the orders of magnitude of the values for the microscopic mechanisms can be trusted despite lack of comprehensive experimental investigation.

Similar studies [188] have allowed to obtain the diffusion and evaporation characteristic times for other clusters deposited on amorphous carbon. For Bi_{90} , one finds $D \sim 3 \cdot 10^{-13}\text{cm}^2\text{s}^{-1}$ and $X_S \sim 8 \text{ nm}$ and for In_{100} : $D \simeq 4 \cdot 10^{-15}\text{cm}^2\text{s}^{-1}$ and strong coalescence (the incident clusters are liquid).

3. Au_{250} on graphite

Fig. 22 shows the morphology of a gold submonolayer film obtained by deposition of Au_{250} (± 100) clusters prepared by a laser source on graphite in a UHV chamber for different substrate temperatures.

The structures are strikingly similar to those obtained in the Sb_{2300} case : large, ramified islands. We can conclude that Au_{250} clusters do move on graphite, and that they do not completely coalesce. A more careful examination of the island morphology indicates that the size of the branches is not the same as the size of the incident clusters, as was the case for Sb_{2300} . Here the branches are larger, meaning that there is a partial coalescence, limited by the *kinetics* of the growth. This is a very interesting experimental test for coalescence models that are presented later. I first try to estimate the diffusion coefficient of the gold clusters. We have to be careful here because the incident flux is *chopped* with the laser frequency, roughly 10Hz. The active portion of the period (i.e. when the flux is "on") is $\simeq 100\mu\text{s}$.

An analysis of the growth in presence of a chopped flux has been reported elsewhere [116,138]. Fig. 23a shows the values of N_{sat} as a function of the diffusion time τ in these experimental conditions ($F_i=6 \text{ ML/s}$) for two hypothesis : only the monomers move or islands up to the pentamer move too (island mobility is supposed to be inversely proportional to its mass). Note that there is a range of diffusion times (up to two orders of magnitude) which lead to the same island saturation value, a strange situation in homogeneous nucleation : see Refs. [116,138] for details.

Given the experimental island densities, the diffusion coefficients in both hypothesis are shown in Fig. 23b. The values of the diffusion coefficient seem too high, especially in the case of exclusive monomer diffusion, but there is no experimental evidence of island mobility for the moment. I note however that since the incident clusters do significantly coalesce, it is not unreasonable to assume that the smallest islands (which are spherical as the incident clusters) can move too. We are presently carrying additional tests (on cluster reevaporation or non brownian cluster diffusion) to confirm the observation of such high diffusion coefficients.

4. Au_{250} on $NaCl$

Given the surprising high mobility of Au_{250} (± 100) on HOPG, it was worth testing gold cluster mobility on other substrates. I present here recent results obtained by depositing Au_{250} clusters on $NaCl$ [139]. The high island density (Fig. 24a) shows that gold clusters are not very mobile on this substrate, with an upper limit on the diffusion coefficient of $D \simeq 10^{-15}\text{cm}^2/\text{s}$. This is in agreement with the low mobilities observed by other authors [140] in the seventies. The diffraction pattern (Fig. 24b) is similar to that obtained in Figs. 15 c and d of Ref. [140]. The authors interpreted their results with the presence of multi-twinned Au particles with two epitaxial orientations : $Au(111)/NaCl(100)$ and $Au(100)/NaCl(100)$. This is reasonable taking into account the interatomic distances for these orientations : $d_{Au_{Au}(111)}=0.289\text{nm}$, $d_{NaCl(100)}=0.282\text{nm}$ and $d_{Au_{Au}(100)}=0.408\text{nm}$ $1/2d_{NaCl(100)}=0.398\text{nm}$ (along the face diagonal). These preliminary results suggest that epitaxy may prevent clusters from moving rapidly

on a surface, a result which has also been observed by other groups (see next section). They also show that, at least in this case, forming the clusters on the surface by atomic aggregation or depositing preformed clusters does not change the orientation nor the diffusion of the clusters on the surface. Work is in progress to determine the precise atomic structure of the clusters, their orientation on the substrate and their diffusion at higher temperatures [139].

VII. TOWARDS A PICTURE OF CLUSTER DIFFUSION AND COALESCENCE AT THE ATOMIC SCALE

In the preceding sections I have tried to analyze the growth with the help of two main ingredients : diffusion of the clusters on the surface and their interaction. I have taken the diffusion as just one number quantifying the cluster motion, without worrying about the microscopic mechanisms which could explain it. For *atomic* diffusion, these mechanisms have been extensively studied [28,136,141] and are relatively well-known. In the (simplest) case of compact (111) flat surfaces, diffusion occurs by site to site jumps over bridge sites (the transition state). Therefore, diffusion is an activated process and plotting the diffusion constant vs. the temperature yields the height of the barrier, which gives information about the microscopics of diffusion. This kind of simple interpretation is not valid for *cluster* diffusion. It is always possible to infer an "activation" energy from an Arrhenius plot (see Fig. 19c) but the meaning of this energy is not clear since the precise microscopic diffusion mechanism is unknown.

Similarly, cluster-cluster coalescence (Fig. 6) has been supposed to be total or null (i.e. pure juxtaposition) but without considering the kinetics nor the intermediate cases which can arise (see the experimental results for gold on graphite for example).

In this section, I describe some preliminary results which can shed some light on the microscopic mechanisms leading to cluster diffusion or coalescence.

A. Diffusion of the clusters

Before turning to the possible microscopic mechanisms, one must investigate whether cluster diffusion is indeed such a general phenomenon. Let me review now the available experimental data concerning the diffusion of *three-dimensional* (3D) clusters. I already presented in the previous section several examples of high cluster mobilities over surfaces. In the case of Sb_{2300} on graphite, mobilities as high as $D = 10^{-8} cm^2 s^{-1}$ are obtained at room temperature, and similar values can be inferred for Ag cluster deposition [61,62]. On a-C substrates, diffusion is not that rapid, but has to be taken into account to understand the growth. More than twenty years ago, the Marseille group [131,140,142,143] carefully studied the mobility of nanometer-size gold crystallites on ionic substrates (MgO, KCl, NaCl). By three different methods, they proved that these 3D clusters - grown by atomic deposition at room temperature - are significantly mobile at moderately high temperatures ($T \sim 350K$). The three different methods were : direct observation under the electron microscope beam [142], comparison of abrupt concentration profiles [140] or the radial distribution functions [131] before and after annealing. All these results are carefully reviewed in Ref. [143]. I will focus here on the last method [131]. Fig. 25 shows the radial distribution functions of the gold clusters obtained just after deposition (the flat curve) and after annealing (the oscillating curve) a similar deposit for a few minutes at 350K (Fig. 4 of Ref. [131]). The flat curve is a standard as-grown radial distribution function (see for example Ref. [101]). The other curve is significantly different from the first, although the cluster size distribution remains identical (Fig. 25). This shows that gold clusters move as an entity on KCl(100) at 350K, since the conservation of the size distribution rules out atomic exchange between islands (the (EC) mechanism presented below (Section VII A 1)). From the shape of the radial distribution function some features of the cluster-cluster interaction could be derived, mainly that it is a *repulsive* interaction. The detailed interaction mechanisms are not clear [131,143]. A different study [140] showed that the clusters were mobile only for a limited amount of time (several minutes), and then stopped. It turns out that clusters stop as soon as they reach epitaxial orientation on the substrate. Indeed, the gold(111) planes can orient on the KCl(100) surface, reaching a stable, minimum energy configuration (for more details on the epitaxial orientations of gold clusters on *NaCl*, see Refs. [144,145]). Therefore, 3D cluster diffusion might be quite a common phenomenon, at least when there is no epitaxy between the clusters and the substrate.

What are the possible microscopic mechanisms? Unfortunately for the field of cluster *deposition*, recent theoretical and experimental work has focused mainly on one atom thick, two-dimensional islands, whose diffusion mechanisms might be different from those of 3D islands. The focus on 2D islands is due to the technological impetus provided by applications of atomic deposition - notably MBE for which one wants to achieve flat layers. Let's briefly review the current state of the understanding of 2D island diffusion to see what inspiration we can draw for 3D cluster diffusion.

1. 2D island diffusion mechanisms

There are two main types of mechanisms proposed to account for 2D island diffusion : single adatom motion and collective (simultaneous) atom motion. It should be noted that small islands (less than ~ 15 atoms) are likely to move by specific mechanisms, depending on the details of the island geometry and atomic energy barriers [146–148]. Therefore I concentrate here on larger 2D islands.

a. Individual mechanisms The most common mechanism invoked to account for 2D island diffusion has been that of individual atomic motion. By individual I mean that the movement of the whole island can be decomposed in the motion of *uncorrelated* single atom moves. There are two main examples of such a diffusion : evaporation-condensation (EC) and periphery-diffusion (PD). Theoretical investigations on these individual mechanisms have generated much interest since it was conjectured that this diffusion constant D_{ind} is proportional to the island number of atoms (island mass) to some power which depends on the precise mechanism (EC or PD) causing island diffusion but not on temperature or the chemical nature of the system. If true, this conjecture would prove very useful, for it would allow to determine experimentally the mechanism causing island migration by measuring the exponent and some details of the atom diffusion energetics by measuring how D_{ind} depends on temperature. Unfortunately, recent studies have shown that this prediction is too simplistic, as I show now for the two different mechanisms.

(i) Periphery diffusion

Fig. 26 shows the elementary mechanism leading to island diffusion via atomic motion on the edge of the island (label PD). Assuming [105] that

- each atomic jump displaces the center of mass of the island by a distance of order $1/N$ (where N is the number of atoms of the island),
- each edge atom (density n_s) jumps with a rate $k \sim \exp(-E_{ed}/k_B T)$ where E_{ed} is the activation energy for jumping from site to site along the border and k_B is Boltzmann constant

One obtains [105] :

$$D_{ind} \sim k n_s 1/N^2 \sim \exp(-E_{ed}/k_B T) N^{-3/2} \quad (7.1)$$

if one postulates that n_s , the mean concentration of edge atoms is proportional to the perimeter of the island (i.e. to $N^{1/2}$). This equation allows in principle to determine the edge activation energy by measuring the temperature dependence of D_{ind} .

However, recent experiments [150] and Kinetic Monte-Carlo simulations [82,105,149,151] have suggested that Eq. 7.1 is wrong. First, the size exponent is not universal but depends on the precise energy barriers for atomic motion (and therefore on the chemical nature of the material) and, second, the measured activation energy does not correspond to the atomic edge diffusion energy. The point is that the limiting mechanism for island diffusion is *corner breaking*, for islands would not move over long distances simply by edge diffusion of the outer atoms [105]. Further studies are needed to fully understand and quantify the PD mechanism.

(ii) Evaporation-Condensation

An alternative route to diffusion is by exchange of atoms between the island and a 2D atomic gas. This is the usual mechanism leading to Ostwald ripening [152]. Atoms can randomly evaporate from the island and atoms belonging to the 2D gas can condensate on it (Fig. 26). This leads to fluctuations in the position of the island center of mass, which are difficult to quantify because of the possible *correlations* in the atomic evaporation and condensation. Indeed, an atom which has just evaporated from an island is likely to condensate on it again, which cannot be accounted by a mean-field theory of island-gas exchange of atoms [153]. The latter leads to a diffusion coefficient scaling as the inverse radius of the island [154], while correlations cause a slowing down of diffusion, which scales as the inverse *square* radius of the island [108,151,153].

Experimentally, Wen et al. [154] have observed by STM the movement of Ag 2D islands on Ag(100) surfaces. They measured a diffusivity almost independent of the island size, which rules out the PD mechanism and roughly agrees with their [154] calculation of the size dependence of the EC mechanism. Since this calculation has been shown to be only approximate, further theoretical and experimental work is needed to clarify the role of EC in 2D island diffusion. However, the work by Wen et al. [154] has convincingly shown that these islands move significantly and that, for

silver, island diffusion is the main route to the evolution of the island size distribution, contrary to what was usually assumed (Ostwald ripening exclusively due to atom exchange between islands, via atom diffusion on the substrate).

b. Collective diffusion mechanisms These individual mechanisms lead in general to relatively slow diffusion of the islands (of order $10^{-17} \text{cm}^2/\text{s}$ at room temperature [154]). For small clusters, different (and faster) mechanisms such as dimer shearing, involving the simultaneous displacement of a dimer, have been proposed [155]. More generally, Hamilton et al. [156] have proposed a different mechanism, also involving *collective* motions of the atoms, which leads to *fast* island motion. By collective I mean that island motion is due to a simultaneous (correlated) motion of (at least) several atoms of the island.

Specifically, Hamilton et al. [156] proposed that *dislocation* motion could cause rapid diffusion of relatively small (5 to 50 atoms) *homoepitaxial* islands on fcc(111) surfaces. Fig. 27 shows the basic idea : a row of atoms move simultaneously from fcc to hcp sites, thus allowing the motion of the dislocation and consequently of the island center of mass. Alternative possibilities suggested by Hamilton et al. for dislocation mediated island motion are the "kink" mechanism (the same atomic row moves by *sequential* but correlated atomic motion) or the "gliding" mechanism studied below, where *all* the atoms of the island move simultaneously. Molecular Dynamics simulations, together with a simple analytical approach [156] suggest that for the smallest islands ($N < 20$) the gliding mechanism is favored, for intermediate sizes ($20 < N < 100$) the dislocation motion has the lowest activation energy, while for the largest studied islands ($N > 100$) the preferential mechanism is that of "kink" dislocation motion. It is interesting to quote at this point recent direct observations of cluster motion by field ion microscopy [157]. Fig. 28 shows successive images of a compact Ir_{19} cluster moving on Ir(111). By a careful study, the authors have ruled out the individual atomic mechanisms discussed above as well as the dislocation mechanism. Instead, they suggest that gliding of the cluster as a whole is likely to explain the observed motion [157].

Hamilton later studied the case of *heteroepitaxial*, strained islands [158]. He has shown that - due to the misfit between the substrate and the island structures - there can exist islands for which introducing a dislocation does not cost too much extra energy. These metastable misfit dislocations would propagate easily within the islands, leading to "magic" island sizes with a very high mobility [158].

2. 3D island diffusion mechanisms

For the 3D clusters, the three microscopic mechanisms presented above are possible in principle. However, as noted above, the individual atom mechanisms lead to a diffusivity smaller than the diffusion of Sb_{2300} on graphite by several orders of magnitude. These mechanisms have also been ruled out for the diffusion of gold crystallites on ionic substrates [143]. Several tentative explanations based on the gliding of the cluster as a whole over the substrate have been proposed [143]. Reiss [159] showed that, for a *rigid* crystallite which is not in epitaxy on the substrate, the activation energy for rotations might be weak, simply because during a rotation, the energy needed by atoms that have to climb up a barrier is partially offset by the atoms going into more stable positions. Therefore, the barrier for island diffusion is of the same order as that for an atom, as long as the island does not reach an epitaxial orientation. Kern et al. [143,160] allowed for a partial rearrangement of the interface between the island and the substrate when there is a misfit. The interface would be composed of periodically disposed zones in registry with the substrate, surrounded with perturbed ("amorphous") zones, weakly bound to the substrate. This theory - similar in spirit to the dislocation theory proposed by Hamilton [156,158] for 2D islands - leads to reasonable predictions [143] but is difficult to test quantitatively.

To clarify the microscopic mechanisms of 3D cluster diffusion, I now present in detail Molecular Dynamics (MD) studies carried out recently [161]. These simulations aimed at clarifying the generic aspects of the question rather than modeling a particular case. Both the cluster and the substrate are made up of Lennard-Jones atoms [162], interacting through potentials of the form :

$$V(r) = 4\epsilon \left(\left(\frac{\sigma}{r} \right)^{12} - \left(\frac{\sigma}{r} \right)^6 \right).$$

Empirical potentials of this type, originally developed for the description of inert gases, are now commonly used to model generic properties of condensed systems. Lennard-Jones potentials include only pair atom-atom interaction and ensure a repulsive interaction at small atomic distances and an attractive interaction at longer distances, the distance scale being fixed by σ and the energy scale by ϵ . For a more detailed discussion of the different interatomic potentials available for MD simulations and their respective advantages and limitations, see Ref. [163]. The substrate is modeled by a single layer of atoms on a triangular lattice, attached to their equilibrium sites by weak harmonic springs that preserve surface cohesion. The Lennard-Jones parameters for cluster atoms, substrate atoms and for the interaction between the substrate and the cluster atoms are respectively $(\epsilon_{cc}, \sigma_{cc})$, $(\epsilon_{ss}, \sigma_{ss})$ and $(\epsilon_{sc}, \sigma_{sc})$. ϵ_{cc} and σ_{cc} are used as units of energy and length. ϵ_{sc} , σ_{ss} and T , the temperature of the substrate, are the control parameters of the simulation. The last two parameters are then constructed by following the standard combination rules : $\epsilon_{ss} = \sigma_{ss}^6$ and $\sigma_{sc} = \frac{1}{2}(\sigma_{cc} + \sigma_{ss})$. Finally, the unit of time is defined as $\tau = (M\sigma_{cc}^2/\epsilon_{cc})^{1/2}$, where M is the mass of the atoms which is identical for cluster and substrate atoms. The simulation uses a standard molecular dynamics technique with thermostatting of the *surface* temperature [164].

In these simulations, the clusters take the spherical cap shape of a solid droplet (Fig. 29) partially wetting the substrate. The contact angle, which can be defined following reference [165], is roughly independent of the cluster size (characterized by its number of atoms n , for $50 < n < 500$). This angle can be tuned by changing the cluster-substrate interaction. For large enough ϵ_{sc} , total wetting is observed. The results presented below have been obtained at a reduced temperature of 0.3 for which the cluster is solid. This is clearly visible in Fig. 29, where the upper and lower halves of the cluster, colored white and grey at the beginning of the run, clearly retain their identity after the cluster *center of mass* has moved over 3 lattice parameters. Hence the cluster motion appears to be controlled by *collective* motions of the cluster as a whole rather than by single atomic jumps.

The MD simulations have confirmed that one of the most important parameters for determining the cluster diffusion constant is the ratio of the cluster lattice parameter to the substrate lattice parameter. The results for the diffusion coefficient are shown in Fig. 30a. When the substrate and cluster are commensurate ($\sigma_{ss} = \sigma_{cc} \equiv 1$), the cluster can lock into a low energy epitaxial configuration. A global translation of the cluster would imply overcoming an energy barrier scaling as $n^{2/3}$, the contact area between the cluster and the substrate. In that case diffusion will be very slow, unobservable on the time scale of the MD simulations. What is interesting to note is that even small deviations from this commensurate case lead to a measurable diffusion on the time scale of the MD runs. This can be understood from the fact that the effective potential in which the center of mass moves is much weaker, as the cluster atoms, constrained to their lattice sites inside the rigid solid cluster, are unable to adjust to the substrate potential (see above, Reiss model [159]). The effect is rather spectacular : a 10% change on the lattice parameter induces an increase of the diffusion coefficient by several orders of magnitude.

Finally, I show in Fig. 30b the effect of cluster size on the diffusion constant for different lattice parameter values. As the number n of atoms in the cluster is varied between $n = 10$ and $n = 500$, the diffusion constant decreases, roughly following a power law $D \sim n^\alpha$. This power law exponent α depends significantly on the mismatch between the cluster and the substrate lattice parameters. For high mismatches ($\sigma_{ss} = 0.7, 0.8$), α is close to -0.66 . As the diffusion constant is inversely proportional to the cluster-substrate friction coefficient, this result is in agreement with a simple "surface of contact" argument yielding $D \sim n^{-2/3}$. On the other hand, when the lattice mismatch is equal to 0.9, one obtains $\alpha \approx -1.4$, although the shape of the cluster, characterized by the contact angle, does not appreciably change. It is instructive to follow the trajectory followed by the cluster center of mass (Fig. 31). In the runs with a large mismatch (Fig. 31a), this trajectory is "brownian-like", with no apparent influence of the substrate. This is consistent with the simple "surface of contact" argument. Instead, when the mismatch is small (Fig. 31b), the center of mass of the cluster follows a "hopping-like" trajectory, jumping from site to site on the honeycomb lattice defined by the substrate. When $\sigma_{ss} = \sqrt{3}/2$, there seems to be a transition between the two regimes around $n = 200$.

It is interesting to consider the interpretation of cluster motion in terms of dislocation displacement within the cluster, a mechanism which has been proposed to explain rapid 2D cluster diffusion [156,158] (see the discussion in Section VII A 1). For this, one can "freeze" the internal degrees of freedom of the cluster deposited on a thermalized substrate. The center of mass trajectory is integrated using the quaternion algorithm [161,164]. Surprisingly, the diffusion constant follows the same power law as in the free cluster case [161]. This result proves that the diffusion mechanism in this case cannot be simply explained in terms of dislocation migration within the cluster as proposed to explain the diffusion of 2D islands in [156,158]. As the substrate atoms are tethered to their lattice site, strong elastic deformations or dislocations within the lattice are also excluded. Hence, the motor for diffusion is here the vibrational motion of the substrate, and its efficiency appears to be comparable to that of the internal cluster modes.

Very recently, U. Landmann performed MD simulations of diffusion of large gold clusters on HOPG substrates [166]. He finds high cluster mobility, in agreement with the preceding simulations. His studies show that cluster diffusion in this case proceeds by two different mechanisms : long (several cluster diameters) linear "flights" separated

by relatively slow diffusive motion as observed in the preceding simulations. Further work is needed to ascertain the atomic mechanisms leading to this kind of motion.

3. Discussion

What are the (partial) conclusions which can be drawn from these studies of cluster diffusion? I think that the main parameter determining the mobility of 3D islands on a substrate is the possible epitaxy of the cluster on the substrate. Indeed, if the island reaches an epitaxial orientation, it is likely to have a mobility limited by the individual atomic movements, which give a small diffusion constant (of order $10^{-17} \text{cm}^2 \text{s}^{-1}$ at room temperature). Diffusivities of this magnitude will not affect the growth of cluster films during typical deposition times, and clusters can be considered immobile. The effect of these kind of diffusion rates can only be seen by annealing the substrates at higher temperatures or for long times. According to Hamilton [156], dislocations could propagate even for epitaxial islands, but it is likely that this mechanism is more important in the case of heteroepitaxial islands which I now proceed to discuss. Indeed, if the island is not in epitaxy on the substrate, high mobilities can be observed because the cluster sees a potential profile which is not very different from that seen by a single atom. It should be noted that this non-epitaxy can be obtained when the two lattice parameters (of the substrate and the island) are very different, or also when they are compatible if there is relative misorientation. The latter has been observed for gold on ionic substrates [143] and mobility is relatively high until the crystallites reach epitaxy. The MD simulations presented above show that, for Lennard-Jones potentials, only homoepitaxy prevents clusters from moving rapidly on a surface. It should be noted that relaxation of the cluster or the substrate - which would favor a locking of the cluster in an energetically favorable position at the expense of some elastic energy - has not been observed in these LJ simulations, nor has dislocation propagation. This is probably realistic for the low interaction energies which correspond to metal clusters on graphite. It could also be argued that dislocation motion is more difficult in 3D clusters than in 2D islands since the upper part of the particle (absent in 2D islands) tends to keep a fixed structure. Another important parameter is the cluster-substrate interaction : one can think that a large attractive interaction (for metal on metal systems for example) can induce an epitaxial orientation and prevent the cluster from diffusing, even in the heteroepitaxial case. The differences between the diffusion of clusters grown on a substrate by atom deposition and aggregation and those previously formed in a beam and deposited must also be investigated. One could anticipate that islands formed by atom aggregation *on* the substrate would accommodate easily to the substrate geometry, whereas preformed clusters might keep their (metastable) configuration. However, it is not at all clear that island nucleation and epitaxy are simultaneous phenomena, for it has been observed that islands can form in a somewhat arbitrary configuration and subsequently orient on the substrate after diffusion and rotation (see Ref. [143]).

B. Cluster-Cluster coalescence

What happens now when two clusters meet? If they remain simply juxtaposed, morphologies similar to Fig. 18a are observed. In this case, the incident clusters have retained their original morphology, and the supported particles are identical to them, even if they are in contact with many others after cluster diffusion. It is clear, by looking for example to Fig. 22 that this is not always the case. In these cases, the supported islands are clearly larger than the incident clusters : some *coalescence* has taken place. How can one understand and predict the size of the supported particles? Which are the relevant microscopic parameters? This section tries to answer these questions, which are of dramatic interest for catalysis, since the activity of the deposits crucially depends on its specific area and therefore on the sintering process (See for example Refs. [168]).

I will first briefly examine the classical theory for sphere-sphere coalescence (i.e. ignoring the effect of the substrate) and then review recent molecular dynamics simulations which suggest that this classical theory may not be entirely satisfactory for nanoparticles.

1. Continuum theory of coalescence

The standard analysis of kinetics of sintering is due to Mullins and Nichols [169,170]. The "motor" of the coalescence is the diffusion of *atoms* of the cluster (or island) surface from the regions of high curvature (where they have less neighbors and therefore are less bound) towards the regions of lower curvature. The precise equation for the atom flux is [170]

$$\vec{J}_s = -\frac{D_s \gamma \Omega \nu}{k_B T} \nabla_s \vec{K} \quad (7.2)$$

where D_s is the surface diffusion constant (supposed to be isotropic), γ the surface energy (supposed to be isotropic too), Ω the atomic volume, ν the number of atoms per unit surface area, k_B Boltzmann's constant, T the temperature and K the surface curvature ($K=1/R_1 + 1/R_2$) where R_1 and R_2 are the principal radii of curvature). For sphere-sphere coalescence, an order of magnitude estimation of the shape changes induced by this flux is [170] :

$$\frac{\partial n}{\partial t} \sim 2B \frac{\partial^2 K}{\partial s^2} (y = s = 0) \quad (7.3)$$

where dn is the outward normal distance traveled by a surface element during dt , s the arc length and $B = D_s \gamma \Omega^2 \nu / k_B T$ (the z axis is taken as the axis of revolution). For this geometry, Eq. 7.3 becomes (Fig. 32) :

$$\frac{\partial l}{\partial t} \sim \frac{B}{l^3} \left(1 - \frac{l}{R} \right) \quad (7.4)$$

where I have made an order of magnitude estimation of the second derivative of the curvature : $\partial K / \partial s \sim (K(R) - K(l)) / l$ and similarly $\partial^2 K / \partial s^2 \sim (1 - l/R) / l^3$ (see Fig. 32). Integrating Eq. 7.4 leads to

$$l \sim (r^4 + 4Bt)^{1/4} \text{ for } l \ll R \quad (7.5)$$

Eq. 7.5 gives an estimation of the coalescence kinetics for two spheres of radius r and R .

However, despite its plausibility, Eq. 7.5 has to be used with care. First, the calculation leading to it from the expression of the flux (Eq. 7.2) is only approximate. More importantly, Eq. 7.2 assumes *isotropic* surface tension and diffusion coefficients. While this approximation may be fruitful for large particles (in the μm range, [171]), it is clearly wrong for clusters in the nanometer range. These are generally faceted [172–174] as a result of anisotropic surface energies. This has two important consequences : first, since the particles are not spherical, the atoms do not feel a uniform curvature. For those located on the planar facets, the curvature is even 0, meaning that they will not tend to move away spontaneously. This effect should significantly reduce the atomic flux. Second, the diffusion is hampered by the edges between the facets [175] which induce a kind of "Schwoebel" effect [176]. Then, the effective mass transfer from one end of the cluster to the other may be significantly lower than expected from the isotropic curvatures used in Eq. 7.2. For these anisotropic surfaces, a more general formula which takes into account the dependence of γ on the crystallographic orientation should be used (see for example Ref. [94]). However, this formula is of limited practical interest for two reasons. First, the precise dependence of the surface energy on the crystallographic orientation is difficult to obtain. Second, as a system of two touching faceted clusters does not in general show any symmetry, the solution to the differential equation is hard to find. One possibility currently explored [177] is to assume a simple analytical equation for the anisotropy of 2D islands and integrate numerically the full (anisotropic) Mullins' equations.

2. Molecular Dynamics simulations of coalescence

Since continuum theories face difficulties in characterizing the evolution of nanoparticle coalescence, it might be useful to perform molecular dynamics (MD) studies of this problem. Several studies [172,178,179] have been performed, showing that two distinct and generally subsequent processes lead to coalescence for particles in the nanometer range : plastic deformation [179] and slow surface diffusion [172,178].

Zhu and Averback [179] have studied the first stages (up to 160 ps) of the coalescence of two single-crystal copper nanoparticles (diameter 4.8 nm). Fig. 33 presents four stages of the coalescence process, demonstrating that plastic deformation takes place (see the arrows indicating the sliding planes) and that a relative rotation of the particles occurs during this plastic deformation (c and d). During the first 5 ps, the deformation is elastic, until the elastic limit (roughly 0.8 nm [179]) is reached : after this, since the shear stress (Fig. 34) is very high, dislocations are formed and glide on (111) planes in the $\langle 110 \rangle$ direction, as usually seen in fcc systems. Fig. 34 also shows that after 40ps (i.e. Fig. 33c) the stress on the glide plane is much smaller and dislocation motion is less important : the two particles rotate until a low-energy grain boundary is found (Fig. 33d). This initial stage of the coalescence, where the two particles reorient and find a low-energy configuration, is very rapid, but does not lead in general to thorough coalescence. An interesting exception might have been found by Yu and Duxbury [178] : their MD simulations showed that for very small clusters (typically less than 200 atoms) coalescence is abrupt provided the temperature is sufficiently close to the melting temperature. They argue that this is due to a (not specified) "nucleation process" : plastic deformation is a tempting possibility.

For larger clusters, the subsequent stages are much slower and imply a different mechanism : atom *diffusion* on the surface of the particles. The initial stages of this diffusion-mediated coalescence have been studied by Lewis et al. [172]. The point was to study if Mullins' (continuum) predictions were useful in this size domain. In Lewis et al. simulations, the embedded-atom method (EAM) [167] was used to simulate the behavior of *unsupported* gold clusters for relatively long times (~ 10 ns). Evidently, an important role of the substrate in the actual coalescence of supported clusters is to ensure thermalization, which is taken care of here by coupling the system to a fictitious "thermostat" [180]. One therefore expects these coalescence events to be relevant to the study of supported clusters in the case where they are loosely bound to the substrate, e.g., gold clusters on a graphite substrate. Strong interaction of the clusters with the substrate may be complicated and lead to cluster deformation even for clusters deposited at low energies, for example if the cluster wets the substrate [181,182].

Fig. 35 shows the evolution of the ratio x/R , where x is the radius of the neck between the two particles. After an extremely rapid approach of the two clusters due to the mechanisms studied above (plastic deformation), a slow relaxation to the spherical shape starts (Fig. 36). The time scale for the slow sphericization process is difficult to estimate from Fig. 35, but it would appear to be of the order of a few hundred ns or more. This number is substantially larger than one would expect on the basis of phenomenological theories of the coalescence of two soft spheres. Indeed, Ref. [170] predicts a coalescence time for two identical spheres $\tau_c = k_B T R^4 / (C D_s \gamma a^4)$, where D_s is again the surface diffusion constant, a the atomic size, γ the surface energy, R the initial cluster radius, and C a numerical constant ($C = 25$ according to Ref. [170]); taking $D_s \sim 5 \cdot 10^{-10} m^2 s^{-1}$ (the average value found in the simulations, see [172]), $R = 30 \text{ \AA}$, $\gamma \approx 1 J m^{-2}$, and $a = 3 \text{ \AA}$, this yields a coalescence time τ_c of the order of 40 ns. The same theories, in addition, make definite predictions on the evolution of the shape of the system with time. In particular, in the tangent-sphere model, the evolution of the ratio x/R is found [170] to vary as $x/R \sim (t/\tau_c)^{1/6}$ for values of x/R smaller than the limiting value $2^{1/3}$. In Fig. 35, the prediction of this simple model (full line) is compared with the results of the present simulations. There is no agreement between model and simulations. The much longer coalescence time observed has been attributed [172] to the presence of facets on the initial clusters, which persist (and rearrange) during coalescence. The facets can be seen in the initial and intermediate configurations of the system in Fig. 36; the final configuration of Fig. 36 shows that the cluster is more spherical (at least from this viewpoint), and that new facets are forming. That diffusion is slow can in fact be seen from Fig. 36: even after 10 ns, at a temperature which is only about 200 degrees below melting for a cluster of this size, only very few atoms have managed to diffuse a significant distance away from the contact region.

The precise role of the facets in the coalescence process is a subject of current interest. Experiments have shown that shape evolution is very slow in presence of facets for 3D crystallites (see for example [183]) and recent experiments [184] and computer simulations [185] on 2D islands suggest that the presence of facets can be effective in slowing down the coalescence process. Clearly, more work is needed to get a *quantitative* understanding of nanoparticles coalescence, and to evaluate the usefulness of Mullins' approach, especially if one manages to include the crystalline *anisotropy* (see also Refs. [186]).

C. Island morphology

Now I can turn on to the prediction of one of the essential characteristics of cluster films : the size of the supported particles. As I have already mentioned in the introduction, the size of the nanoparticles controls many interesting properties of the films. Therefore, even an approximate result may be useful, and this is what I obtain in this section.

The experiments shown above demonstrate that the supported particles can have a variety of sizes, from that of the incident clusters (Sb_{2300} /HOPG, Section VIA) up to many times this size (for example Au_{250} /HOPG, Section VIB3). To understand how the size of the supported particles is determined, one can look at a large circular island to which clusters are arriving by diffusion on the substrate (Fig. 32). There are two antagonist effects at play here. One is given by thermodynamics, which commands that the system should try to minimize its surface (free) energy. Therefore one expects the clusters touching an island to coalesce with it, leading to compact (spherical) domains. The other process, driving the system away from this minimization is the continuous arrival of clusters on the island edge. This kinetic effect tends to form ramified islands. What is the result of this competition? Since there is a kinetically driven ramification process, it is essential to take into account the *kinetics* of cluster-cluster coalescence, as sketched in the previous section. I will use Eq. 7.5 even if it is only approximate, to derive an upper limit for the size of the compact domains grown by cluster deposition. It is an *upper* limit since, as pointed out in the previous section, coalescence for faceted particles could be *slower* than predicted by Eq. 7.5, hence diminishing the actual size of these domains.

We first need an estimate of the kinetics of the second process : the impinging of clusters on the big island. A very simple argument is used here (see also [187] for a similar analysis for atomic growth) : since the number of clusters

reaching the surface is F per unit surface per second and the total number of islands is N_t per unit surface, each island receives in average a cluster every $t_r = N_t/F$.

We are now in a position to quantify the degree of coalescence in a given growth experiment. Let me suppose that a cluster touches a large island at $t=0$. If no cluster impinges on the island before this cluster completely coalesces (in a time τ_c according to Eq. 7.5), then the islands are compact (circular). Instead, if a cluster touches the previous cluster before its total coalescence has taken place, it will almost freeze up the coalescence of the previous cluster. The reason is that now the atoms on the (formerly) outer surface of the first cluster do not feel curvature since they have neighbors on the second cluster. The mobile atoms are now those of the second cluster (see Fig. 32, label a) and the coalescence takes a longer time to proceed (the atoms are farther from the big island). Then, if $t_r \ll \tau_c$, the islands formed on the surface are ramified. For intermediate cases, the size R_c of the compact domains can be estimated from Eq. 7.5 as $R_c = x(\tilde{t}_r)$ where \tilde{t}_r takes into account the fact that, to freeze the coalescence of a previous cluster, one cluster has to touch the island at roughly the same point : $\tilde{t}_r \simeq t_r 2\pi R/r$ and

$$R_c^4 = r^4 + 4B \frac{2\pi R_c}{r} \frac{N_t}{F} \quad (7.6)$$

Eq. 7.6 describes the limiting cases ($B \sim \infty$ or $B \sim 0$) correctly. The problem with the intermediate cases is to obtain a reliable estimate of the (average) atomic surface self diffusion. For gold, Chang and Thiel [136] give values which vary between 0.02 eV on compact facets and 0.8 eV on more open surfaces. One solution is to go the other way round and estimate D_s from the experimental data and Eq. 7.6. From Fig. 22, estimating R_c from the thickness of the island arms, and using the experimental values for r (0.85 nm) and the fact that since the flux is pulsed (see Section VIB3), the time between two successive arrivals of clusters is approximately the time between two pulses (0.1 s), and not N_t/F , one obtains $D_s \simeq 3 \cdot 10^{-3} \text{cm}^2 \text{s}^{-1} \exp(-0.69 \text{eV}/(k_B T))$, which seems a sensible value.

Despite the difficulty of defining average diffusion coefficients, one can use Eq. 7.6 to obtain a reasonable guess for the size of the compact domains by assuming that D_s is thermally activated : $D_s(T) = D_0 \exp(-E_a/(k_B T))$ with a prefactor $D_0 = 10^{-3} \text{cm}^2 \text{s}^{-1}$ and an activation energy E_a taken as a fraction of the bonding energy between atoms (proportional to $k_B T_f$). One obtains [188]

$$B = 10^{11} \exp(-4.6 T_f/T) n m^4/s \quad (7.7)$$

Inserting this value in Eq. 7.6 leads to Fig. 37 where the size of the compact domains is plotted as a function of T/T_f . The important feature is that as long as $T/T_f \leq 1/4$, the incident particles do not merge. Note that this 1/4 is sensitive to the assumed value of D^* , but only via its logarithm. Again, this estimation of R_c/r is an upper limit since coalescence could be slower than predicted by Eq. 7.5.

What would happen now if the incident clusters were *liquid*? An experimental example of this liquid coalescence is given by the deposition of In_{100} on a-C (see above). A rough guess of the coalescence time is given by a hydrodynamics argument [189]: the driving force of the deformation is the surface curvature γ/R^2 where γ is the liquid surface tension and R the cluster radius. This creates a velocity field which one can estimate using the Navier-Stokes equation : $\eta \Delta v = \gamma/R^2$ where η is the viscosity and v is the velocity of the fluid. This leads to $\tau_c(\text{liquid}) \sim R/v \sim \eta R/\gamma$. Inserting reasonable values for both η (.01 Pa s) and γ (1 J m^{-2}) leads to $\tau_c(\text{liquid}) \sim 0.01 R$ which gives $\tau_c(\text{liquid}) = 10 \text{ps}$ for $R \sim 1 \text{nm}$. This is the good order of magnitude of the coalescence times found in simulations of liquid gold clusters ($\tau_c(\text{liquid}) \sim 80 \text{ps}$ [172]). Now, since $\tau_c(\text{liquid}) \ll t_r$ ($t_r \sim 0.1 \text{s}$, see above) cluster-cluster coalescence is almost instantaneous, which would lead to $R_c \sim \infty$. In fact, R_c is limited in this case by *static* coalescence between the big islands formed during the growth. The reason is that the big islands may be solid or pinned by defects leading to a slow coalescence. The analysis is similar here to what has been done for atomic deposition [190].

D. Thick films

The preceding section has studied the first stages of the growth, the submonolayer regime, which interests researchers trying to build nanostructures on the surface. I attempt here a shorter study of the growth of thick films, which are known to be very different from the bulk material in some cases [5,8,13]. The main reason for this is their nanostructuration, as a random stacking of nanometer size crystallites. Therefore, it is interesting to understand how the size of these crystallites is determined and how stable the nanostructured film is. One can anticipate that the physical mechanism for cluster size evolution is, as in the submonolayer case, sintering by atomic diffusion. For thick films however, surface diffusion can only be effective before a given cluster has been "buried" by the subsequent deposited clusters. Thus, most of the size evolution takes place during growth, for after the physical routes to

coalescence (bulk or grain boundary diffusion) are expected to be much slower. Studies of compacted nanopowders [5,192] have shown that nanoparticles are very stable against grain growth. Siegel [5] explains this phenomenon in the following way. The two factors affecting the chemical potential of the atoms, and potentially leading to structure evolutions are local differences in cluster size or in curvature. However, for the relatively uniform grain size distributions and flat grain boundaries observed for cluster assembled materials [5], these two factors are not active, and there is nothing telling locally to the atoms in which direction to migrate to reduce the global energy. Therefore, the whole structure is likely to be in a deep local (metastable) minimum in energy, as observed in closed-cell foams. The stability of such structures has been confirmed by several computer simulations [193,194] which have indicated a possible mechanism of grain growth at very high ($T/T_f \sim 0.8$) temperatures : grain boundary amorphization or melting [193].

What determines the size of the supported particles *during* the growth? For thick films, a reasonable assumption is that a cluster impinging on a surface already covered by layer of clusters does *not* diffuse, because it forms strong bonds with the layer of the deposited clusters. This hypothesis has been checked for the growth of Sb_{2300} on graphite [115]. There are two main differences with submonolayer growth : first, an impinging cluster has more than one neighbor and the sphere-sphere kinetics is not very realistic; second the relevant time for ramification I have used in the preceding section is no more useful here since clusters do not move. As a first approximation, to obtain an upper limit in the size of the domains, we can use the same coalescence kinetics and take a different "ramification" time : the average time for the arrival of a cluster touching another is roughly $t_f \sim 1/(Fd^2)$ where $d = 2r$ is the diameter of the cluster. If the same formula (Eq. 7.5) is used, one finds

$$R_c^4 = r^4 + \frac{B}{Fr^2} \quad (7.8)$$

The results obtained using the same approximation as in the preceding section for B (Eq. 7.7) are shown in Fig. 37.

Experimentally, there are observations for deposition of Ni and Co clusters [191]. The size of the crystallites is comparable to the size of the incident (free) clusters. This is compatible with Eq. 7.8 since the T_f of these elements is very high ($\simeq 1800K$). Therefore, Eq. 7.8 predicts that films grown at $T = 300K$, ($T/T_f \sim 0.17$) should keep a nanostructuration with $R_c \simeq r$, as is observed experimentally [191]. I stress again that a structure obtained with cluster deposition with this characteristic size is not likely to recrystallize in the bulk phase (thereby loosing its nanophase properties) unless brought to temperatures close to T_f [5,193,194].

VIII. CONCLUSIONS, PERSPECTIVES

What are the principal ideas presented in this paper?

First, useful models to analyze the first stages of thin film growth by cluster deposition have been presented in detail (Section III). These models are useful at a fundamental level, and I have shown in Section VI how many experimental results concerning *submonolayer* growth can be interpreted by combining these few simple processes (deposition, diffusion, evaporation . . .). Specifically, by comparing the experimental evolution of the island density as a function of the number of deposited particles to the predictions of computer simulations, one can obtain *quantitative* information about the relevant elementary processes.

Second, the quantitative information on diffusion has shown that large clusters can move rapidly on the surface, with diffusion constants comparable to the atomic ones. A first attempt to understand this high diffusivity at the atomic level is given in Section VII : the conclusion is that rapid cluster diffusion might be quite common, provided the cluster and the substrate do not find an epitaxial arrangement. Concerning cluster-cluster coalescence, it has been suggested that this process can be much slower than predicted by the usual sintering theories [170], probably because of the cluster *facets*.

Third, despite all the approximations involved in its derivation, Fig. 37 gives an important information on the morphology of the film : an *upper* limit for the ratio of the size of the compact domains over the size of the incident clusters. This helps understanding why cluster deposition leads to nanostructured films provided the deposition temperature is low compared to the fusion temperature of the material deposited ($T_s \leq T_f/4$). Clearly, further experimental and theoretical work is needed in order to confirm (or invalidate) Fig. 37.

It is clear that we still need to understand many aspects of the physics of cluster deposition. Possible investigation directions include the following, given in an arbitrary order. First, the coalescence of nanoparticles has yet to be understood and quantified. This is a basic question for both submonolayer and thick materials. Second, one has to characterize better the interactions between clusters and the substrate, and especially its influence on the cluster diffusion. It is also important to investigate the possible interactions between the clusters, which could dramatically

affect the growth. Obtaining *ordered* arrays of nanoparticles is a hot topic at this moment. A possibility is the pinning of the clusters on surface "defects" which demands a better understanding of cluster interaction with them. Another idea is to use the self-organization of some bacteria to produce an ordered array on which one could arrange the clusters (See Ref. [195], especially Chap. 5). Clearly, investigating the interaction of clusters with biological substrates is not an easy task, but it is known that practical results are not always linked to a clear understanding of the underlying mechanisms . . .

Acknowledgments : This article could never be written without all the experimental and theoretical work carried out in our group in Lyon and in collaboration with other groups. On the experimental side, the Center for the study of small clusters ("Centre pour l'étude des petits agrégats") gathers researchers from solid state physics ("Département de Physique des Matériaux", DPM), the gas phase ("Laboratoire de Spectrométrie Ionique et Moléculaire", LASIM) and catalysts ("Institut de Recherche sur la Catalyse", IRC). I therefore acknowledge all their researchers for their help, and especially those who have done part of the research presented here : Laurent Bardotti, Michel Broyer, Bernard Cabaud, Francisco J. Cadete Santos Aires, Véronique Dupuis, Alain Hoareau, Michel Pellarin, Brigitte Prével, Alain Perez, Michel Treilleux and Juliette Tuaillon. On the theoretical side, this work was carried out in collaboration with Jean-Louis Barrat, Pierre Deltour and Muriel Meunier (DPM, Lyon), my friend Hernán Larralde (Instituto de Física de Cuernavaca, Mexico), Laurent Lewis (Université de Montréal, Canada) and Alberto Pimpinelli (Université Blaise Pascal Clermont-2, France). I am happy to thank Claude Henry (CRMC2, Marseille) and Horia Metiu (University of California) for a careful reading of the manuscript, Jean-Jacques Métois (CRMC2, Marseille) for interesting discussions, Michael Moseler (Freiburg University) for sending me Fig. 3 and Simon Carroll for Fig. 20.

* e-mail address : jensen@dpm.univ-lyon1.fr

-
- [1] S. S. Schweber, *Physics Today* (November 1993) p. 34.
 - [2] H. Gleiter, *Nanostructured Materials* **1** 1 (1992)
 - [3] R. E. Palmer, *New. Sci.* **2070**, 38 (1997)
 - [4] Special issue on clusters, *Science* **271**, 920 (1996)
 - [5] R. W. Siegel, *Cluster Assembly of Nanophase Materials*, in *Materials Science and Technology* **15** 584 (1991) (R. W. Cahn, Ed. VCH, Weinheim, Germany); see also R. W. Siegel more recent contribution to Ref. [8].
 - [6] *Cluster Assembled Materials* Ed. Sattler, *Materials Science Forum* **232**, Trans Tech Publications (Zürich, Switzerland, 1996)
 - [7] J. H. Fendler (Ed.) *Nanoparticles and Nanostructured Films* (Wiley-VCH, Weinheim, Germany, 1998)
 - [8] *Nanomaterials : Synthesis, Properties and Applications*, A. S. Edelstein and R. C. Cammarata (Eds.) (IOP Publishing, Bristol, 1996)
 - [9] For a short and clear introduction to this enormous field, see for example J. R. Arthur, *Thin-Film deposition* in *Encyclopedia of Applied Physics* (Ed. G. L. Trigg, Wiley-VCH, Weinheim, Germany) **21**, 409 (1997) and references therein; For more complete information, see : R. F. Bunshah *Handbook of Deposition Technologies for Films and Coatings*, 2nd ed., Noyes (Park Ridge, NJ, USA, 1994) and D. A. Glocker, *Handbook of Thin Film Process Technology*, IOP (Philadelphia, USA, 1995)
 - [10] C. C. Koch, *Mechanical milling and alloying*, in *Materials Science and Technology* **15** 584 (1991) (R. W. Cahn, Ed. VCH, Weinheim, Germany)
 - [11] *Nanostructured Materials: Clusters, Composites and Thin Films*, ACS Symposium series **679**, V. M. Shalaev and M. Moskovits Eds. (American Chemical Society Editions, Washington DC, USA, 1997)
 - [12] C. G. Granqvist and R. A. Buhrman, *J. Appl. Phys.* **47**, 2200 (1976)
 - [13] P. Melinon et al. *Int. J. of Mod. Phys. B* **9**, 339 (1995); A. Perez et al, *J. Physics D* **30**, 709 (1997).
 - [14] W. de Heer, *Rev. Mod. Phys.* **65**, 611 (1993)
 - [15] P. Joyes, *Les agrégats inorganiques élémentaires*, Ed. de Physique (Paris, 1990)
 - [16] *Microclusters*, Springer Series in Materials Science **4**, Ed. S. Sugano, Y. Nishina and S. Ohnishi (Springer-Verlag, Berlin, 1987)
 - [17] Averback (Eds.) *Cluster and Cluster-Assembled Materials*, *MRS Proceedings* **206** (1991); *Mat. Sci. and Eng.* **A 217/218**

- (1996); Surf. Rev. Lett. **3**(1), Proceedings of ISSPIC 7 (1996); *Small Particles and Inorganic Clusters*, Proceedings of ISSPIC 8 (Copenhagen); Z. Phys. D **40** 1-574 (1997), Ed. H. H. Anderson (Springer-Verlag, Berlin)
- [18] G. Fuchs, P. Mélinon, F. Dos Santos Aires, M. Treilleux, B. Cabaud and A. Hoareau, Phys. Rev. B **44**, 3926 (1991)
- [19] C. Bréchnignac, Ph. Cahuzac, F. Carlier, M. de Frutos, A. Masson, C. Colliex, C. Mory and B. Yoon, Z. Phys. D **40**, 515 (1997); B. Yoon, Ph. D. Thesis, University of Orsay (France) (1997); C. Bréchnignac, Ph. Cahuzac, F. Carlier, C. Colliex, C. Mory, M. de Frutos, A. Masson and B. Yoon, Phys. Rev. B **57**, R2084 (1998)
- [20] V. Paillard, P. Melinon, J. P. Perez, V. Dupuis, A. Perez and B. Champagnon, Phys. Rev. Lett. **71**, 4170 (1993)
- [21] V. P. Zhdanov and P. R. Norton, Appl. Surf. Sci. **81**, 109 (1994); M. C. Bartelt, L. S. Perkins and J. W. Evans, Surf. Sci. Lett. **344**, L1193 (1995); C. Ratsch, P. Smilauer, A. Zangwill and D. D. Vvedensky, Surf. Sci. Lett. **329**, L599 (1995)
- [22] Nanostructured Materials (Pergamon Press); Physica E (Elsevier Science);
- [23] <http://www.msel.nist.gov/structure/metallurgy/techactv95/nanostruc.html> <http://nanoweb.mit.edu/http://www.eas.asu.edu/~nano/nano2.html>
- [24] Europhysics News **28**(3) 89 (1997).
- [25] Special edition of Physics Today, February 1990
- [26] Special edition of Phys. Today **46** (June 1993);
- [27] M. A. Herman and H. Sitter, *Molecular Beam Epitaxy*, Springer-Verlag (Berlin, 1989); A. Y. Cho, *Molecular Beam Epitaxy* American Institute of physics (Woodbury, NY, USA, 1994)
- [28] M. Lagally, Physics Today **46**(11), 24 (1993) and references therein.
- [29] *Nanophase Materials: Synthesis-Properties-Applications*, NATO Advanced Study Series, Series E **260** (1994) Ed. C. Hadjiapanayis and R. W. Siegel (Dordrecht: Martinus Nijhoff)
- [30] P. Jena et al. in *Cluster Assembled Materials* Ed. Sattler, Materials Science Forum **232**, Trans Tech Publications (Zürich, Switzerland, 1996) p. 1. See also P. Jena and S. N. Khanna, Mat. Sci. and Eng. **A 217/218**, 218 (1996)
- [31] R. Turton, *The quantum dot* (W. H. Freeman and Company Ltd. 1995)
- [32] A. P. Alivisatos, *Science* **271**, 933 (1996); L. Banyai and S. W. Koch, *Semiconductor Quantum Dots*, World Scientific, Singapore (1993); MRS Bulletin **23** (2) (February 1998); C. Weisbuch and B. Binter *Quantum Semiconductor Structures* (Academic Press, New York, 1991)
- [33] H.J. Freund, Angew. Chem. Int. Ed. **36**, 452 (1997) P.L.J. Gunter, J.W.H. Niemantsverdriet, T.H. Ribeiro and G.A. Somorjai, Catal. Rev.Sci. Engine. **39**, 77 (1997); C.R. Henry, C.Chapon, S.Giorgio and C.Goyhenex, in *Chemistry and Reactivity of Clusters and Thin Films*, Eds. R.M.Lambert and G. Pacchioni, NATO-ASI Series E, **331**, (Kluwer 1997), p. 117
- [34] C. R. Henry, Surf. Sci. Rep. **31**, 231 (1998)
- [35] M. Che and C.O. Bennett, Adv. Catal. **36**, 55 (1989)
- [36] G. Pacchioni and N. Roesch, Surf. Sci. **306**, 169 (1994)
- [37] P.W. Jacobs, S.J. Wind, F.H. Ribeiro and G.A. Somorjai, Surf. Sci. **372** L249 (1997)
- [38] D. M. Schaefer, A. Patil, R. P. Andres and R. Reifengerger, Phys. Rev. B **51**, 5322 (1995)
- [39] H. Brune, Surf. Sci. Rep. **31** 121 (1998)
- [40] G. Springholz, V. Holy, M. Pinczoltis and G. Bauer, *Science* **282**, 734 (1998)
- [41] D. J. Eaglesham and M. Cerullo, Phys. Rev. Lett. **64**, 1943 (1990);
- [42] For a review, see H. Ibach, Surf. Sci. Rep. **29**, 193 (1997) and MRS Bulletin **21** (2) (April 1996) D. Leonard et al., Appl. Phys. Lett. **63**, 23 (1993); J. M. Moison et al., Appl. Phys. Lett. **64**, 196 (1994); H. Brune and K. Kern, "Heteroepitaxial metal growth: the effects of strain", in Growth and Properties of ultrathin epitaxial layers, D. A. King and D. P. Woodruff Eds., The Chemical Physics of Solid Surfaces, Vol. 8 (Elsevier, Amsterdam 1997), p.149; H. Brune et al. Phys. Rev. B **52**, R14380 (1995);
- [43] J. L. Vialle et al. Rev. Sci. Instrum. **68**, 2312 (1997)
- [44] J. L. Rousset et al. J. Chem. Phys. **102**, 8574 (1995) J. L. Rousset et al. Surf. Sci. **352-354**, 583 (1996)
- [45] C. Ray et al. Phys. Rev. Lett. **80**, 5365 (1998)
- [46] T. Michely, M. Hohage, M. Bott and G. Comsa, Phys. Rev. Lett. **70**, 3943 (1993).
- [47] M. Kalff, G. Comsa, and T. Michely, Phys. Rev. Lett. **81**, 1255 (1998).
- [48] R. P. Andres et al. *Science* **273**, 1690 (1996)
- [49] J. Schiotz, T. Rasmussen, K. W. Jacobsen and O. H. Nielsen, Phil. Mag. Lett. **74**, 339 (1996)
- [50] V. Dupuis et al. J. Appl. Phys. **76** 6676 (1994)
- [51] I. Yamada and G. H. Takakoa, Jpn. J. Appl. Phys. **32**, 2121 (1993) and references therein; I. Yamada, Mat. Sci. and Eng. **A 217/218**, 82 (1996)
- [52] I. Yamada, H. Inokawa and T. Takagi, Japan. J. Appl. Phys. **56**, 2746 (1984)
- [53] R. Biswas, G. S. Grest and C. M. Soukoulis, Phys. Rev. B **38**, 8154 (1988)
- [54] Z. Insepov and I. Yamada, Nucl. Instr. and Meth. in Phys. Res. **B 99**, 248 (1995)
- [55] D. Turner and H. Shanks, J. Appl. Phys. **70**, 5385 (1991)
- [56] R.L.McEachern, W.L.Brown, M.F.Jarrold, M. Sosnowski, G. Takaoka, H. Usui and I. Yamada, J. Vac. Sci. Technol. **A9**, 3105 (1991)
- [57] H. Haberland, M. Karrais, M. Mall and Y. Thurner, J. Vac. Sci. Technol. **A 10**, 3266 (1992)

- [58] H. Haberland, Z. Insepov and M. Moseler, Phys. Rev. B **51**, 11061 (1995)
- [59] C. Massobrio and B. Nacer, Z. Phys. D **40** 526 (1997) and references therein.
- [60] S. J. Carroll, S. G. Hall, R. E. Palmer and R. Smith, Phys. Rev. Lett. **81**, 3715 (1998)
- [61] I. M. Goldby, L. Kuipers, B. von Issendorff and R. E. Palmer, Appl. Phys. Lett. **69**, 2819 (1996)
- [62] G. M. Francis, I. M. Goldby, L. Kuipers, B. von Issendorff and R. E. Palmer, J. Chem. Soc., Dalton Trans. **1** 665 (1996)
- [63] G. H. Wang, H. Q. Zhang, M. Han, J. X. Ma, Q. Wang, Phys. Lett. A **189**, 218 (1994)
- [64] J. X. Ma, M. Han, H. Q. Zhang, Y. C. Gong and G. H. Wang, Appl. Phys. Lett. **65**, 1513 (1994)
- [65] E. Ganz, K. Sattler and J. Clarke, Surf. Sci. **219**, 33 (1989); O. F. Hagen, Rev. Sci. Instrum. **63**, 2374 (1992); O. F. Hagen, G. Knop, R. Fromknecht and G. Linker, J. Vac. Sci. Technol. **A 12**, 282 (1994); A. Wawro, R. Czajka, A. Kasuya and Y. Nishina, Surf. Sci. **365**, 503 (1996);
- [66] J.F. Roux et al. Appl. Phys. Lett. **64**, 1212 (1994)
- [67] C. L. Kelchner and A. E. De Pisto, Nanostructured Materials **8**, 253 (1997)
- [68] A. Canning, G. Galli and J. Kim, Phys. Rev. Lett. **78**, 4442 (1997)
- [69] J. F. Roux, L. Bardotti, B. Cabaud, M. Treilleux, P. Jensen and A. Hoareau, Mat. Sci. Eng. B. **49**, 110 (1997). See also E. Kay, Z. Phys. D **3**, 251 (1986).
- [70] K. Sattler, J. Muhlbach et E. Recknagel, Phys. Rev. Lett. **45**, 821 (1980)
- [71] D. Rayane, P. Melinon, B. Tribollet, B. Cabaud, A. Hoareau, M. Broyer, J. Chem. Phys. **91** (1989) 3100
- [72] M. Samy El-Shall and A. S. Edelstein, Chapter 2 of Ref. [8].
- [73] P. Milani and W. A. de Heer, Rev. Sci. Instrum. **61** 147 (1990)
- [74] G. Vandoni, C. Felix, R. Monot, J. Buttet and W. Harbich, Chem. Phys. Lett. **229**, 51 (1994)
- [75] H.-P. Cheng and U. Landman, *Science* **260**, 1304 (1993);
- [76] I. M. Vitomirov, C. M. Aldao, G. D. Waddill, C. Capasso and J. H. Weaver, Phys. Rev. B **41**, 8465 (1990)
- [77] W. D. Luedtke and U. Landman, J. Vac. Sci. Technol. B **9**, 414 (1991)
- [78] J. J. Pascual, J. Méndez, J. Gómez-Herrero, A. M. Baró, N. García and V. T. Binh, Phys. Rev. Lett. **71**, 1852 (1993)
- [79] Z. Zhang and M. G. Lagally, *Science* **276**, 377 (1997).
- [80] P. Jensen, *La Recherche* **283** 42 (1996)
- [81] P. Meakin, Phys. Rev. Lett. **51**, 1119 (1983); M. Kolb, R. Botet and R. Jullien, Phys. Rev. Lett. **51** (1983) 1123; for a comprehensive review, see H. J. Herrmann, Phys. Rept. **136**, 153 (1986).
- [82] A. F. Voter, Phys. Rev. B **34**, 6819 (1986);
- [83] M. Schroeder, P. Smilauer and D. E. Wolf, Phys. Rev. B **55**, 10814 (1997)
- [84] T. Shitara et al. Phys. Rev. B **46**, 6815 (1992); **46**, 6825 (1992)
- [85] T. R. Linderroth et al. Phys. Rev. Lett. **77**, 87 (1996)
- [86] J.W. Evans and M.C. Bartelt, J. Vac. Sci. Technol. A **12**, 1800 (1994)
- [87] C. Mottet, R. Ferrando, F. Hontinfinde and A. C. Levi, Surf. Sci. (1998)
- [88] G. Zinsmeister, Vacuum **16**, 529 (1966); Thin Solid Films **2**, 497 (1968); Thin Solid Films **4**, 363 (1969); Thin Solid Films **7**, 51 (1971)
- [89] M. Smoluchovsky, Phys. Z. **17**, 557 and 585 (1916)
- [90] J. A. Venables, Phil. Mag. **27**, 697 (1973)
- [91] J. A. Venables, G. D. T. Spiller, and M. Hanbücken, Rep. Prog. Phys. **47**, 399 (1984)
- [92] S. Stoyanov and D. Kaschiev, *Current Topics in Mat. Science*, Ed. E. Kaldis, (North-Holland, 1981)
- [93] J. Villain, A. Pimpinelli, L.-H. Tang, and D. E. Wolf, J. Phys. I France **2**, 2107 (1992); J. Villain, A. Pimpinelli and D.E. Wolf, Comments Cond. Mat. Phys. **16**, 1 (1992)
- [94] J. Villain and A. Pimpinelli *Physique de la Croissance Cristalline* (Eyrolles, 1995) (english edition to be published by Cambridge University Press, 1998)
- [95] A. Pimpinelli, P. Peyla, P. Jensen and H. Larralde, in *Directions in Condensed Matter Physics* Ed. Z. Zhang and M. Lagally (World Scientific, 1997)
- [96] G.S. Bales and D.C. Chrzan, Phys. Rev. B **50**, 6057 (1994)
- [97] N. Metropolis et al. J. Chem. Phys. **21**, 1087 (1953)
- [98] K. Binder (ed.) *Monte Carlo methods in statistical physics* (Springer-Verlag, Berlin, 1986);
- [99] K. Binder *Mechanics : Classical to Monte Carlo Methods*, in *Encyclopedia of Applied Physics*, **10**, G. L. Trigg (Ed.) (John Wiley & Sons, London, 1994); K. Binder, Rep. Prog. Phys. **60**, 487 (1997)
- [100] L.-H. Tang, J. Phys. I France **3**, 935 (1993)
- [101] J. W. Evans and M. C. Bartelt, in *Directions in Condensed Matter Physics* Ed. Z. Zhang and M. Lagally (World Scientific, 1997); (1994). For a review, see ref [103] and [94].
- [102] P. Jensen, A.-L. Barabási, H. Larralde, S. Havlin, and H. E. Stanley, Nature **368**, 22 (1994); Physica A **207**, 219-227 (1994); Phys. Rev. B **50**, 15316 (1994)
- [103] A.-L. Barabasi and H. E. Stanley, *Fractal Concepts in Surface Growth* (Cambridge University Press, 1995).
- [104] K. Binder, p. 1 of Ref. [98]
- [105] A. Bogicevic, S. Liu, J. Jacobsen, B. Lundqvist and H. Metiu, Phys Rev B **57** R9459 (1998)
- [106] H. C. Kang and W. H. Weinberg, J. Chem. Phys. **90**, 2824 (1989)

- [107] S. V. Khare et al. Phys. Rev. Lett. **75**, 2148 (1995)
- [108] S. V. Khare and T. L. Einstein, Phys. Rev. B **54**, 11752 (1996)
- [109] A. B. Bortz, M. H. Kalos and J. L. Lebowitz, J. Comp. Phys. **17** 10 (1975)
- [110] C. Ratsch, A. Zangwill and P. Smilauer, Surf. Sci. **314**, L937 (1994)
- [111] B. Z. Noshov, V. Bressler-Hill, S. Varma and W. H. Weinberg, Surf. Sci. **364**, 164 (1996); M. Schroeder and D. E. Wolf, Surf. Sci. **375**, 129 (1997)
- [112] J. C. Hamilton, Phys. Rev. B **55**, R7402 (1997)
- [113] J. Frenkel and T. Kontorova, Phys. Z. Sowj. **13**, 1 (1938)
- [114] P. Jensen, Comments At. Mol. Phys. (1998)
- [115] L. Bardotti, P. Jensen, M. Treilleux, A. Hoareau and B. Cabaud, Phys. Rev. Lett. **74**, 4694 (1995); Surf. Sci. **367** 276 (1996)
- [116] P. Jensen and B. Niemeyer, Surf. Sci. Lett. **384**, 823 (1997)
- [117] P. Jensen, H. Larralde and A. Pimpinelli, Phys. Rev. B **55**, 2556 (1997) : note that in this paper, a mistake was made in the normalization of the island size distributions (Fig. 9).
- [118] P. Jensen, L. Bardotti, A.-L. Barabási, H. Larralde, S. Havlin, and H. E. Stanley, *Disordered Materials and Interfaces* [PROC. SYMPOSIUM OF MATERIALS RESEARCH SOCIETY, 1995], edited by H. Z. Cummins, D. J. Durian, D. L. Johnson, and H. E. Stanley (Materials Research Society, Pittsburgh, 1996), p. 391.
- [119] C. Ratsch, P. Smilauer, A. Zangwill and D. D. Vvedensky, Surf. Sci. Lett. **329**, L599 (1995)
- [120] P. Jensen, A.-L. Barabási, H. Larralde, S. Havlin, and H. E. Stanley, Fractals **4**, 321 (1996).
- [121] J. A. Strosio and D. T. Pierce, J. Vac. Sci. Technol. B **12** 1783 (1994)
- [122] J. Evans and M. C. Bartelt, Phys. Rev. B **54**, R17359 (1996)
- [123] D. Stauffer, A. Aharony *Introduction to Percolation Theory* (2nd edition, Taylor & Francis, London, 1992)
- [124] P. Melinon, P. Jensen, J. Hu, A. Hoareau, B. Cabaud and D. Guillot, Phys. Rev. B **44**, 12562 (1991)
- [125] B. Lewis and J. C. Anderson in *Nucleation and Growth of thin films* (Academic Press, New York, 1978); J. L. Robins and T. N. Rhodin, Surf. Sci. **2**, 346 (1964); H. Larralde, P. Jensen, M. Meunier and A. Pimpinelli, Proceedings of the Materials Research Society, Fall Meeting, Boston, December 1996
- [126] S. Liu, L. Bönig and H. Metiu, Phys. Rev. B **52** 2907 (1995)
- [127] L. Kuipers and R. E. Palmer, Phys. Rev. B **53**, R7646 (1996)
- [128] I. Furman and O. Biham, Phys. Rev. B **55**, 7917 (1997)
- [129] M. Meunier, Ph. D. thesis (Université Aix-Marseille, 1995); M. Meunier and C.R. Henry, Surf. Sci. **307**, 514 (1994)
- [130] M. Harsdorff, Thin Sol. Films **116**, 55 (1984)
- [131] J. C. Zanghi, J. J. Métois and R. Kern, Phil. Mag. **31**, 743 (1975)
- [132] X. Xiao, Y. Xie, C. Jakobsen and Y. R. Shen, Phys. Rev. B **56**, 12529 (1997) and references therein; K. Haug, Z. Zhang, D. John, C. F. Walters, D. M. Zehner and W. E. Plummer, Phys. Rev. B **55**, R10233 (1997); S. Liu, L. Bönig, J. Detch and H. Metiu, Phys. Rev. Lett. **74**, 4495 (1995) and references therein.
- [133] C. R. Henry, C. Chapon and B. Mutaftschiev, Thin Solid Films **33**, 1 (1976)
- [134] P. Jensen, M. Meunier, H. Larralde and A. Pimpinelli, Surf. Sci. **412-13**, 458 (1998)
- [135] H. Brune, H. Röder, C. Boragno, and K. Kern, Phys. Rev. Lett. **73**, 1955 (1994)
- [136] S.-L. Chang and P. A. Thiel, Critical Reviews in Surface Chemistry **3**, 239-296 (1994)
- [137] F. Dos Santos Aires, PhD Thesis (University of Lyon, 1990)
- [138] N. Combe and P. Jensen, Phys. Rev. B **57**, 15553 (1998)
- [139] M. Treilleux et al. (in preparation)
- [140] A. Masson, J.J. Métois and R. Kern, Surf. Sci. **27** 463 (1971)
- [141] R. Gomer, Rep. Prog. Phys. **53** (1990) 917
- [142] J.J. Métois, K. Heinemann and H. Poppa, Phil. Mag. **35**, 1413 (1977)
- [143] R. Kern, G. Le Laye and J.J. Métois, Current Topics in Materials Science, vol 3 chap 3, North Holland (1979)
- [144] J. W. Matthews and E. Grünbaum, J. Vac. Sci. Technol. **3**, 133, (1966)
- [145] L. Y. Kuo, P. Shen, Surf. Sci. Lett. **373**, L350 (1997)
- [146] G. L. Kellogg, Phys. Rev. Lett. **73**, 1833 (1994)
- [147] G.L. Kellogg, Surf. Sci. Rep. **21** 1 (1994)
- [148] S. Liu, Z. Zhang, J. Norskov and H. Metiu, Surf. Sci. **321** 161 (1994)
- [149] H. Shao, P. C. Weakliem and H. Metiu, Phys. Rev. B **53**, 16041 (1996)
- [150] W. W. Pai, A. K. Swan, Z. Zhang and J. F. Wendelken, Phys. Rev. Lett. **79**, 3210 (1997)
- [151] D. S. Sholl and R. T. Skodje, Phys. Rev. Lett. **75**, 3158 (1995)
- [152] M. Zinke-Allmang, L. C. Feldman and M. H. Grabow, Surf. Sci. Rep. **16** 377 (1992)
- [153] J. M. Soler, Phys. Rev. B **53**, R10540 (1996); C. deW. Van Siclen, Phys. Rev. Lett. **75**, 1574 (1995);
- [154] J.M. Wen, S.L. Chang, J.W. Burnett, J.W. Evans, and P.A. Thiel, Phys. Rev. Lett. **73**, 2591 (1994); J.M. Wen, S.L. Chang, J.W. Burnett, J.W. Evans, and P.A. Thiel, Phys. Rev. Lett. **76**, 562 (1996)
- [155] Z. P. Shi, A. K. Swan, Z. Zhang and J. F. Wendelken, Phys. Rev. Lett. **76**, 4927 (1996)
- [156] J. C. Hamilton, M. S. Daw and S. M. Foiles, Phys. Rev. Lett. **74**, 2760 (1995)

- [157] S. C. Wang and G. Ehrlich, Phys. Rev. Lett. **79**, 4234 (1997)
- [158] J. C. Hamilton, Phys. Rev. Lett. **77**, 885 (1996) J. C. Hamilton, Phys. Rev. B **55**, R7402 (1997)
- [159] H. Reiss, J. Appl. Phys. **39**, 5045 (1968)
- [160] A. Masson, J.J. Metois and R. Kern, Surf. Sci. **27** 483 (1971);
- [161] P. Deltour, P. Jensen, and J-L. Barrat, Phys. Rev. Lett. **78**, 4597 (1997)
- [162] J. E. Lennard-Jones, Proc. Roy. Soc. London A **106** 463 (1924)
- [163] MRS Bulletin, **21(2)**, February 1996.
- [164] M. P. Allen and T. E. Tidesley, Computer simulation of Liquids, Oxford University Press (1987)
- [165] J. Hautman et al., Phys. Rev. Lett. **67**, 1763 (1991)
- [166] U. Landmann (unpublished) : oral presentation at ISSPIC9 (Lausanne, Switzerland, 1998)
- [167] S.M. Foiles, M.I. Baskes, and M.S. Daw, Phys. Rev. B **33**, 7983 (1986).
- [168] E. Ruckenstein and B. Pulvermacher, J. Catal. **29** 224 (1973); D.B. Dadybujor, S.P. Marsh and M.E. Glicksman, J. Catal. **99** 358 (1986); S. A. Stevenson, J. A. Dumesic, R. T. K. Baker and E. Ruckenstein, *Metal-Support Interactions in Catalysis, Sitering and Redispersion* (Van Nostrand Reinhold, New York, 1987)
- [169] W.W. Mullins, J. Appl. Phys. **28**, 333 (1957)
- [170] F.A. Nichols and W.W. Mullins, J. Appl. Phys. **36**, 1826 (1965); F.A. Nichols, J. Appl. Phys. **37**, 2805 (1966).
- [171] J. C. Heyraud, J. J. Métois and J. M. Bermond, J. Cryst. Growth **98**, 355 (1989)
- [172] L. Lewis, P. Jensen, and J-L. Barrat, Phys. Rev. B **56**, 2248 (1997)
- [173] M. Flüeli, P. A. Buffat, and J. P. Borel, Surf. Sci. **202**, 343 (1988).
- [174] Ph. Buffat and J-P. Borel, Phys. Rev. A **13**, 2287 (1976)
- [175] S. Valkealahti and M. Manninen, Phys. Rev. B, **57**, 15533 (1998)
- [176] R. L. Schwoebel, J. Appl. Phys. **40**, 614 (1969); R. L. Schwoebel and E. J. Shipsey, J. Appl. Phys. **37**, 3682 (1966); J. Villain, J. Physique I **1**, 19 (1991)
- [177] N. Combe, P. Jensen, A. Pimpinelli and C. Misbah (unpublished)
- [178] X. Yu and P. M. Duxbury, Phys. Rev. B **52**, 2102 (1995)
- [179] H. Zhu and R. S. Averback, Phil. Mag. Lett. **73**, 27 (1996)
- [180] See for instance D. Frenkel and B. Smit *Understanding Molecular Simulation* (Academic Press, 1996); M.P. Allen and D.J. Tildesley, *Computer Simulation of Liquids* (Clarendon Press, Oxford, 1987).
- [181] W. D. Luedtke and U. Landman, Phys. Rev. Lett. **73**, 569 (1994)
- [182] M. Hou, Nucl. Instr. and Methods B **135**, 501 (1998)
- [183] M. Dreschler, J. J. Métois and J. C. Heyraud, Surf. Sci. **108** 549 (1981); J. J. Métois and J. C. Heyraud, Thin Solid Films **75** 1 (1981); C. R. Henry and M. Meunier, Mat. Sci. Eng. **A 217/218**, 239 (1996)
- [184] C. R. Stoldt, A. M. Cadilhe, C. J. Jenks, J.-M. Wen, J. W. Evans and P. A. Thiel, Phys. Rev. Lett. **81**, 2950 (1998)
- [185] P. Jensen, N. Combe, H. Larralde, J. L. Barrat, C. Misbah and A. Pimpinelli (Eur. Phys. J. B, to be published)
- [186] W. Selke and P. M. Duxbury, Z. Phys. B **94**, 311 (1994); E. Adam, A. Chame, F. Lancon and J. Villain, J. Phys. I France **7** 1455 (1997)
- [187] A. Pimpinelli, J. Villain and D. E. Wolf, J. Phys. I (France) **3**, 447 (1993); G.S. Bales and D.C. Chrzan, Phys. Rev. Lett. **74**, 4879 (1995)
- [188] P. Jensen, unpublished
- [189] J.L. Barrat (private communication)
- [190] G. Jeffers, M. A. Dubson and P. M. Duxbury, J. Appl. Phys. **75**, 5016 (1994)
- [191] J. Tuillon, Ph. D. Thesis (Université de Lyon, 1995); J. Tuillon et al., Phil. Mag. A **76** 493 (1997)
- [192] G. W. Nieman, J. R. Weertman and R. W. Siegel, J. Mater. Res. **6**, 1012 (1991)
- [193] H. Zhu and R. S. Averback, Mat. Sci. Eng. **A204**, 96 (1995)
- [194] M. Celino, G. D'Agostino, V. Rosato, Mat. Sci. Eng. **A204**, 101 (1995); Phys. Rev. B **48**, 22 (1993)
- [195] *Biomimetic Materials Chemistry*, Ed. S. Mann, (VCH Publishers, New York, USA (1996)

FIG. 1. Ag nanoislands grown on two monolayers of Ag deposited on Pt(111) and annealed at 800K. The inset shows a fast fourier transform of the spatial distribution. From Ref. [39])

FIG. 2. By changing the mean size of the incident antimony clusters, one can dramatically change the morphology of the submonolayer film. The four micrographs have been obtained for the same thickness (1 nm) and deposition rate ($5 \times 10^{-3} \text{ nm s}^{-1}$). The mean sizes are : (a) Sb₄, (b) Sb₁₆, (c) Sb₃₆, (d) Sb₂₄₀. The changes in morphology are interpreted by the different mobilities of the clusters as a function of their size, as well as their different coalescence dynamics and sensitivity to surface defects. From Ref. [18].

FIG. 3. Molecular Dynamics simulations of the morphology of films obtained by Mo₁₀₄₃ cluster deposition for increasing incident kinetic energies per atom (as indicated in the figures) onto a Mo(001) substrate. From Ref. [58]

FIG. 4. Principle of a Kinetic Monte Carlo simulation (see text).

FIG. 5. Main elementary processes considered in this paper for the growth of films by cluster deposition. (a) adsorption of a cluster by deposition; (b) and (d) diffusion of the isolated clusters on the substrate; (c) formation of an island of two monomers by juxtaposition of two monomers (nucleation) (d) growth of a supported island by incorporation of a diffusing cluster (e) evaporation of an adsorbed cluster. I also briefly consider the influence of island diffusion (f).

FIG. 6. Possible interaction of two clusters touching on the surface : (a) pure juxtaposition (b) total coalescence. Intermediate cases (partial coalescence) are possible and will be described later.

FIG. 7. Time scales of some elementary processes considered in this paper for the growth of films by cluster deposition. The relevant processes are those whose time scale are smaller than the deposition time scale shown by the arrow in the left. In this case, models including only cluster diffusion on the substrate and cluster cluster coalescence are appropriate. "Island diffusion" refers to the motion of islands of clusters as a whole, "cluster dissociation" to the evaporation of atoms from the cluster and "interdiffusion" to the exchange of atoms in the cluster with substrate atoms.

FIG. 8. Evolution of the monomer and island densities as a function of the thickness (in monolayers), for islands formed by pure juxtaposition : (a) complete condensation, $F = 10^{-8}$, $\tau_e = 10^{10}$ ($\tau = 1$). These values mean : $X_S = 10^5$ and $\ell_{CC} = 22$ (b) important evaporation, $F = 10^{-8}$, $\tau_e = 600$ ($\tau = 1$) ($X_S = 25$ and $\ell_{CC} = 22$). ℓ_{CC} represents the mean island separation at saturation for the given fluxes when there is no evaporation [117]. The length units correspond to the incident cluster (monomer) diameter. In (b) the "condensation" curve represents the total number of particles actually present on the surface divided by the total number of particles sent on the surface ($F t$). It would be 1 for the complete condensation case, neglecting the monomers that are deposited on top of the islands. The solid line represents the constant value expected for the monomer concentration, while the dashed line corresponds to the linear increase of the island density (see text).

FIG. 9. Morphology of a submonolayer deposit in the case of growth with complete condensation and pure juxtaposition : (a) $\theta = 0.1\%$; (b) $\theta = 15\%$. The values of the parameters are : $F = 10^{-8} \text{ ML/s}$, $\tau = 1$ and $L=300$.

FIG. 10. Saturation island density as a function of the normalized flux ($\tau = 1$) for different growth hypothesis indicated on the figure, always in the case of island growth by pure juxtaposition. "no evap" (circles) means complete condensation. Triangles show the densities obtained if there is evaporation, for $\tau_e = 100$. In the preceding cases, islands are supposed to be immobile. This hypothesis is relaxed for the last set of data, *mobile islands* (squares), where island mobility is supposed to decrease as the inverse island size [102] (there is no evaporation). The dashed line is an extrapolation of the data for the low normalized fluxes. Fits of the different curves in the low-flux region give : "no evap" (solid line): $N_{sat} = 0.53(F\tau)^{0.36}$; "evap" (dotted line) : $N_{sat} = 0.26F^{0.67}\tau^{-1/3}\tau_e$ (for the τ and τ_e exponents, see [117] and Appendix A) and "mobile islands" (dashed line) : $N_{sat} = 0.33(F\tau)^{0.42}$

FIG. 11. Evolution of the island density as a function of the thickness for different growth hypothesis. This figure shows that the *same* saturation density can be obtained for films grown in very different conditions. The different sets of data represent : *triangles* : growth with coalescence and evaporation, $\tau_e = 100\tau$ and $F\tau = 1.2 \cdot 10^{-8}$, *circles* : growth with coalescence but without evaporation ($F\tau = 3 \cdot 10^{-10}$), *solid line* : growth with pure juxtaposition without evaporation ($F\tau = 2.5 \cdot 10^{-9}$), *squares* : growth with coalescence on defects (defect concentration : $5 \cdot 10^{-4}$ per site) and $F\tau = 10^{-14}$ (no evaporation), *dashed line* : growth with pure juxtaposition without evaporation but with mobile islands, $F\tau = 10^{-8}$.

FIG. 12. Normalized island size distributions for $F = 10^{-8}$, $\tau = 1$ and different values of τ_e for islands formed by pure juxtaposition (no coalescence). The size distributions were obtained for different coverages θ between .05 and 0.2. The solid line shows the size distribution obtained without evaporation, the dashed line that obtained with mobile dimers and the numbers show the different values of τ_e . The size distributions shown here have been obtained with $F\tau = 10^{-8}$, but the same distributions are obtained if both F , τ and τ_e are changed but the same parameter $\epsilon = (1 + X_S)X_S^5 (F\tau)$ is obtained (see Ref. [117])

FIG. 13. Saturation island density as a function of the normalized flux ($\tau = 1$) for different growth hypothesis in the case of growth by total coalescence (3d islands). I show the densities obtained for the complete condensation case (filled circles) and for two different evaporation times : $\tau_e = 100$ (triangles) and $\tau_e = 20$ (squares). The label *defects* means growth in presence of defects which act as nucleation centers. Their concentration is 10^{-3} per site. The dashed line is an extrapolation of the defect data for the low normalized fluxes. Fitting the simulation data leads to the following numerical relations : $N_{sat} = 0.27(F\tau)^{0.286}$ when there is no evaporation (solid line) ; $N_{sat} \sim 0.039F^{0.55}\tau^{-2/3}\tau_e^{4/3}$ when evaporation is significant (from an approximation for the two dotted curves) : the exponents for τ and τ_e have been derived from a rate-equations treatment (Appendix B)

FIG. 14. Normalized island size distributions obtained for $F = 10^{-8}$, $\tau = 1$ and different values of the evaporation time τ_e for islands formed by total coalescence. The size distributions were obtained for different coverages θ between .05 and 0.2. The solid line shows the size distribution obtained without evaporation. The number next to each symbol corresponds to τ_e .

FIG. 15. Effect of the presence of defects on the island size distribution. The rescaled island size distributions are obtained for $F = 10^{-8}$ and different values of the evaporation time τ_e ($\tau = 1$) for islands formed by total coalescence by nucleation on defects. The size distributions were obtained for different coverages θ between .05 and 0.15. Contrary to what is observed for homogeneous nucleation, (i.e. without defects) the histograms do depend on the coverage for nucleation on defects. The solid line shows the size distribution obtained without evaporation.

FIG. 16. Values of (a) the thickness e_{sat} and (b) island density N_{sat} at the saturation of island density as a function of the evaporation parameter $\eta = F\tau X_S^6$ for growth with pure juxtaposition [117]. The solid lines represent theoretical predictions [117].

FIG. 17. Values of the thickness e_{sat} (a) and the condensation coefficient C_{sat} (b) at the saturation of island density in the total coalescence limit (3d growth for atomic deposition). In the limit of low island densities (i.e. high evaporation rates), C_{sat} is a constant (see Ref. [134], this regime is indicated by the solid line). However, there are crossover regimes which depend on the precise τ_e and which are shown here. Then, from a measure of C_{sat} and N_{sat} one can get an estimate for τ_e for the not too low island densities which correspond to many experimental cases. In the same spirit, (a) shows the evolution of e_{sat} as a function of N_{sat} in the crossover regime. The numbers correspond to the different τ_e/τ used for the simulations and CC refers to the case of complete condensation (no evaporation). The dotted line in the higher left shows the limiting regime $e_{sat} \sim N_{sat}^{-1/2}$.

FIG. 18. Typical island morphologies obtained experimentally by TEM (a) and from the computer simulations (b) at the same coverage. (a) Sb_{2300} deposition on graphite HOPG at $T_s = 353K$ and $f = 610^{-3}nm/s$, corresponding to $F = 1.710^{-3}ML/s$. The deposited thickness is 0.5 nm or $e = 0.14ML$ (b) model including only deposition, diffusion and pure juxtaposition of the incident clusters, $F\tau = 9 \cdot 10^{-11}$

FIG. 19. (a) Evolution of the island density as a function of the deposited thickness. The solid line is a fit to the experimental data with $F\tau = 1.75 \cdot 10^{-8}$. (b) Evolution of the maximum island density (N_{sat}) as a function of the incident flux F at room temperature. The solid line is a fit to the experimental data : we find $N_{sat} = a f^{0.37 \pm 0.03}$ (c) Dependence of the diffusion coefficient on the temperature. From a fit on the experimental data (solid line), one finds $D = D_0 \exp(-E_a/kT)$, with $E_a = 0.7 \pm 0.1$ eV and $D_0 = 10^4 cm^2 s^{-1}$. The island densities are expressed per site, a site occupying the projected surface of a cluster, equivalent to $2.08 \cdot 10^{-13} cm^2$

FIG. 20. Scanning electron microscopy of a submonolayer deposit of Ag_{160} slightly accelerated (50eV) clusters on HOPG. From Ref. [62].

FIG. 21. (a) Morphology of a Sb_{36} film at $e = 1.8ML$. (b) Evolution of the island density (per site) as a function of thickness (ML). The dashed line represents a fit of the data with $F\tau = 10^{-5}$ assuming a pyramidal (half-sphere) shape for the supported islands, while the solid line assumes that islands are spherical and $F\tau = 3 \cdot 10^{-6}$

FIG. 22. Morphologies of a Au_{250} films at $e = 0.12 ML$ and increasing temperatures as indicated in the micrographs. There are less and less islands as the substrate temperature is raised and the islands become more and more compact.

FIG. 23. (a) Saturation island density as a function of the diffusion time τ ($F_i=6$ ML/s) for two hypothesis : only the monomers move (solid line) or islands up to the pentamer move too (dashed line). The lowest island densities have been extrapolated. (b) Temperature dependence of diffusion coefficient as derived from (a) and Fig. 22 in the two hypothesis : only the monomers move (solid line) or islands up to the pentamer move too (dashed line).

FIG. 24. Morphology (a) and diffraction pattern (b) of a Au_{250} submonolayer deposit on NaCl at $e = 0.12$ ML. The supported islands are small (mean diameter $\simeq 5\text{nm}$) and in epitaxy with the substrate as shown by the diffraction pattern.

FIG. 25. Radial distribution functions for gold clusters grown at 293K by atomic deposition before and after annealing at 390 K for several minutes. The right inset shows the size distribution of the clusters, which does not change, demonstrating that no particle-particle coalescence via atomic evaporation takes place. From Ref. [131].

FIG. 26. Individual atomic mechanisms leading to island diffusion. PD refers to diffusion of atoms on the periphery of the island, while the exchange of atoms between the island and the atomic 2D gas is shown by the condensation and evaporation labels. The dashed circles represent the old positions of the atoms, while the continuous circles represent the new positions, after the elementary process.

FIG. 27. Principle of island motion by dislocation propagation. The atomic column in the middle of the island jumps from fcc to hcp sites, moving the island center of mass. From Ref. [156].

FIG. 28. Successive positions of a Ir_{19} 2D cluster on a Ir(111) surface observed by field ion microscopy at low temperature. The motion takes place at $T \sim 690\text{K}$ and the figures correspond to 6, 10 and 14 heating intervals of 10 seconds each. From Ref. [157].

FIG. 29. Configuration of the Lennard-Jones cluster on the crystalline surface. (A) Side view : The cluster is partially wetting the surface. (B) Top view : The two halves of the cluster have been colored at the beginning of the run. After the cluster center of mass has moved by roughly three substrate lattice constants from its original position, the two parts of the cluster are still well distinct. Then, the cluster diffusion cannot be explained in terms of single atom mechanisms ($n=100$, $\sigma_{ss}=0.7$, $\epsilon_{sc}=0.4$, $T=0.3$)

FIG. 30. (a) Dependence of the diffusion coefficient on the mismatch between the lattice parameter of the substrate and the cluster. A small change in the lattice parameter of the cluster leads to a huge change in the diffusivity ($n=100$, $\epsilon_{sc}=0.4$, $T=0.3$, Run Length = 12500 τ) (b) Dependence of the diffusion coefficient of a cluster as a function of its number of atoms. Data correspond to different mismatches between the cluster and the substrate lattice parameters. The diffusion coefficient decreases as a power law with exponent α . The two different slopes correspond to different diffusion regimes : the weaker dependence corresponds to a brownian trajectory; the stronger correspond to a "hopping-like" diffusion. For comparison, the arrow indicates the diffusion coefficient of a single adatom with $\sigma_{ss} = 0.9$.

FIG. 31. Trajectory of a cluster center of mass diffusing on a substrate. The solid line represents the trajectory and the circles the equilibrium position of the surface atoms. (a) large mismatch : the motion is "brownian-like", i.e. the cluster does not "see" the structure of the surface. The values of the parameters are : $\epsilon_{sc} = 0.4$, $\sigma_{ss} = 0.7$, $T=0.3$, $n=100$; (b) small mismatch : the cluster center of mass jumps from one hexagon center to a nearest neighbor one. The values of the parameters are the same as for (a) except for $\sigma_{ss} = 0.9$

FIG. 32. Schematic illustration of the competition between coalescence and kinetic ramification. R is the radius of the largest island, r that of the incident clusters and l stands for the typical length of a coalescing cluster. The label "a" refers to the ramification process when a cluster is touched by another one before coalescence can take place.

FIG. 33. Atomic positions at four different times during partial coalescence of Cu clusters (4.8 nm diameter each). The atomic positions are projected onto the $(12\bar{1})$ plane of the bottom sphere for (a) to (c) and onto the $(10\bar{1})$ plane for (d). The arrows indicate the sliding plane ((a) to (c)) and the grain-boundary dislocation (d). From Ref. [179].

FIG. 34. Distribution of shear stress in the sliding plane at different times during the coalescence shown in Fig. 33. Filled circles : 5ps, open squares : 10ps, open triangles : 20ps, crosses : 30ps and plus : 40ps. From Ref. [179].

FIG. 35. Evolution in time of the ratio of the neck radius, x , to the cluster radius, R . The full line represents the numerical solution obtained by Nichols [170] with an arbitrary time scale, while the crosses are the results of Lewis et al. [172] simulations.

FIG. 36. Successive cluster morphologies during the coalescence of a gold 767-atom liquid cluster with another gold 1505-atom solid cluster. The figures represent three stages of the coalescence process after 0, 1 and 10 ns, i.e. times much longer than those studied in Ref. [179].

FIG. 37. Approximate dependence of the radius of the supported particles R_c as a function of the substrate temperature for submonolayer and thick films. Lines refer to predictions from Eq. 7.6 with different incident cluster radius while symbols represent experimental results shown. The theoretical predictions for the submonolayer regime were obtained by taking $N_t/F = 0.1$ and using Eq. 7.7. For the thick film limit, I have taken $F = 10^{-3} \text{ ML/s}$ and $r = 2.5 \text{ nm}$ (Eq. 7.8). One should consider these theoretical R_c values as an upper limit since coalescence may be much slower at these (nano)scales (see the text). As a consequence, it is no surprise that the predicted values are clearly larger than the experimental ones. Concerning Sb, the huge difference can come from a partial oxidation of the clusters on the substrate because of the relatively bad vacuum conditions (pressure $\sim 10^{-7}$ Torr). Even a thin oxide layer can decrease significantly atomic surface diffusion and transport, thus slowing the coalescence process.

Appendix A

Regimes predicted by rate-equations calculations for the growth of 2D islands with evaporation. These predictions agree with the computer simulations presented in this paper and are relevant for both cluster and atomic deposition (see Ref. [117] for more details).

I will here rapidly recall how the rate-equations can be written [117], and then turn on to the different regimes which can be derived from them.

The rate equation describing the time evolution of the density ρ of monomers on the surface is, to lowest relevant orders in F :

$$\frac{d\rho}{dt} = F(1 - \theta) - \frac{\rho}{\tau_e} - F\rho - 2\sigma_o\rho - \sigma_i N_t \quad (8.1)$$

The first term on the right hand side denotes the flux of monomers onto the island free surface, (θ is the island coverage discussed below). The second term represents the effect of evaporation, i.e. monomers evaporate after an average time τ_e . The third term is due to the possibility of losing monomers by effect of direct impingement of a deposited monomers right beside a monomer still on the surface to form an island. This “direct impingement” term is usually negligible, and indeed will turn out to be very small in this particular equation, but the effect of direct impingement plays a crucial role in the kinetics of the system in the high evaporation regimes. The last two terms represent the loss of monomers by aggregation with other monomers and with islands respectively. The factors σ_o and σ_i are the “cross sections” for encounters and are calculated in Refs. [90,96,117].

The number N_t of islands will be given by:

$$\frac{dN_t}{dt} = F\rho + \sigma_o\rho \quad (8.2)$$

where the first term represents the formation of islands due to direct impingement of deposited monomers next to monomers already on the surface, and the second term accounts for the formation of islands by the encounter of monomers diffusing on the surface.

For the island coverage θ i.e. the area covered by all the islands per unit area, one has:

$$\frac{d\theta}{dt} = 2[F\rho + \sigma_o\rho] + \sigma_i N_t + JN_t \quad (8.3)$$

The term in brackets represents the increase of coverage due to formation of islands of size 2 (i.e. formed by two monomers) either by direct impingement or by monomer-monomer aggregation. The next term gives the increase of coverage due to the growth of the islands as a result of monomers aggregating onto them by diffusion, and the last term represents the growth of the islands due to direct impingement of deposited monomers onto their boundary, or directly on the island. This last term depends on X_S^* , the desorption length of monomers diffusing on top of the islands [117]. In all the simulations presented here (Section III), I have taken $X_S^* = 0$. The total surface coverage is given by $\theta + \rho \sim \theta$ except at very short times.

The cross sections can be evaluated in the quasistatic approximation, which consists in assuming that R does not vary in time and that the system is at a steady state. One finds [90,96,117]

$$\sigma_i = 2\pi R D \left(\frac{dP}{dr} \right)_{r=R} = 2\pi D \rho \left(\frac{R}{X_S} \right) \frac{K_1(R/X_S)}{K_0(R/X_S)} \quad (8.4)$$

The cross section for monomer-monomer encounters σ_o is obtained from the same formula substituting R by the monomer radius, and D by $2D$ as corresponds to relative diffusion.

After some additional approximations, one finds [117] three principal regimes which are spanned as the evaporation time τ_e decreases. They have been called : *complete condensation* regime where evaporation is not important, *diffusion* regime where islands grow mainly by diffusive capture of monomers and finally *direct impingement* regime where evaporation is so important that islands can grow only by capturing monomers directly from the vapor. Within each of these regimes, there are several subregimes characterized by the value of X_S^* . I use $l_{CC} \equiv (F\tau)^{-1/6}$, the island-island distance at saturation when there is no evaporation and R_{sat} as the maximum island radius, reached at the onset of coalescence.

complete condensation $X_S \gg l_{CC}$

$$N_{sat} \sim F^{1/3} \tau^{1/3} \text{ for any } X_S^* \quad (8.5)$$

diffusive growth $1 \ll X_S \ll l_{CC}$

$$N_{sat} \sim \begin{cases} (F X_S^2 \tau_e)^{2/3} (X_S + X_S^*)^{-2/3} & \text{if } X_S^* \ll R_{sat} \text{ (a)} \\ F \tau_e X_S^2 & \text{if } X_S^* \gg R_{sat} \text{ (b)} \end{cases} \quad (8.6)$$

with $R_{sat} \sim (X_S + X_S^*)^{1/3} (F X_S^2 \tau_e)^{-1/3}$, which gives for the crossover between regimes (a) and (b) : $X_S^*(crossover) \sim (F X_S^2 \tau_e)^{-1/2}$.

direct impingement growth $X_S \ll 1$

$$N_{sat} \sim \begin{cases} (F \tau_e)^{2/3} & \text{if } X_S^* \ll 1 \text{ (a)} \\ (F \tau_e)^{2/3} X_S^{*-2/3} & \text{if } 1 \ll X_S^* \ll R_{sat} \text{ (b)} \\ F \tau_e & \text{if } X_S^* \gg R_{sat} \text{ (c)} \end{cases} \quad (8.7)$$

with $R_{sat} \sim (F \tau_e)^{-1/3} X_S^{*1/3}$, which gives for the crossover between regimes (a) and (b) : $X_S^*(crossover) \sim (F \tau_e)^{-1/2}$.

Appendix B

I present here the summary of the different limits of growth of 3d islands in presence of evaporation and/or defects. These results are derived in detail in Ref. [134] from the resolution of rate-equations similar to those presented in Appendix A. For each regime, I give in the order the saturation island density N_{sat} , the thickness at saturation e_{sat} (i.e. the thickness when the island density first reaches its saturation value), the thickness at coalescence e_c (i.e. the thickness when the island density starts to decrease due to island-island coalescence), and the scaling kinetics of the mean island radius as a function of time before the saturation island density is reached. I use $l_{CC} = (F\tau)^{1/7}$ for 3d islands [134] and $X_S = \sqrt{\tau_e/\tau}$.

Clean substrate (no defects)

high evaporation : $X_S \ll l_{CC} \ll l_{def}$

$$\begin{aligned} N_{sat} &\sim [F\tau_e(1 + X_s^2)]^{2/3} \\ e_{sat} &\sim e_c \sim [F\tau_e(1 + X_s^2)]^{-1/3} \\ R &\sim Ft \end{aligned}$$

low evaporation : $l_{CC} \ll X_S \ll l_{def}$ or $l_{CC} \ll l_{def} \ll X_S$

$$\begin{aligned} N_{sat} &\sim \left(\frac{F}{D}\right)^{2/7} \\ e_{sat} &\sim e_c \sim \left(\frac{D}{F}\right)^{1/7} \\ R &\sim (FDt^2)^{1/9} \sim t^{2/9} \end{aligned}$$

Dirty substrate (many defects)

high evaporation : $X_S \ll l_{def} \ll l_{CC}$

$$\begin{aligned} N_{sat} &\sim c \\ e_{sat} &\sim \frac{1}{[1+X_s^2]} \\ e_c &\sim \frac{1}{c^{1/2}} \\ R &\sim Ft \end{aligned}$$

low evaporation : $l_{def} \ll X_S \ll l_{CC}$ or $l_{def} \ll l_{CC} \ll X_S$

$$\begin{aligned} N_{sat} &\sim c \\ e_{sat} &\sim c \\ e_c &\sim \frac{1}{c^{1/2}} \\ R &\sim \left(\frac{Ft}{c}\right) \text{ for } t \leq c/F, \text{ i.e. before saturation} \\ R &\sim (Ft/c)^{1/3} \text{ between saturation and coalescence } (c/F \leq t \leq 1/Fc^{1/2}). \end{aligned}$$

Table I

Principal symbols and terms used in this paper. The natural length unit in the model corresponds to the mean diameter of an incident cluster.

<i>Symbols and terms</i>	<i>Units, Remarks</i>
<i>island</i>	<i>structure formed on the surface by aggregation of clusters</i>
n	<i>number of atoms of the cluster</i>
d	<i>cluster diameter in nm, $d = d_0 n^{1/3}$ where d_0 depends on the element</i>
<i>site</i>	<i>area occupied by a cluster on the surface $\text{site} = \pi d^2 / 4$</i>
ML	<i>monolayer : the amount of matter needed to cover uniformly the substrate with one layer of clusters (1 cluster per site)</i>
F	<i>Impinging flux expressed in monolayers (or clusters per site) per second</i>
τ	<i>Diffusion time : mean time needed for a cluster to make a "jump" between two sites (in seconds)</i>
τ_e	<i>evaporation time : mean time before a monomer evaporates from the surface</i>
X_S	<i>mean diffusion length on the substrate before desorption : $X_S = \sqrt{D\tau_e}$</i>
ϕ	<i>Normalized flux ($\phi = F\tau$) expressed in clusters per site</i>
D	<i>Diffusion coefficient expressed in $\text{cm}^2 \text{s}^{-1}$ ($D = \text{site} / 4\tau$)</i>
e	<i>mean thickness of the film, $e = Ft$ where t is the deposition time</i>
θ	<i>coverage; fraction of the substrate covered by the clusters</i>
N_t	<i>island density on the surface, expressed per site</i>
N_{sat}	<i>saturation (maximum) island density on the surface, expressed per site</i>
ρ	<i>density of isolated clusters on the surface, expressed per site</i>
C_{sat}	<i>condensation coefficient (ratio of matter actually present on the substrate over the thickness) at saturation</i>
l_{CC}	<i>the island-island distance at saturation when there is no evaporation</i>

This figure "Fig1.jpg" is available in "jpg" format from:

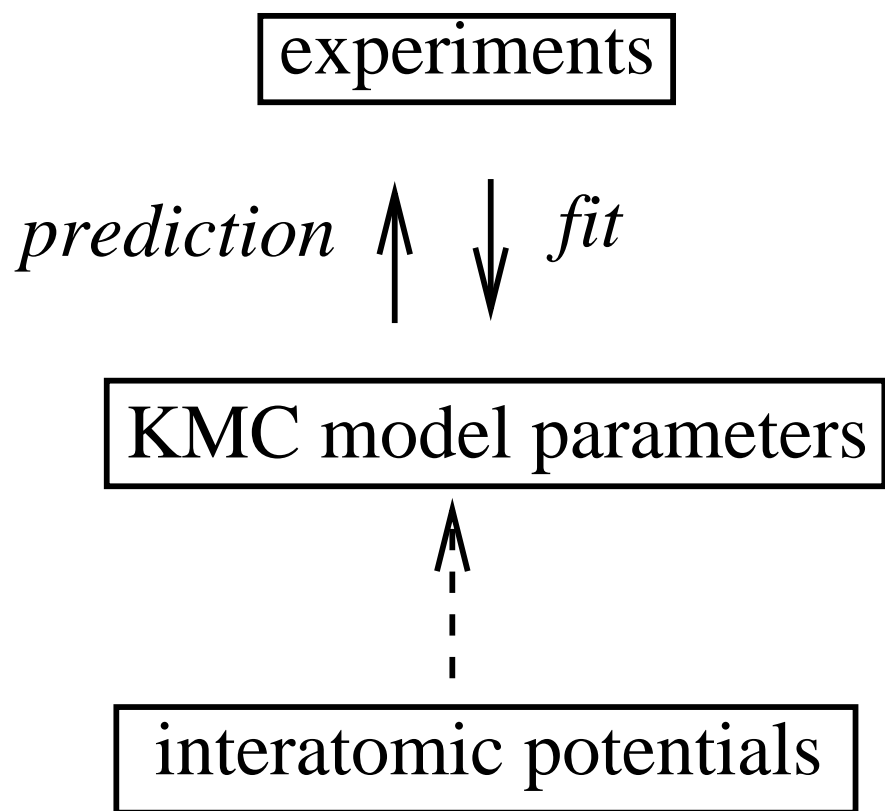
<http://arxiv.org/ps/cond-mat/9903141v1>

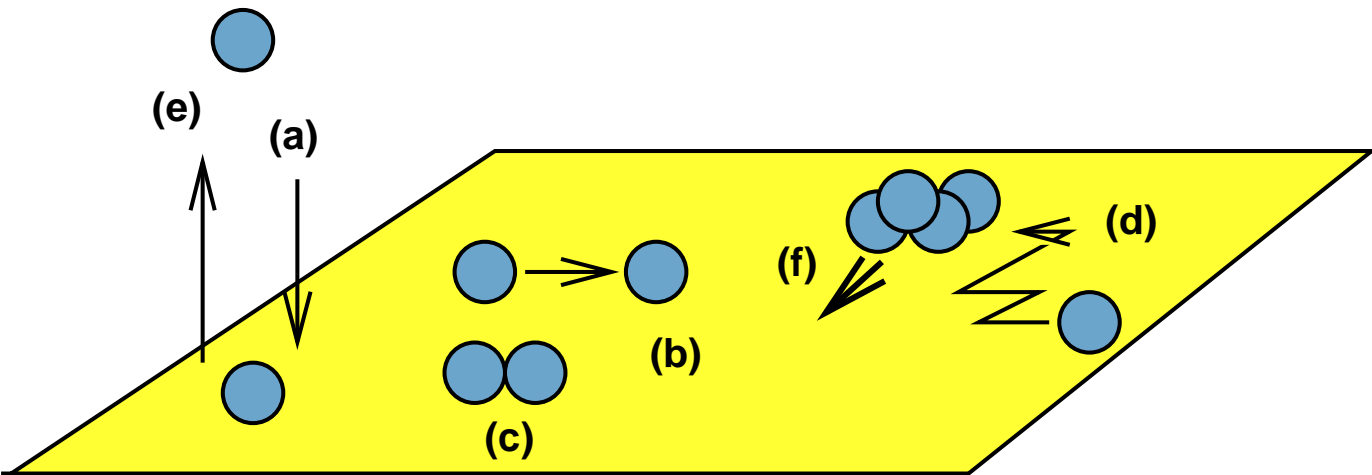
This figure "Fig2.gif" is available in "gif" format from:

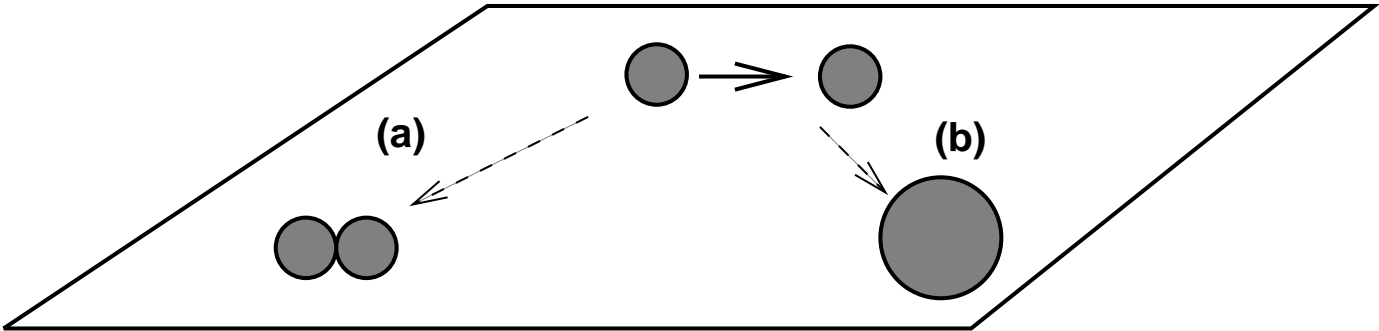
<http://arxiv.org/ps/cond-mat/9903141v1>

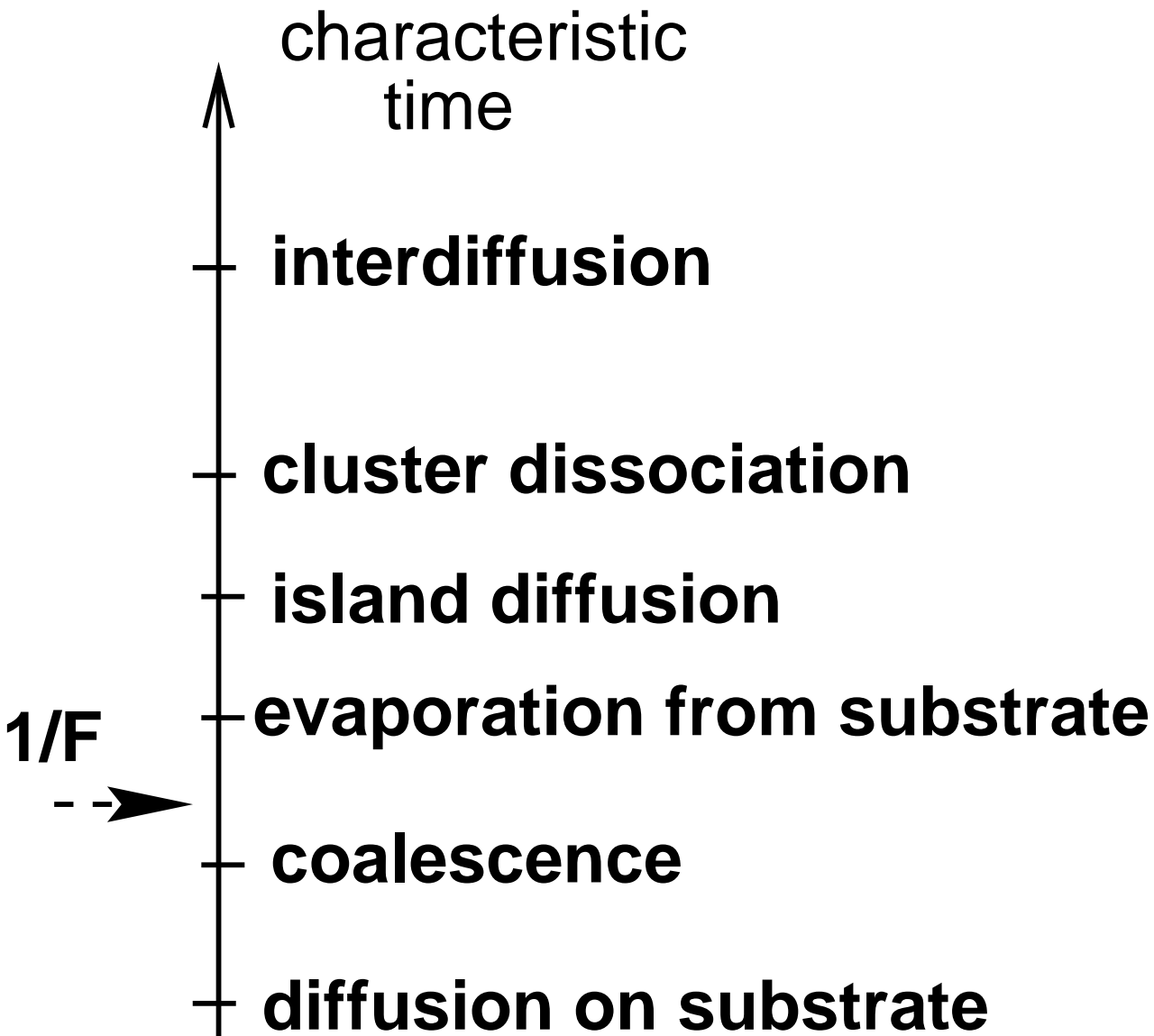
This figure "Fig3.gif" is available in "gif" format from:

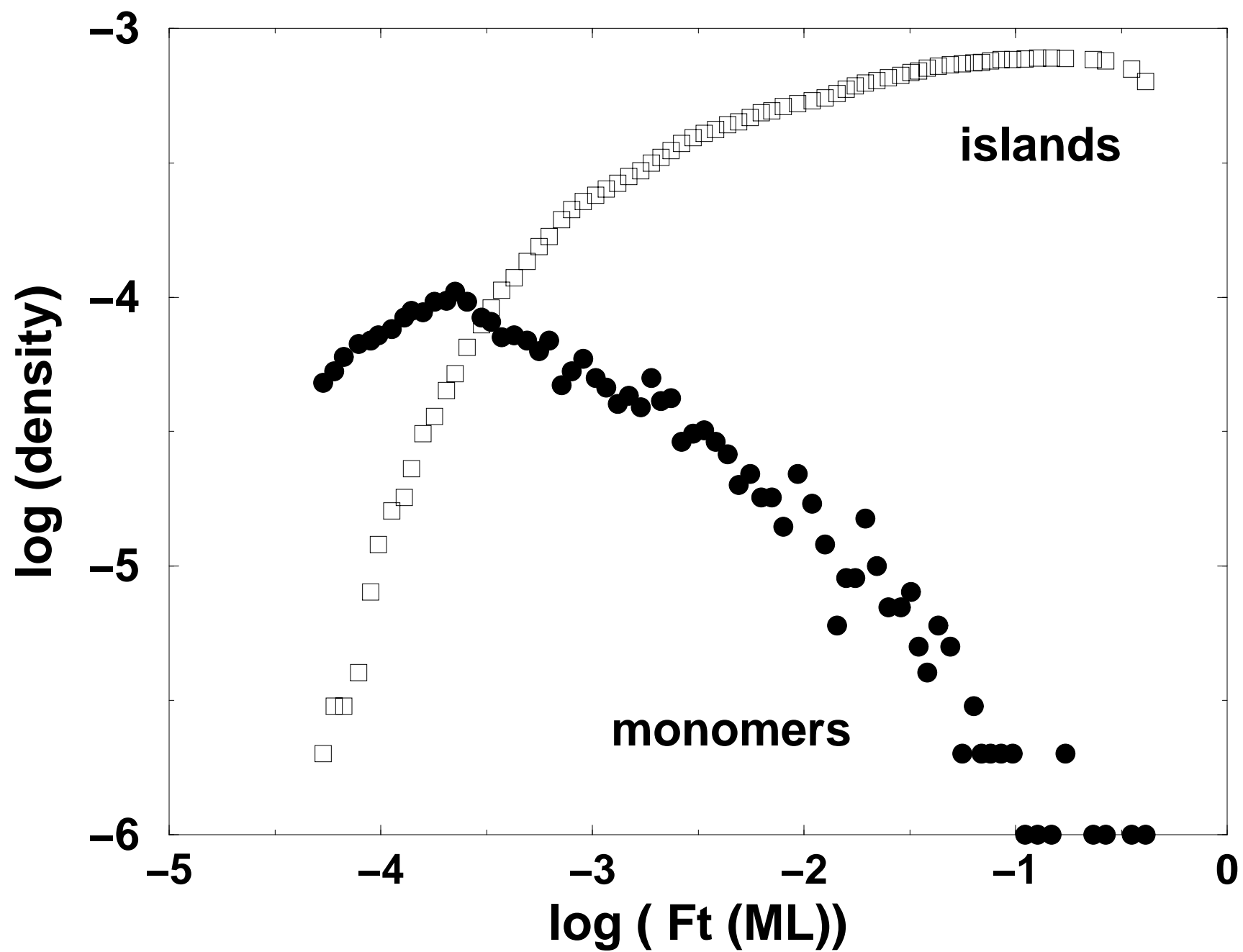
<http://arxiv.org/ps/cond-mat/9903141v1>

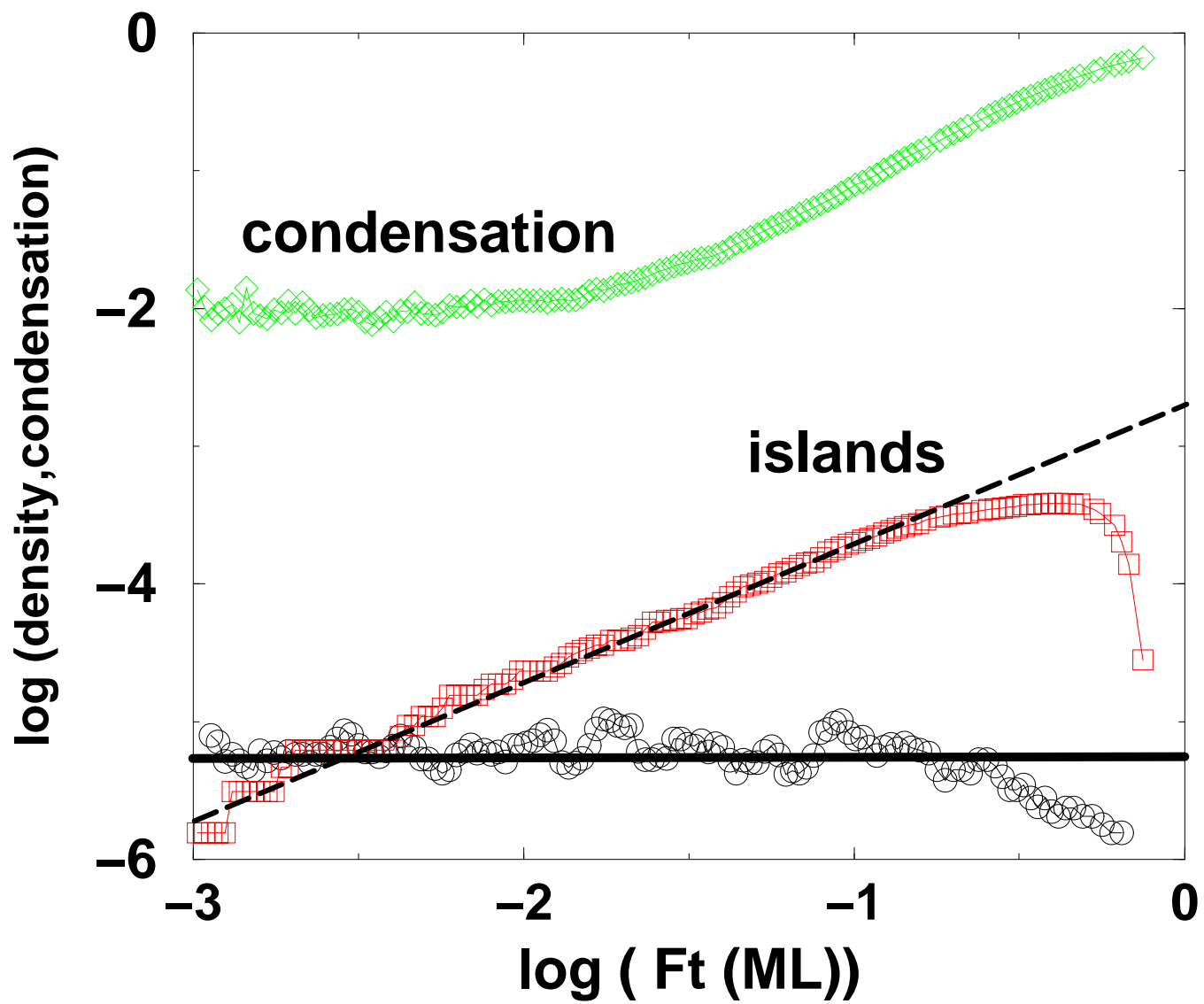












1

2

3

4

5

6

7

8

9

10

11

12

13

14

15

16

17

18

19

20

21

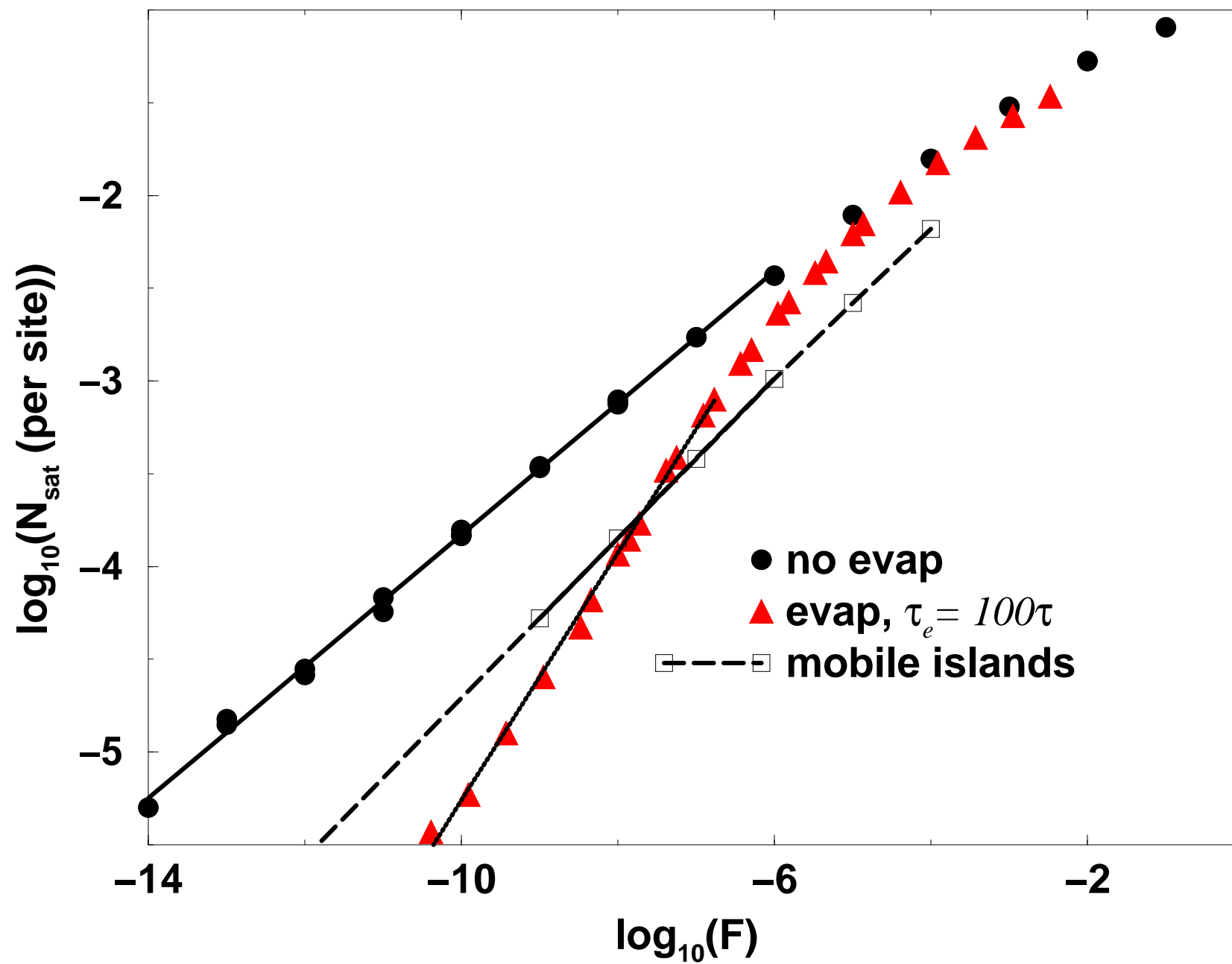
22

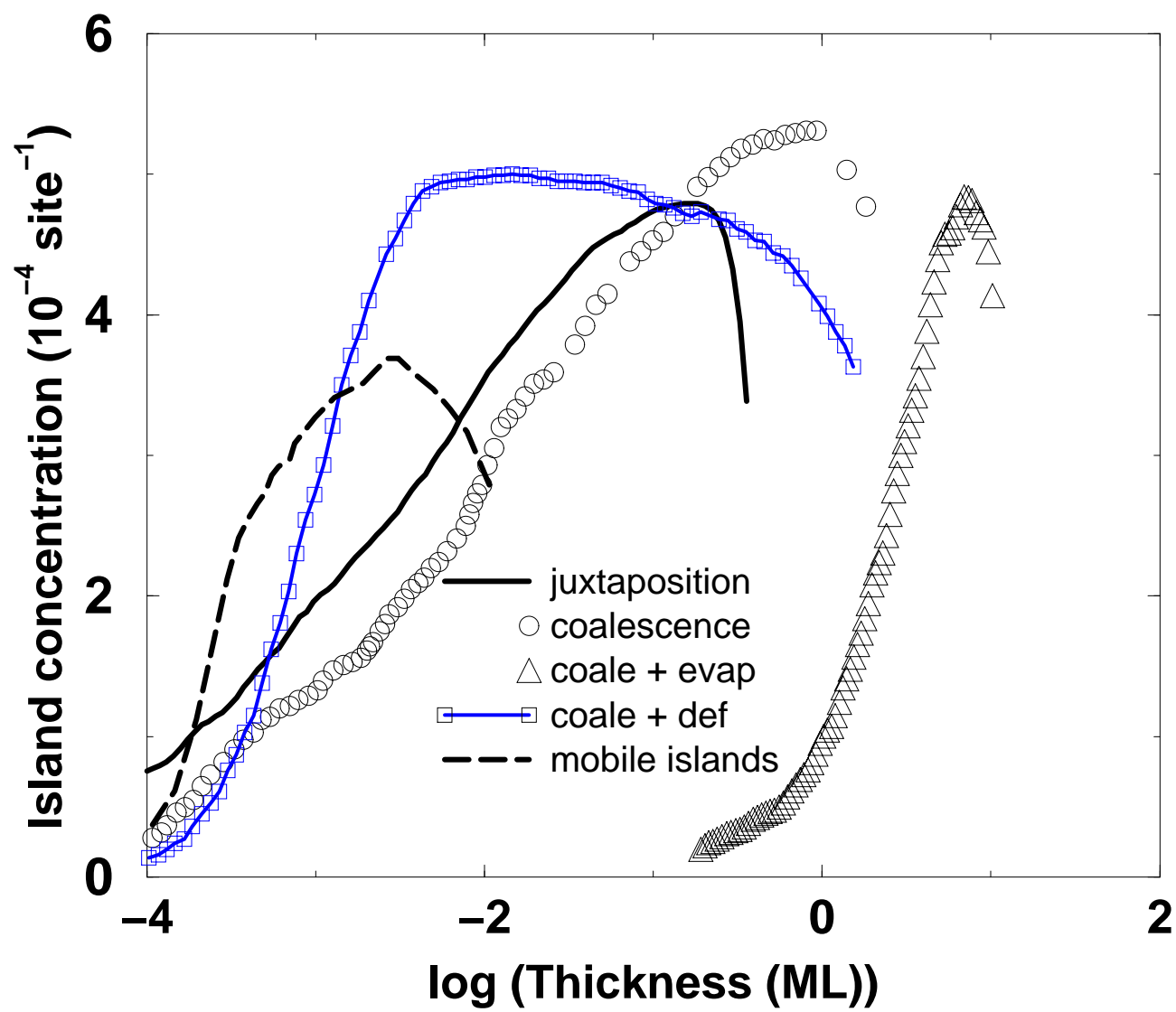
23

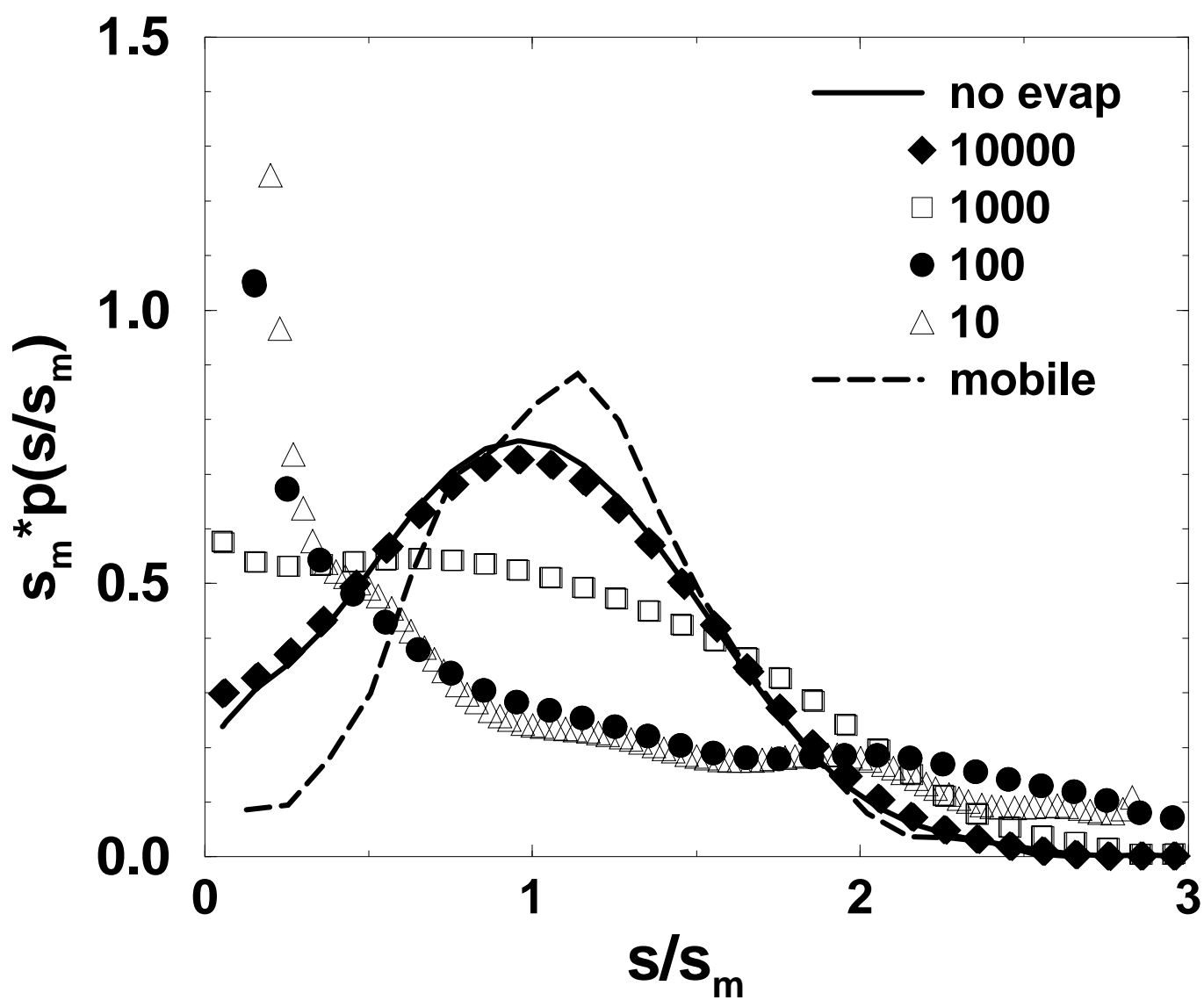
24

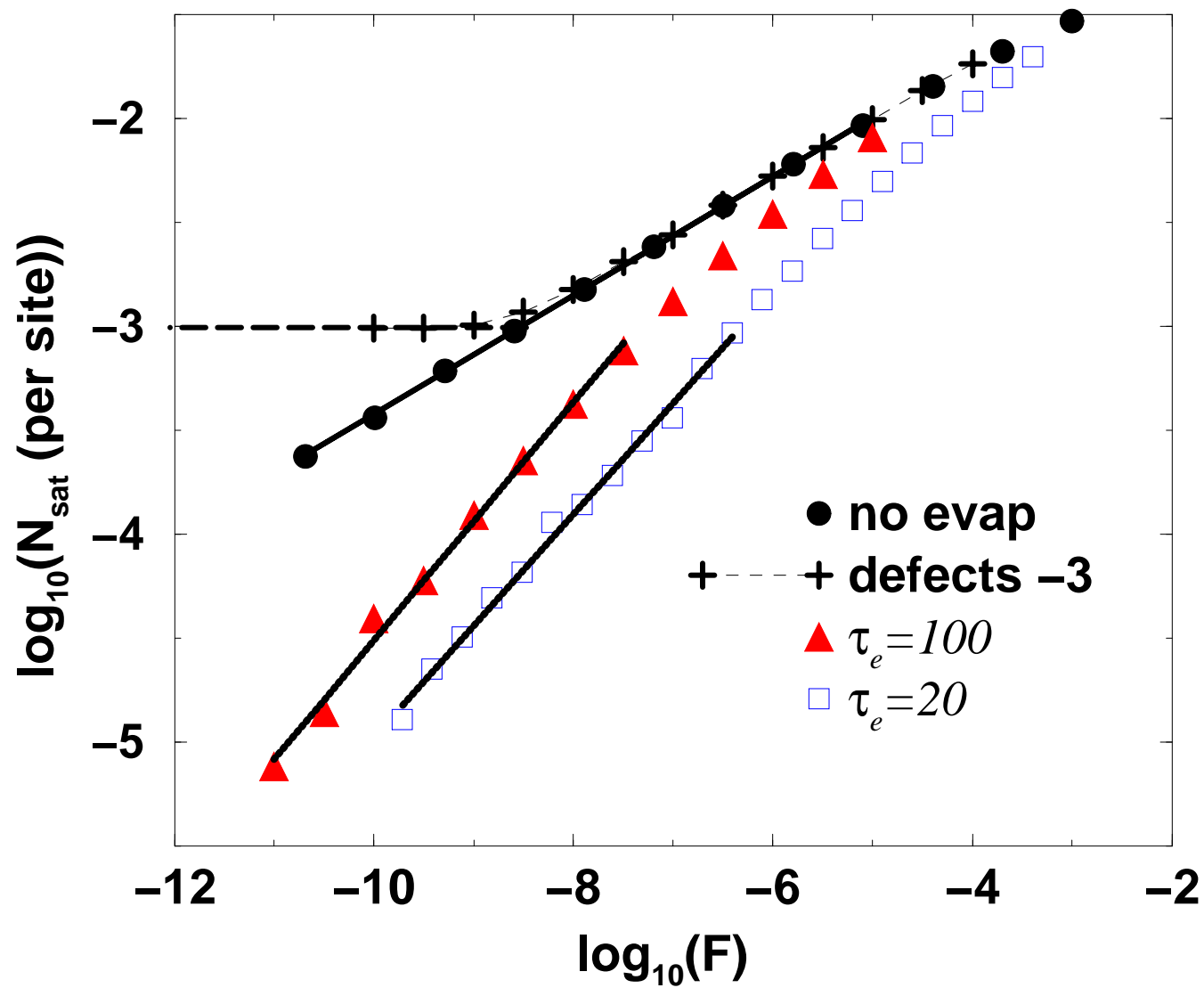
This figure "Fig9b.gif" is available in "gif" format from:

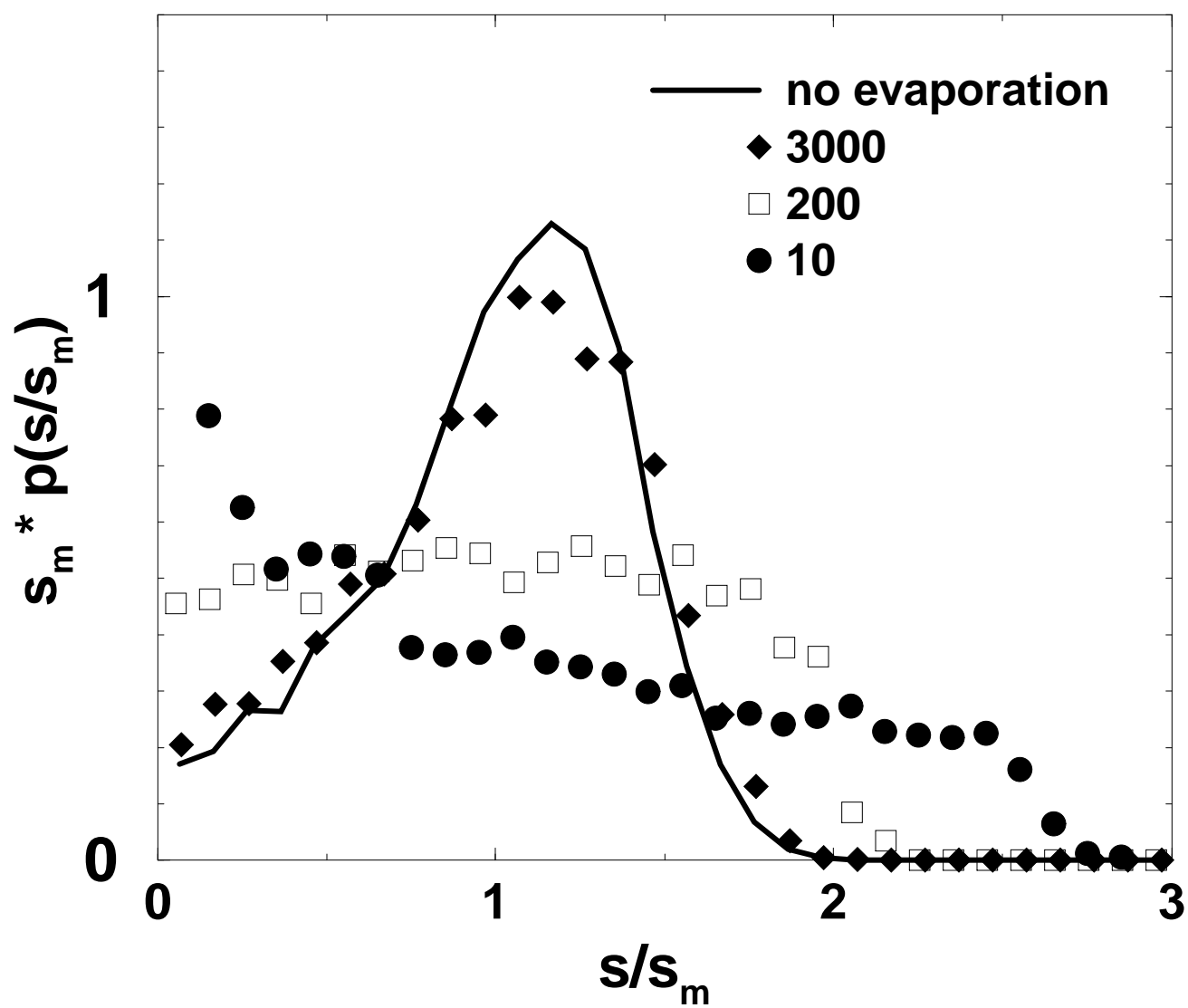
<http://arxiv.org/ps/cond-mat/9903141v1>

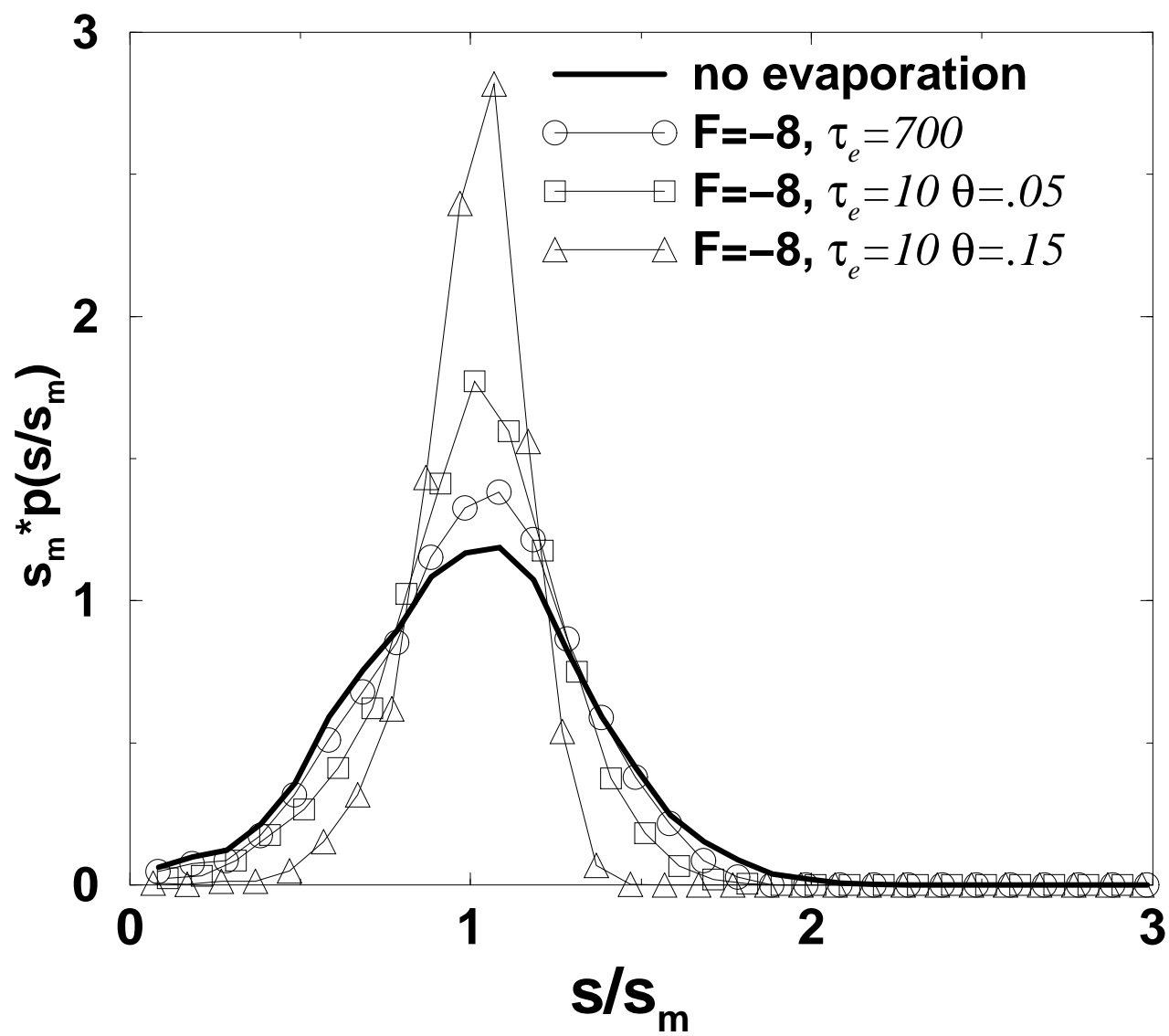


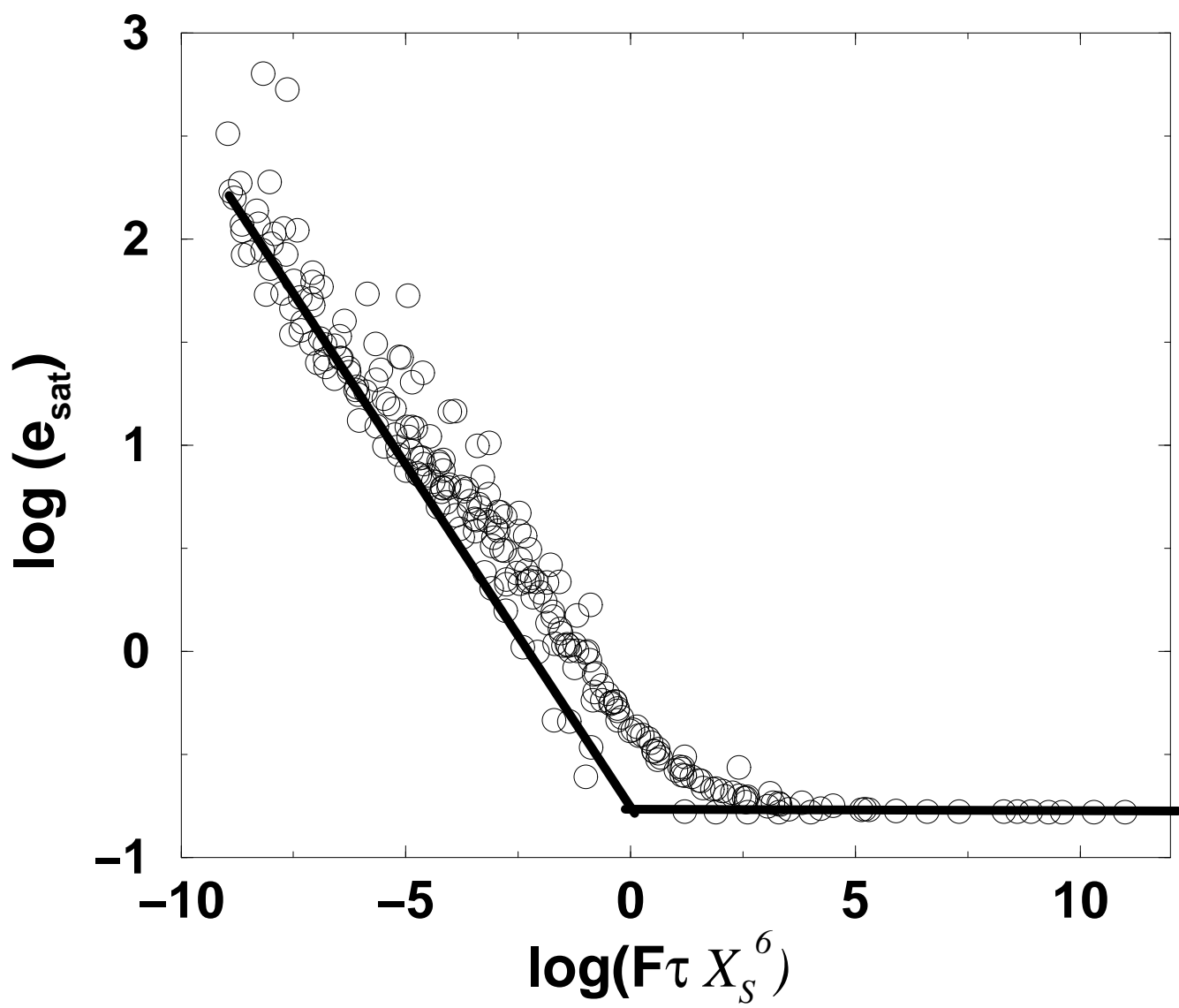


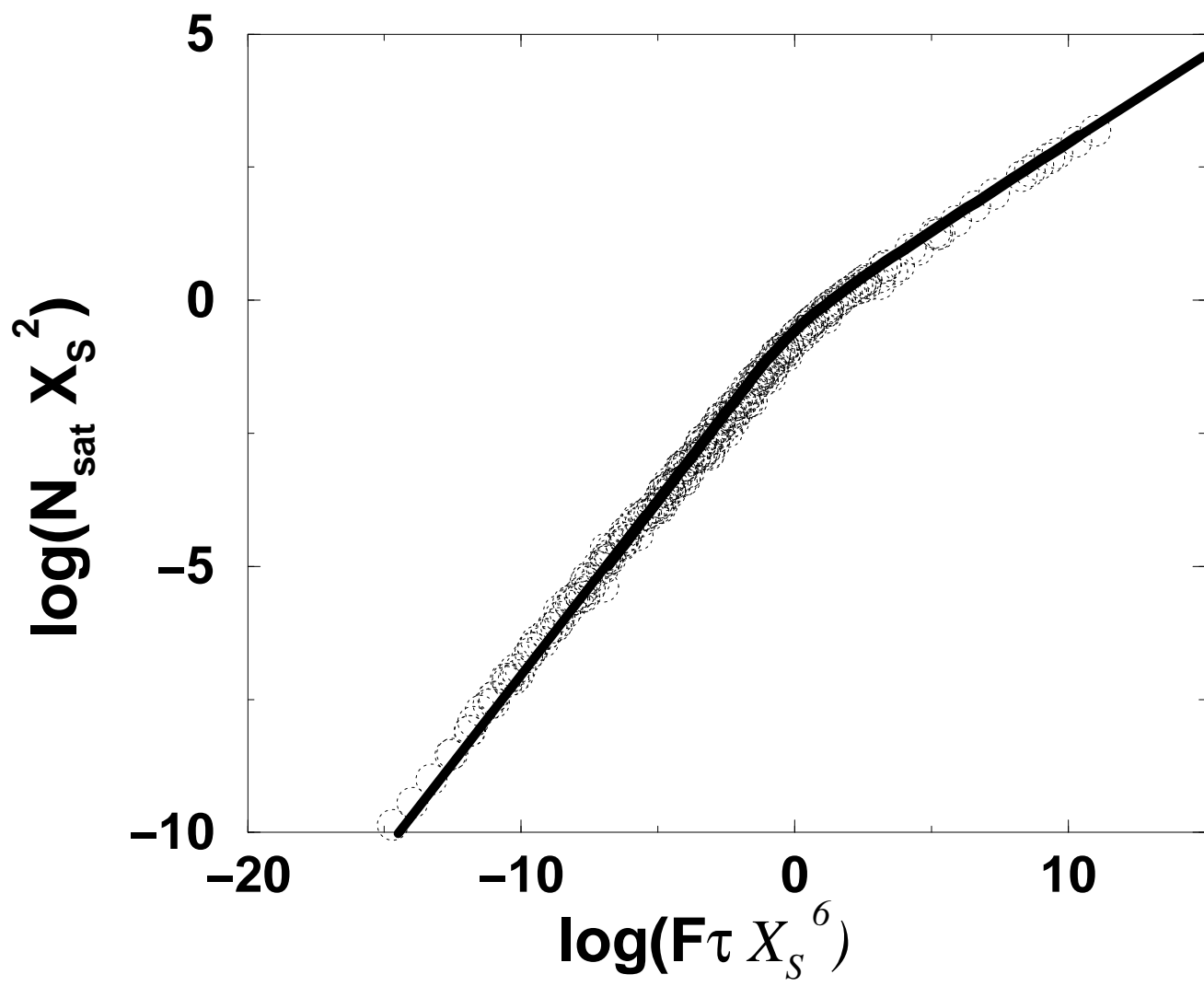


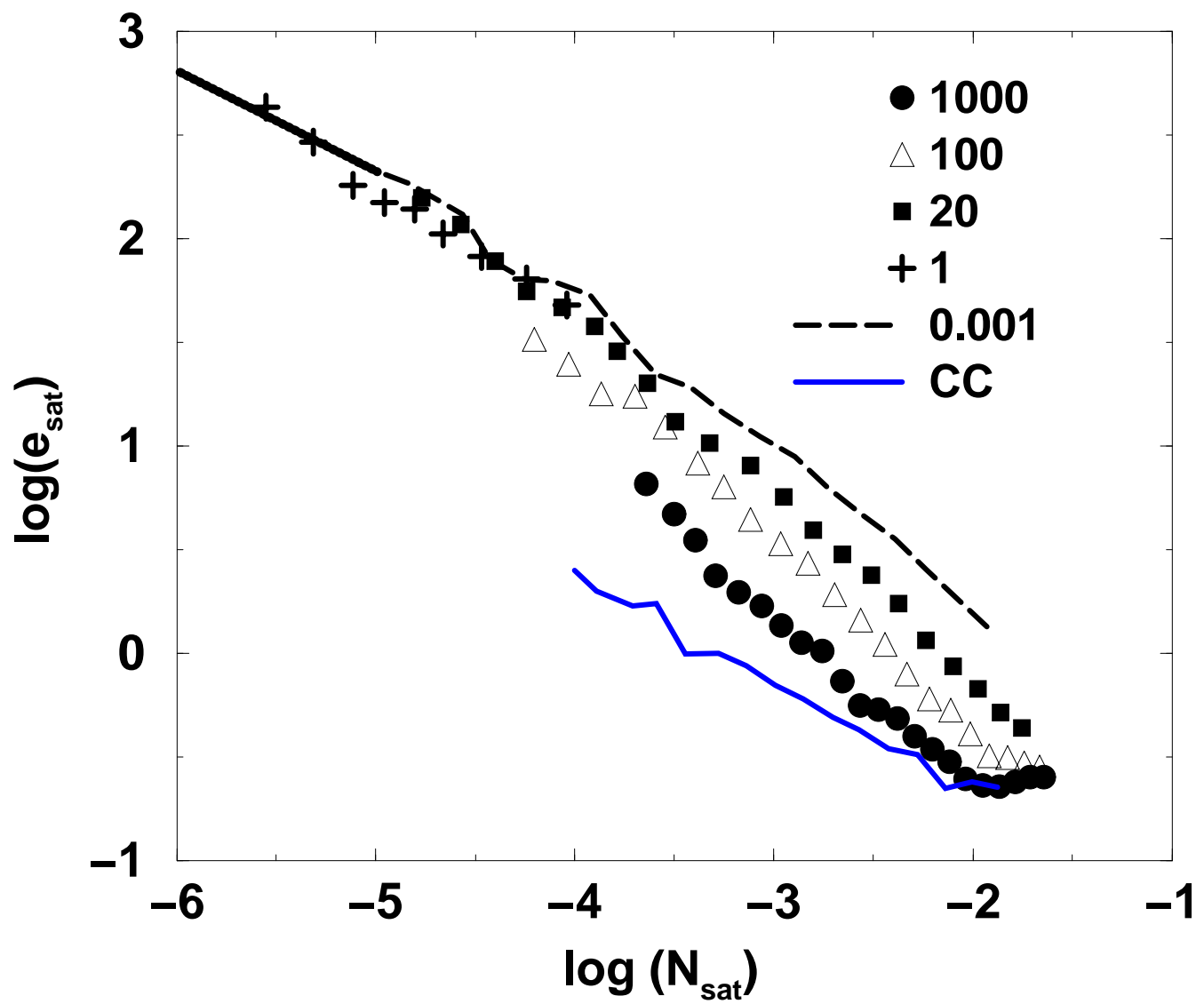


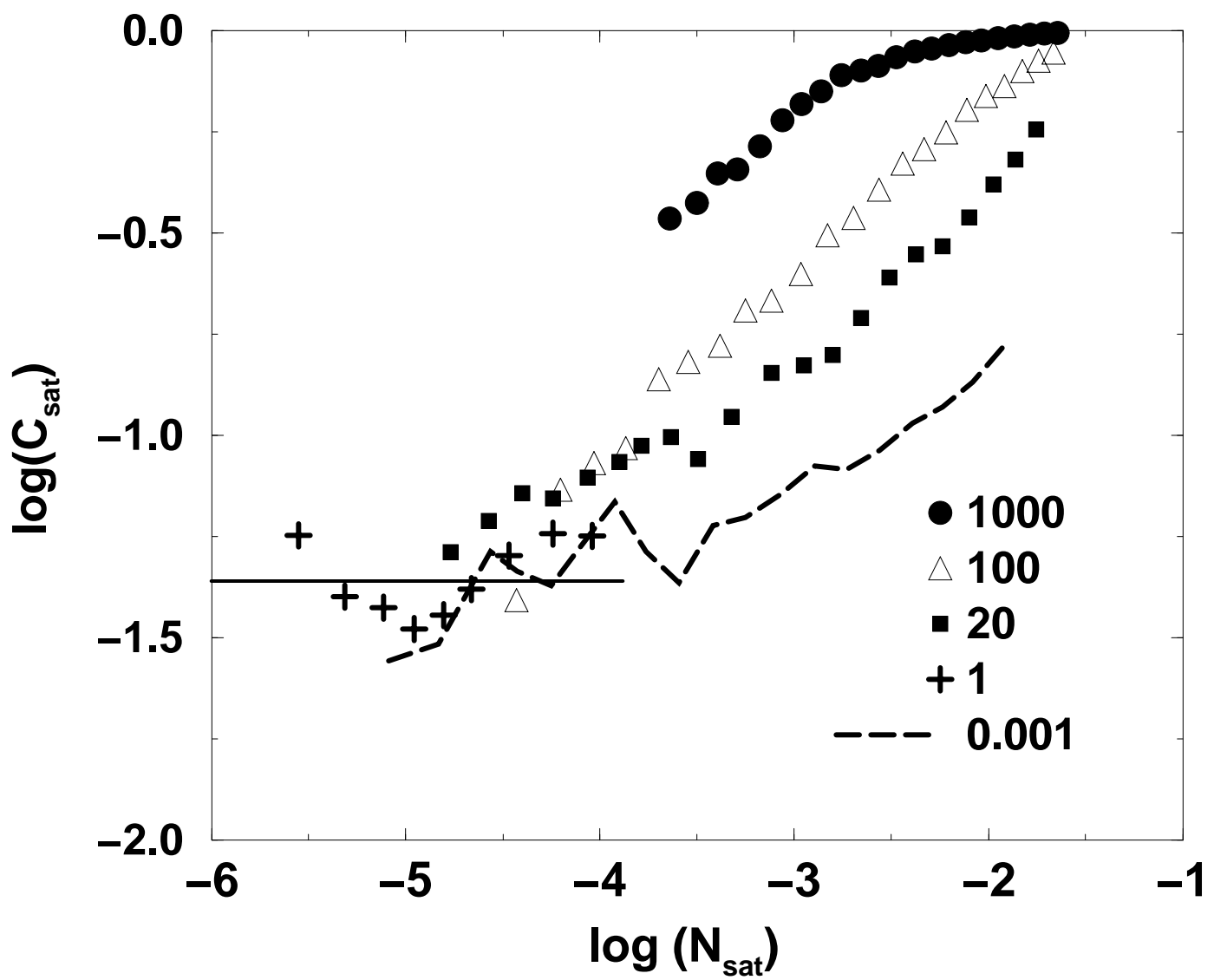






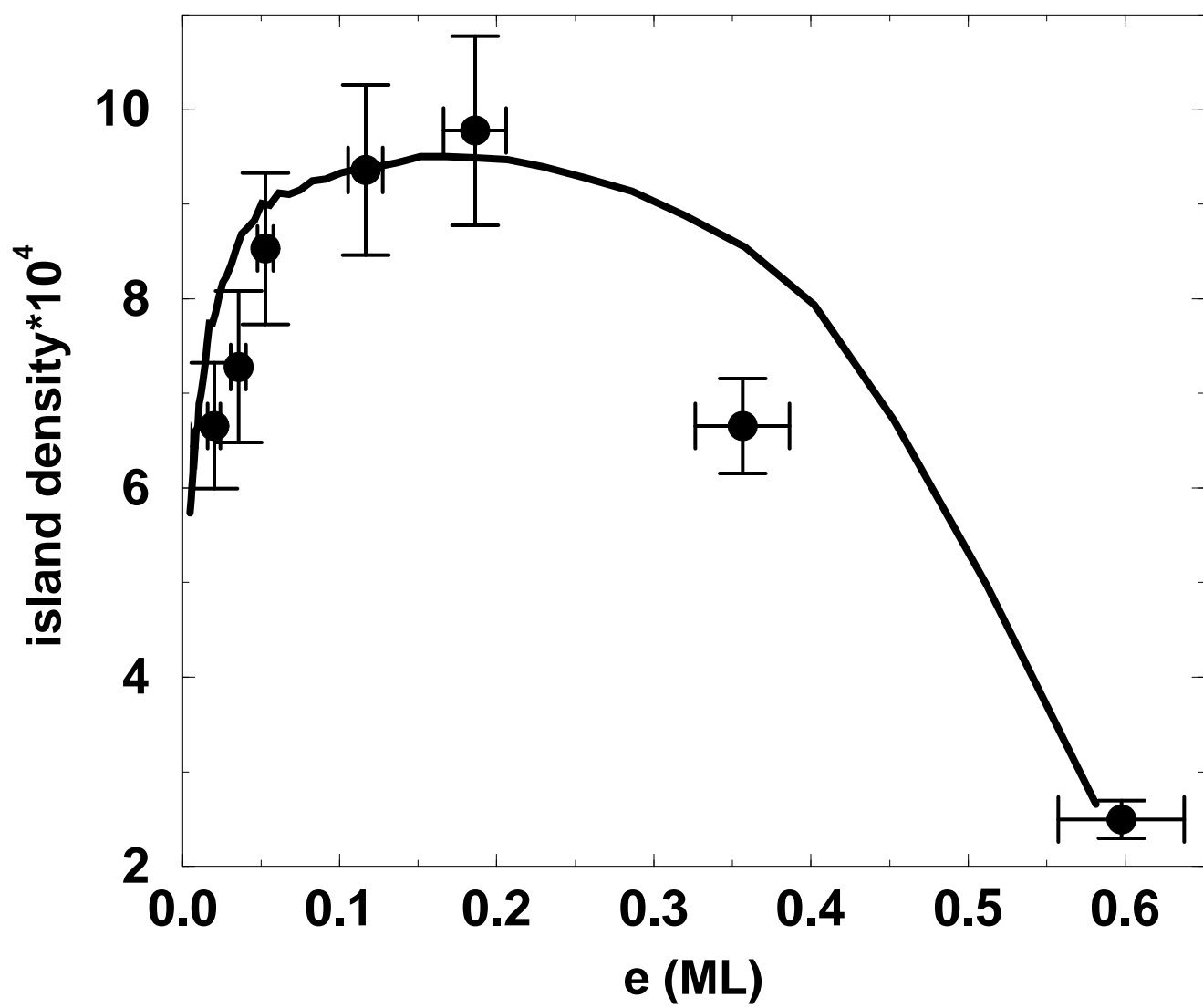


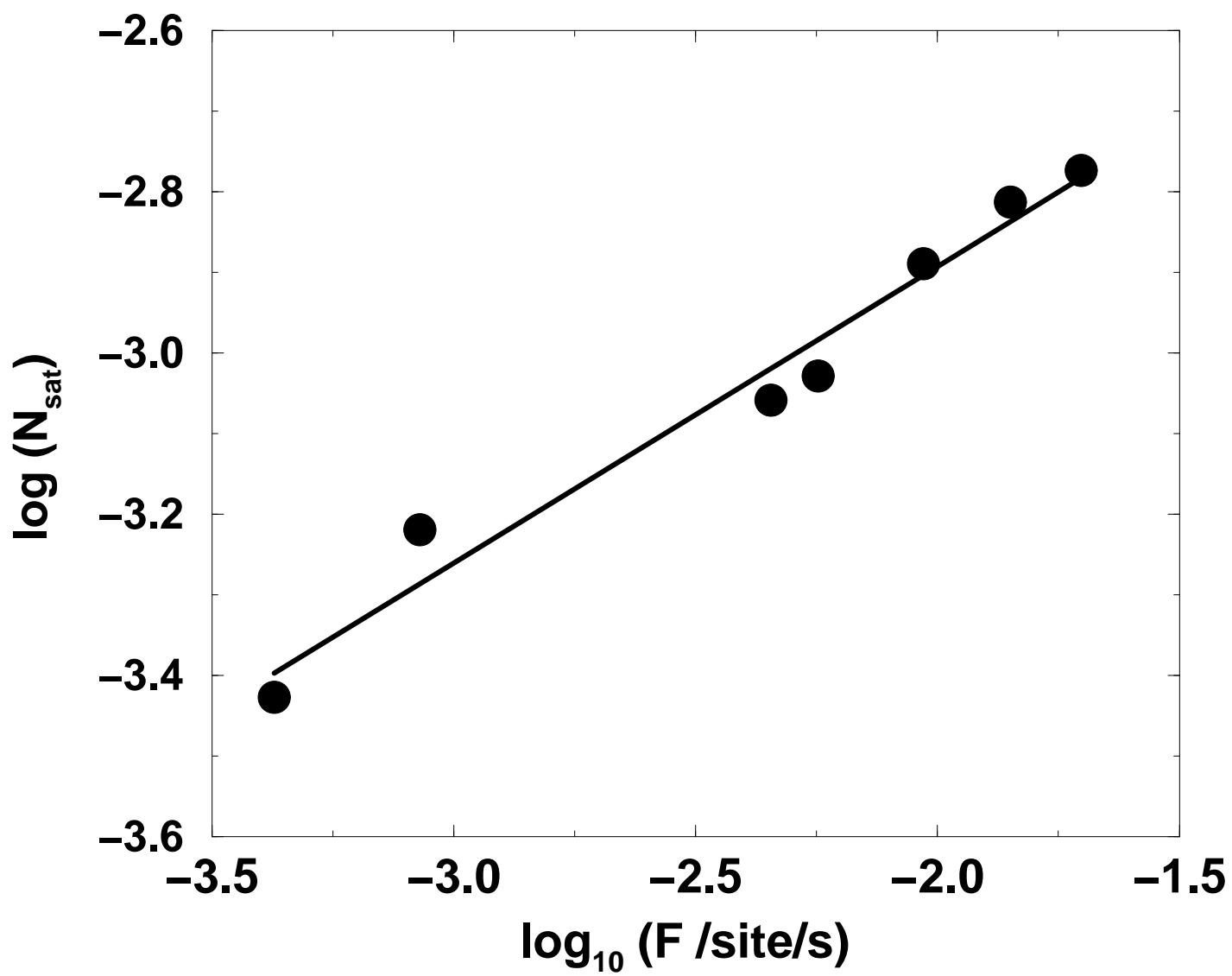


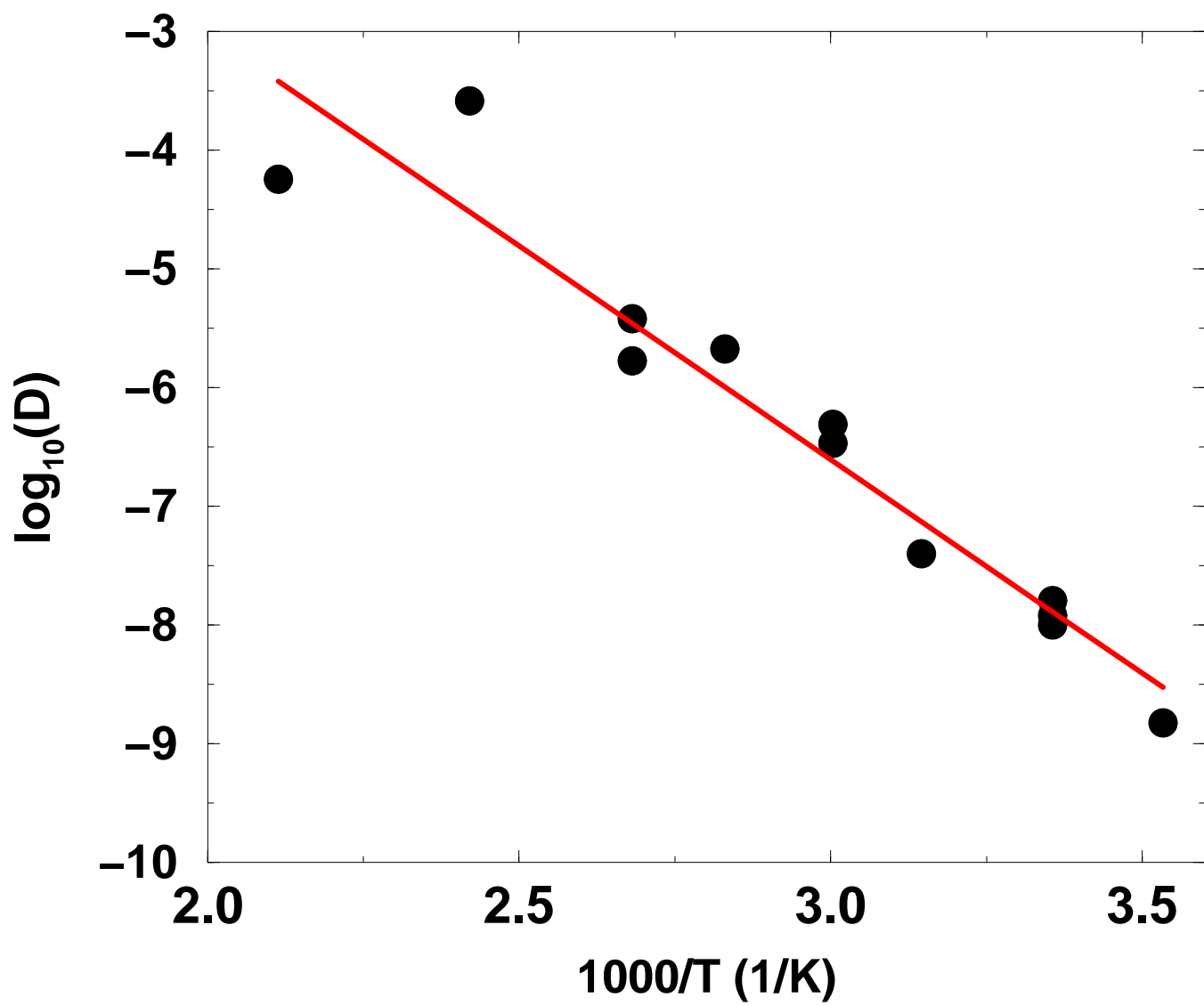


This figure "Fig18.jpg" is available in "jpg" format from:

<http://arxiv.org/ps/cond-mat/9903141v1>





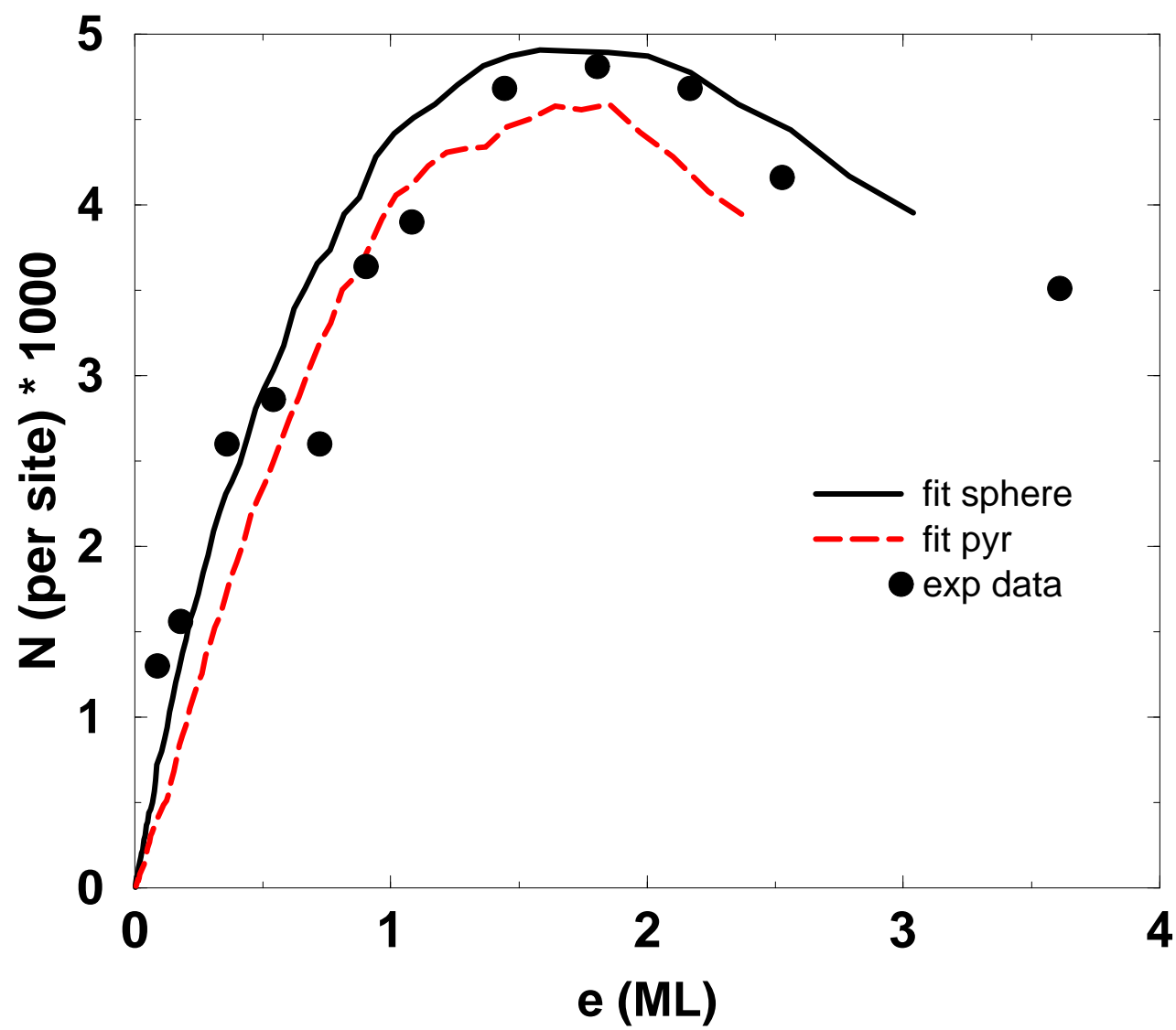


This figure "Fig20.jpg" is available in "jpg" format from:

<http://arxiv.org/ps/cond-mat/9903141v1>

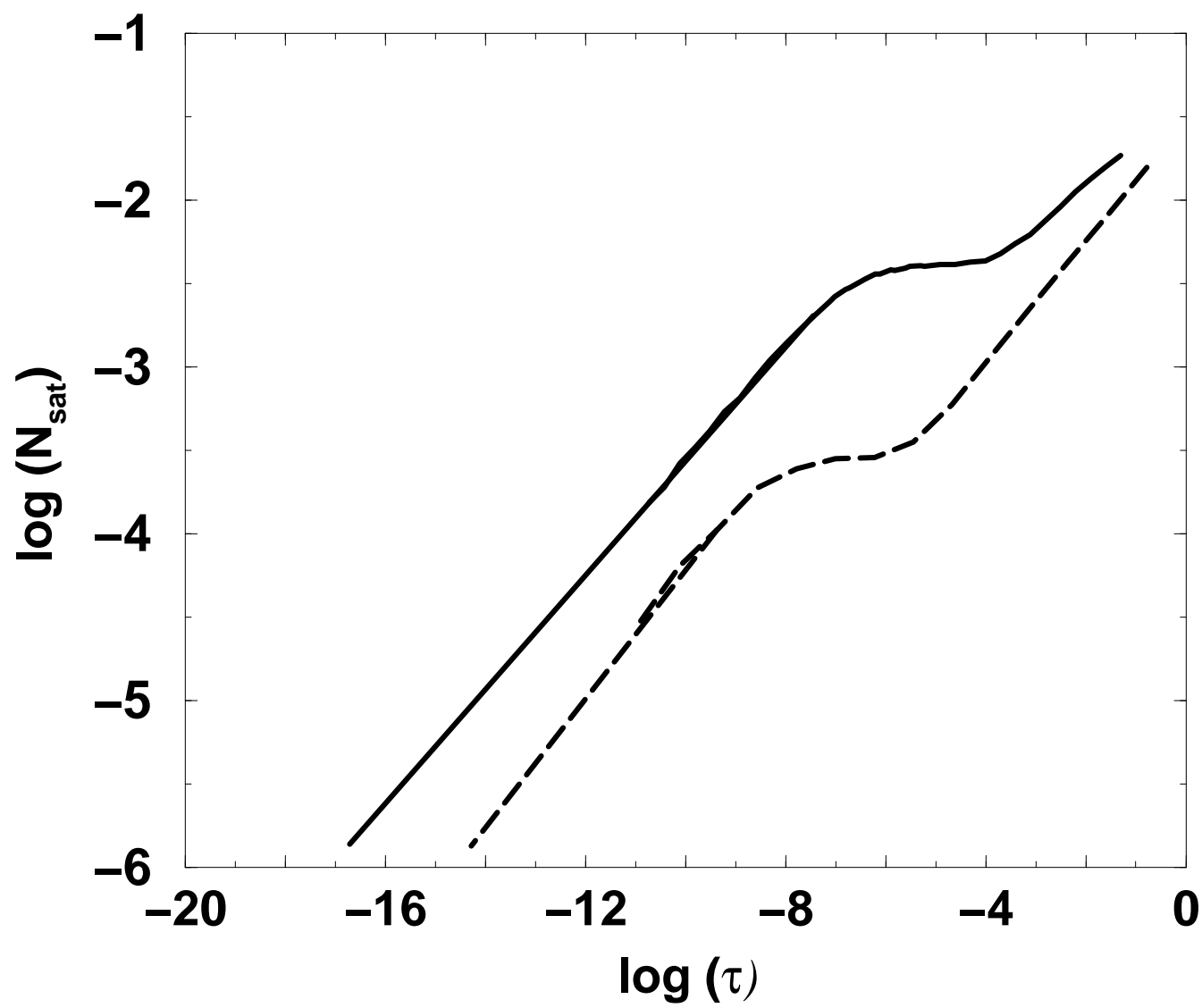
This figure "Fig21a.jpg" is available in "jpg" format from:

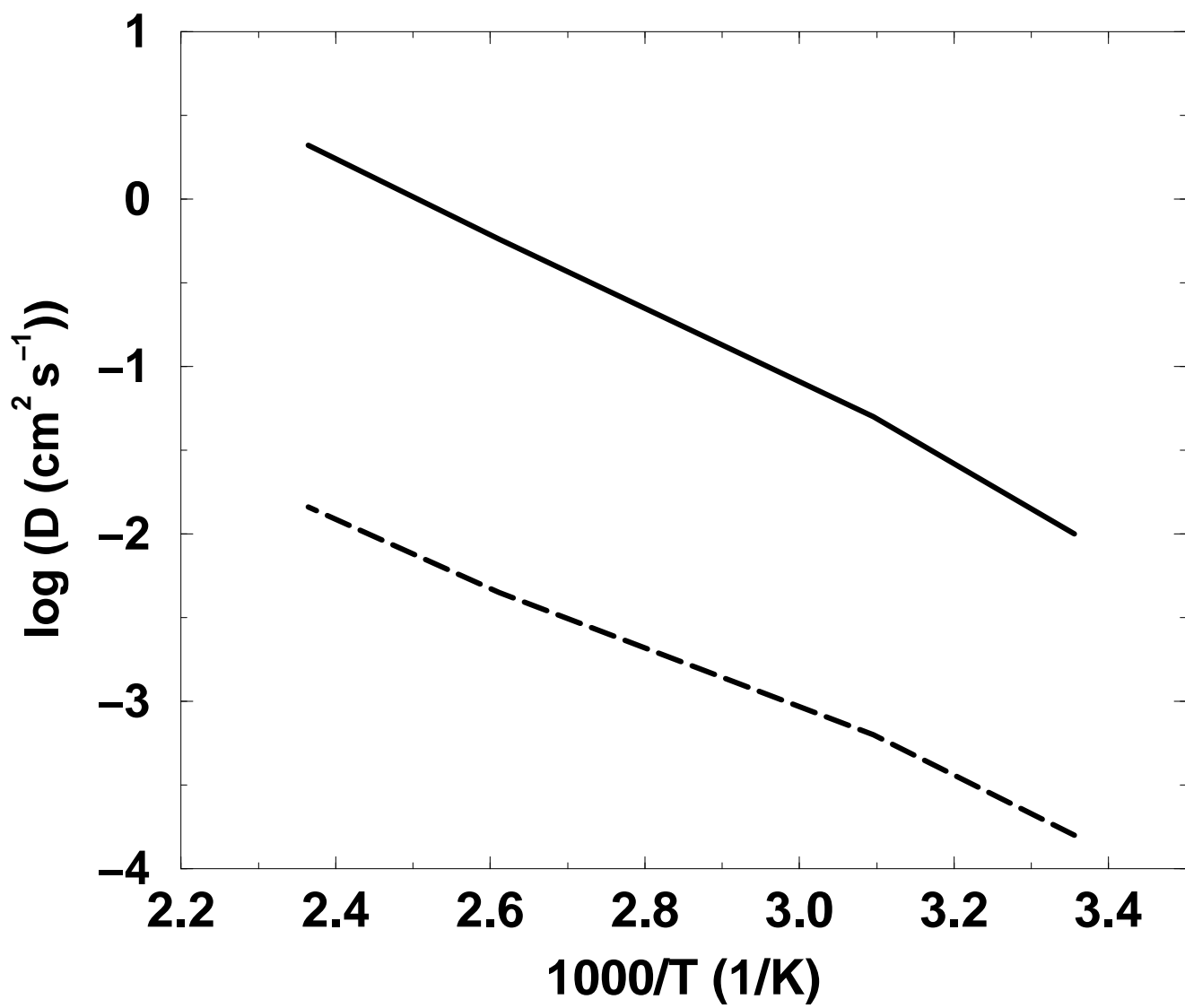
<http://arxiv.org/ps/cond-mat/9903141v1>



This figure "Fig22.jpg" is available in "jpg" format from:

<http://arxiv.org/ps/cond-mat/9903141v1>





This figure "Fig24a.jpg" is available in "jpg" format from:

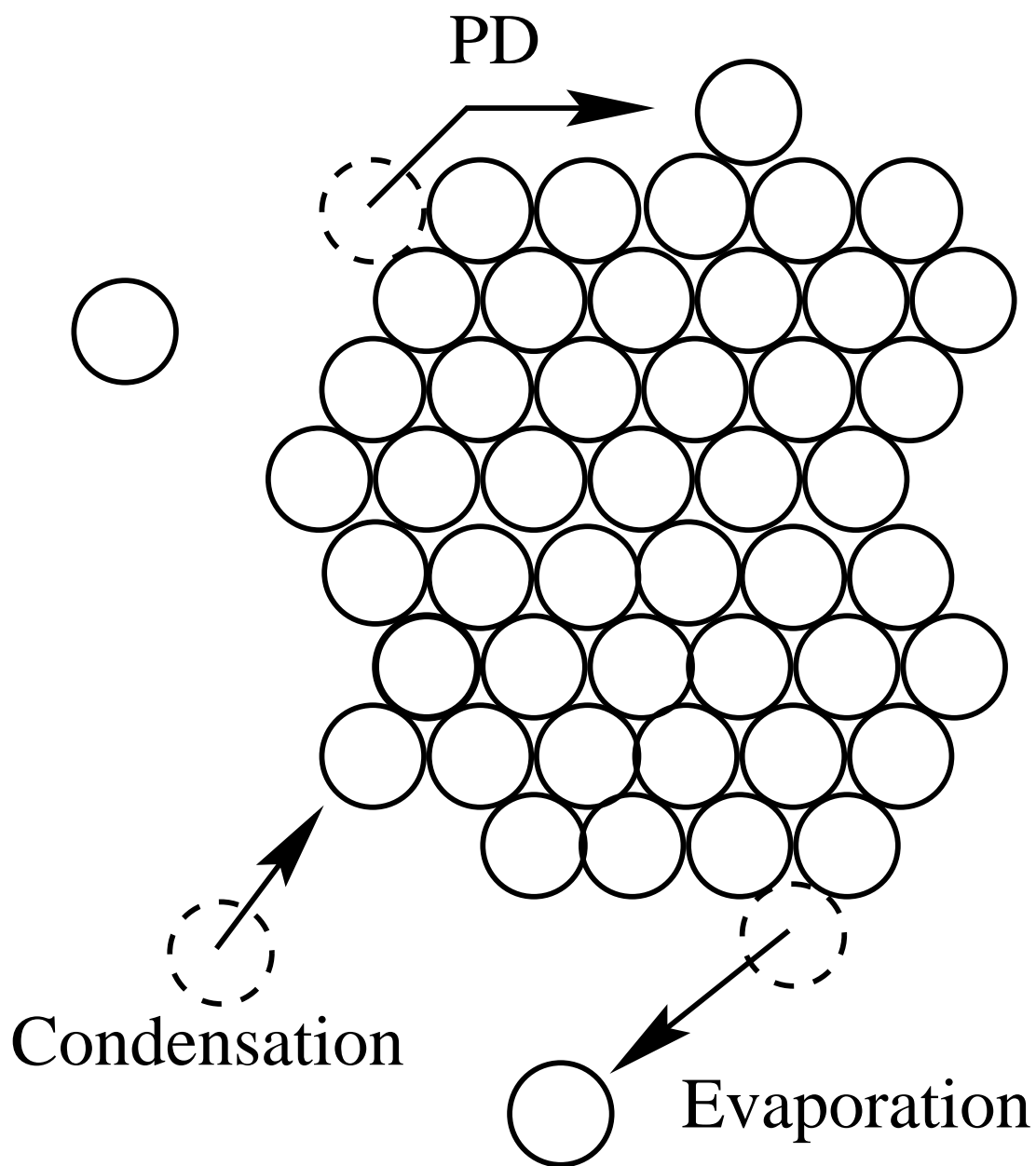
<http://arxiv.org/ps/cond-mat/9903141v1>

This figure "Fig24b.jpg" is available in "jpg" format from:

<http://arxiv.org/ps/cond-mat/9903141v1>

This figure "Fig25.jpg" is available in "jpg" format from:

<http://arxiv.org/ps/cond-mat/9903141v1>



This figure "Fig27.jpg" is available in "jpg" format from:

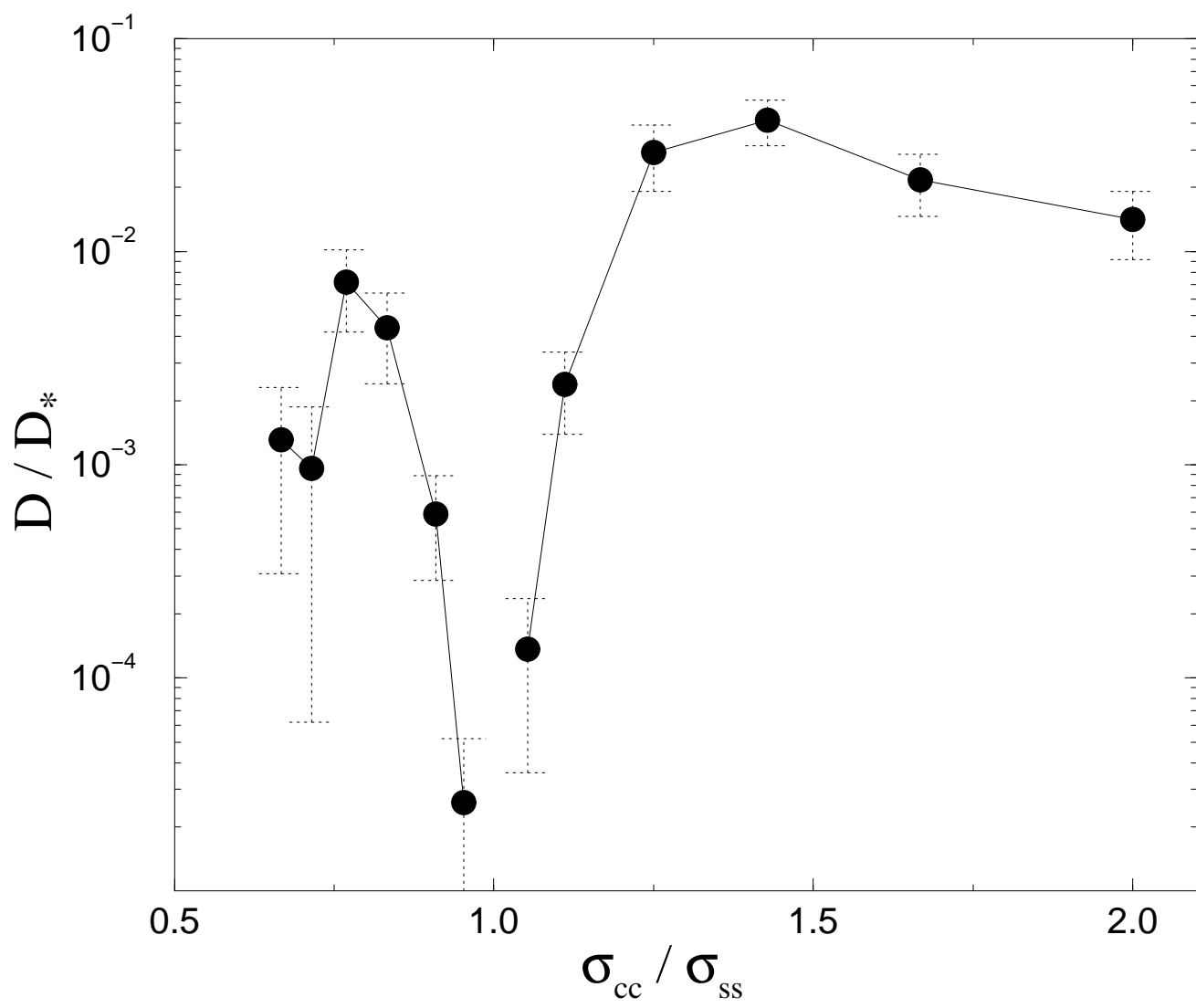
<http://arxiv.org/ps/cond-mat/9903141v1>

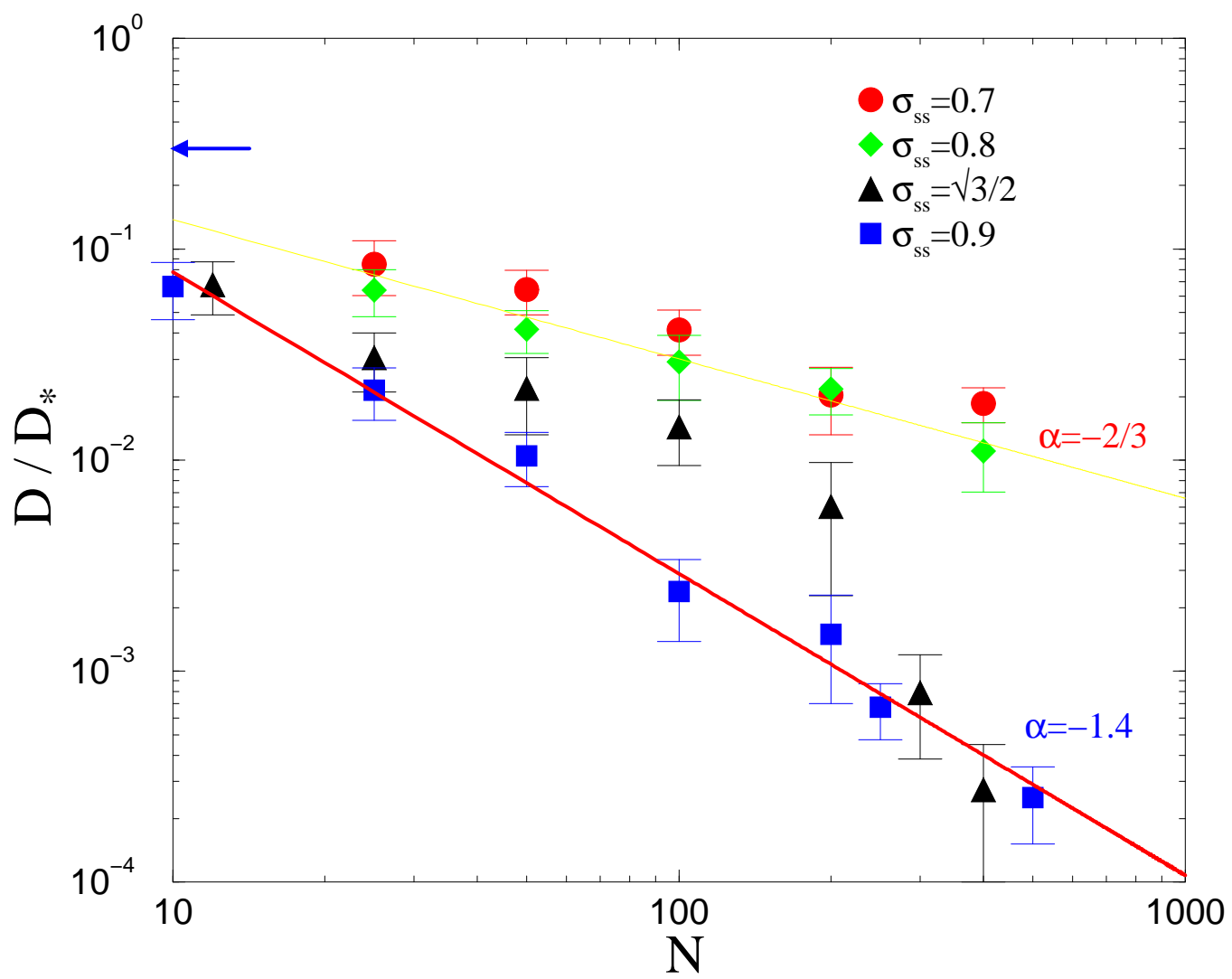
This figure "Fig28.jpg" is available in "jpg" format from:

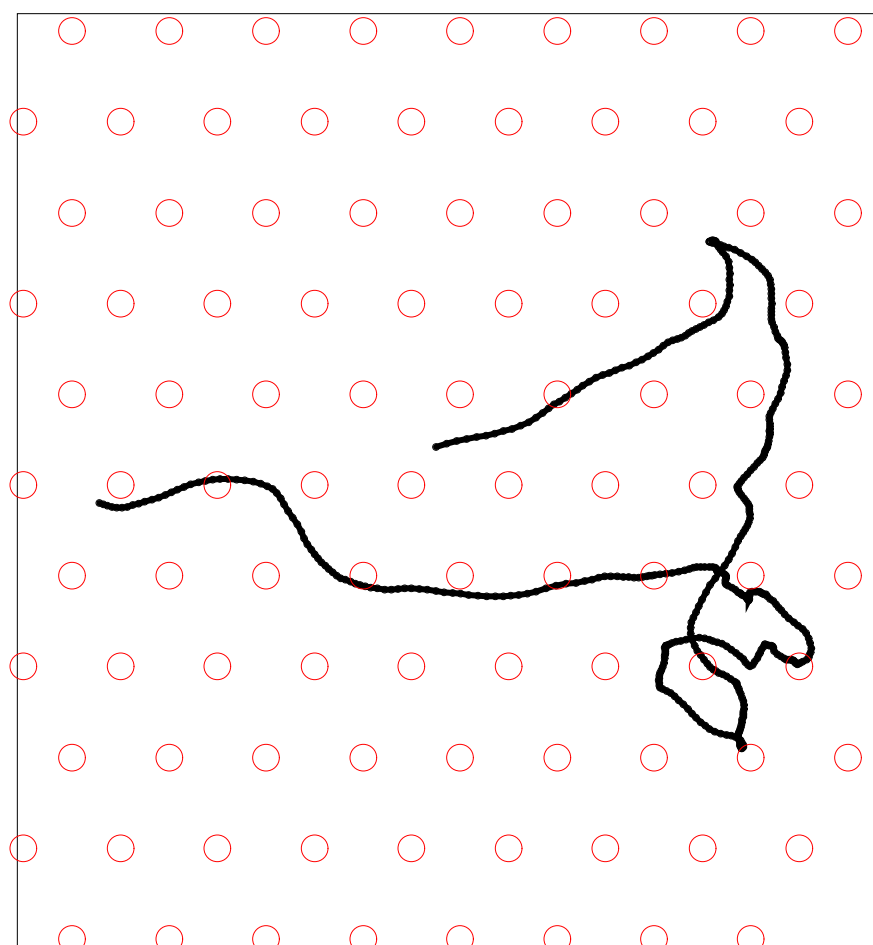
<http://arxiv.org/ps/cond-mat/9903141v1>

This figure "Fig29.jpg" is available in "jpg" format from:

<http://arxiv.org/ps/cond-mat/9903141v1>

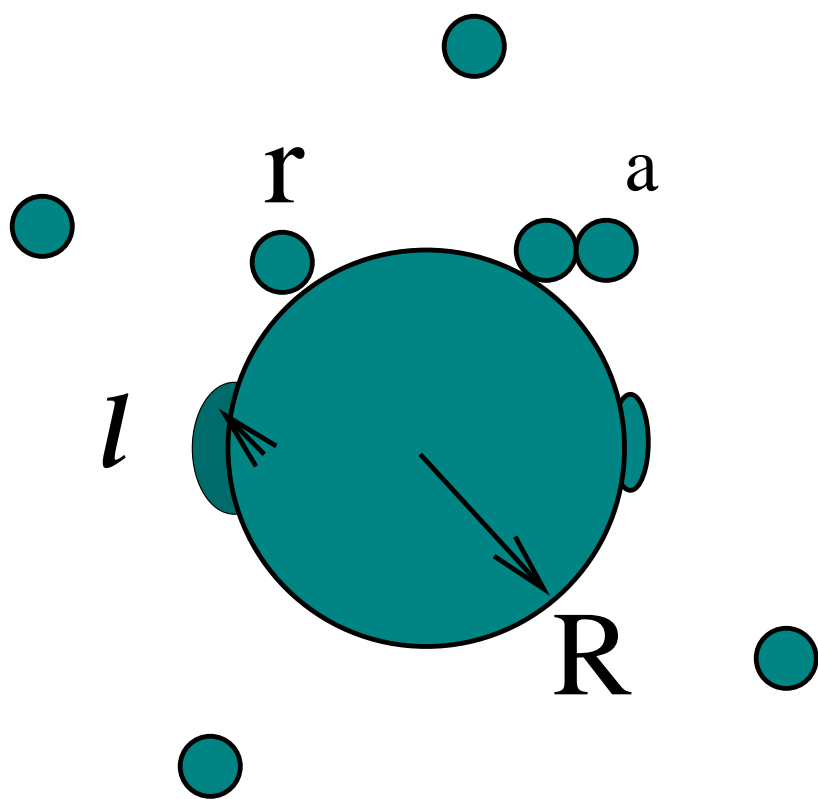






This figure "Fig31b.jpg" is available in "jpg" format from:

<http://arxiv.org/ps/cond-mat/9903141v1>



This figure "Fig33.jpg" is available in "jpg" format from:

<http://arxiv.org/ps/cond-mat/9903141v1>

This figure "Fig34.jpg" is available in "jpg" format from:

<http://arxiv.org/ps/cond-mat/9903141v1>

This figure "Fig35.jpg" is available in "jpg" format from:

<http://arxiv.org/ps/cond-mat/9903141v1>

This figure "Fig36.jpg" is available in "jpg" format from:

<http://arxiv.org/ps/cond-mat/9903141v1>

